Master Thesis

Effect of Post Metallization Annealing for La_2O_3 Gate Thin Film

Supervisor

Professor Hiroshi Iwai

Associate Professor Shun-ichiro Ohmi

Iwai Laboratory

Department of Advanced Applied Electronics

Interdisciplinary Graduate School of Science and Engineering

Tokyo Institute of Technology

02M36107

Atsushi Kuriyama

CONTENTS

Chapter 1

Introduction

1.1 Background

In this section, the general perspective of the present semiconductor technology and the background of this investigation will be described in the pages that follow.

1.1.1 Background of This Study

In recent years, a magnificent influence of silicon LSI technology has appeared in a large number of scenes such as our social, business and domestic lives, and that has supported essential part of them. The higher performance and the lower consumption power equipments using silicon LSI technology like personal computers and cellular phones have been developed with great force as shown in Figure 1-1. The principal element which makes it possible is the improvements of Metal-Oxide-Semiconductor Field Effect Transistor (MOS FET), especially by miniaturizing the physical size of the devices according to scaling method. Scaling method is the way of shrinking the devices with same factor S as shown in Figure 1-2 and Table 1-1. To downsize the devices leads to high speed switching operation and lower power consumption owing to the shrink of the channel length, and whole performance of LSI system also can becomes higher because miniaturizing the devices realizes to contain much higher number of transistor in the same area, which improve high-speed, high-frequency characteristics. Investigating the device for downsizing is hence far important and has continued throughout the world.

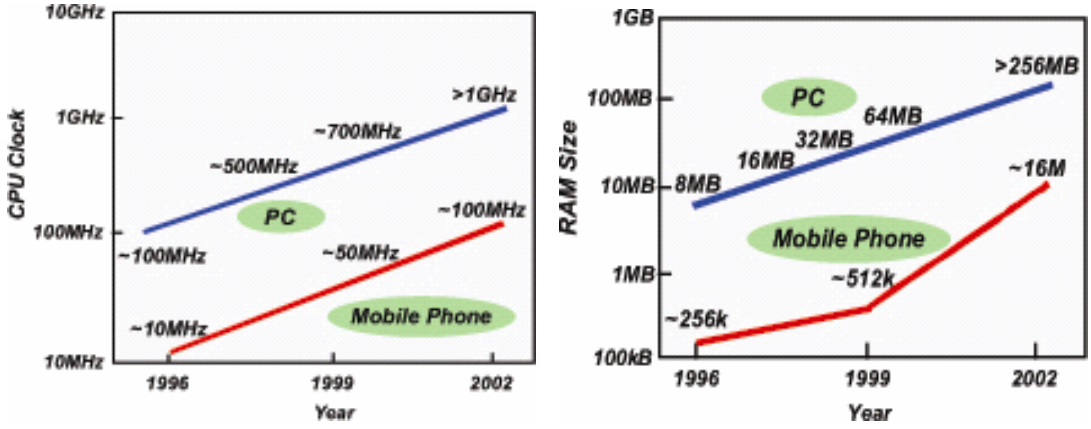

Fig. 1-1: Trends of CPU Clock and RAM Size

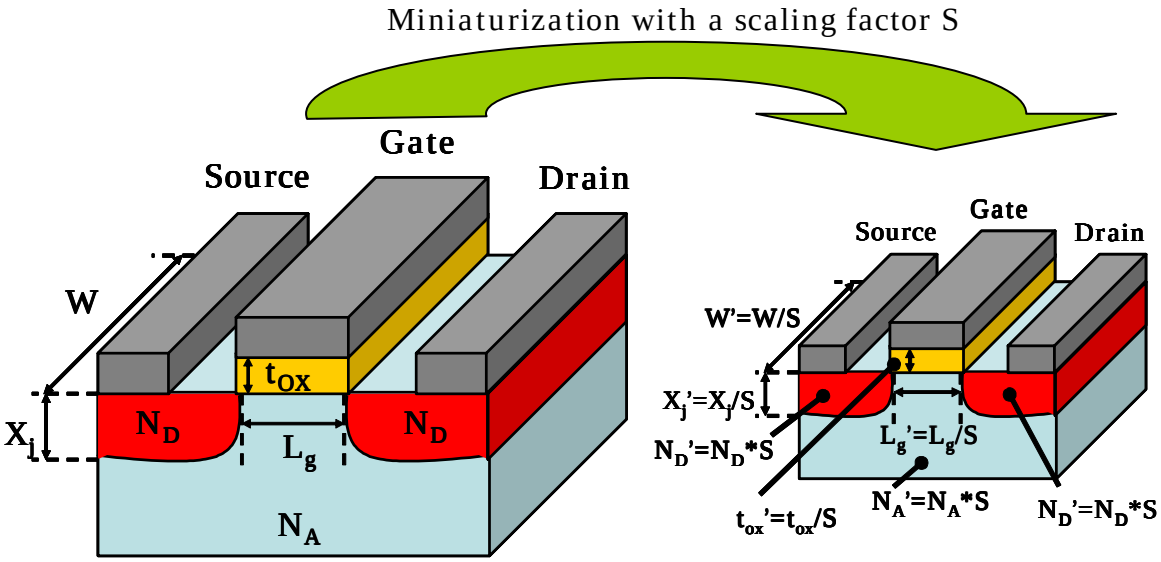

Fig. 1-2: Scaling Method on MOSFET

Table 1-1: Scaling on MOSFET by a scaling factor S

Quantity	Before Scaling	After Scaling
Channel length	L_g	$L'_g = L/S$
Channel Width	W	W' = W/S
Device Area	A	$A' = A/S^2$
Gate Oxide Thickness	t_{OX}	$t_{OX}' = t_{OX}/S$
Gate Capacitance Per Unit Area	C_{OX}	$C_{OX}' = t_{OX}*S$
Junction Depth	X_j	$X_j' = X_j/S$
Threshold Voltage	V_{th}	$V_{th}' = V_{th}/S$
Doping Density (Acceptor)	N_A	$N_A' = N_A*S$
Doping Density (Donor)	N_D	$N_D' = N_D*S$

1.1.2 Limits of Silicon Dioxide (SiO_2) as Gate Insulator

To downsize the size of MOSFET, however, brings various difficulties at the same time. One of them, considered as the decisive factor in future LSI technology, is limits of SiO_2 as gate insulator. As mentioned in former section, shrinking the devices has brought magnificent improvement in LSI technology. At the mention of gate insulator, SiO_2 had been used as gate insulator since MOSFET was invented because SiO_2 has good property such as high stability with silicon substrate at high temperature process or low density of fixed charge, defects in bulk and at the interface. Consequently, SiO_2 had played a significant role of MOSFET and been downsized over a long period of time.

It is said recently, however, that Thinning down SiO_2 has been reaching limits because of direct tunneling current. Table 1-2 shows the electrical properties for 1 nm thickness SiO_2 gate insulator. This table says that leakage current density reaches 100 A/cm^2 and, to make matters worse, when SiO_2 thickness become below 0.8 nm, leakage current density will increase over 1 kA/cm^2 caused by direct tunneling effect. Figure 1-3 shows the schematic band diagram explaining direct tunneling mechanism. In case of the thick insulator, that works as a barrier for carriers. Therefore, leakage current remains low. In case of thin insulator, however, the quantum effect can not be negligible and carriers can get to pass through the insulator directly. Consequently, leakage current becomes huge exponentially. This undesirable effect will lead the increase of power consumption and degradation of LSI reliability and these unacceptable phenomena must be averted.

Table 1-3 shows technology roadmap for various element of MOSFET. This roadmap indicates the value of EOT (Equivalent Oxide Thickness) will reach 0.9 nm in 2007 and 0.5 nm in 2016. However, it is said that practical solutions to realize EOT=0.9 nm are not known yet.

From the foregoing, it is considered that revolutionary change to solve these problems is strongly required and one of the answers is to replace SiO_2 to new material.

Table 1-2: Electrical Properties for 1nm thickness SiO_2 Gate Insulator

EOT [nm]	1.0
Leakage Current Density [A/cm2]	100
Gate Length [0m]	0.1
Gate Width [0m]	5
Gate Area [cm2]	5×10^{-9}
Functions per Chip (Transistors/Chip)	1×10^{8}
Total Gate Area [cm^2]	5×10^{-1}
Total Leakage Current per Chip [A/chip]	50

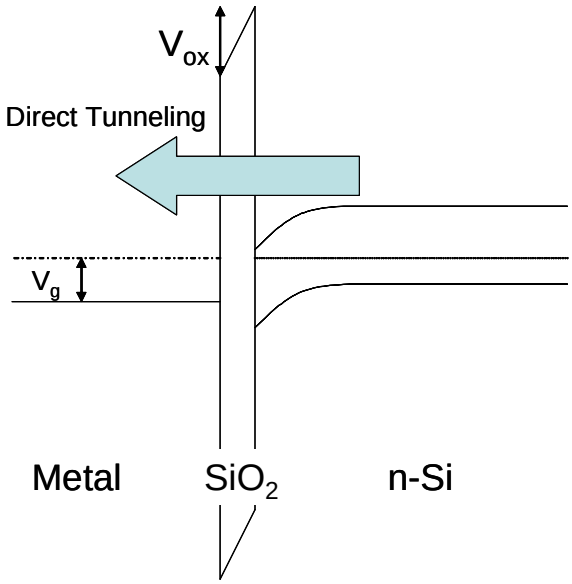

Figure 1-3: The Schematic Band Diagram for Thin SiO_2 MOS Capacitor

Table 1-3: Projections of the sizes of MOSFET

Year	2004	2007	2010	2013	2016
Node [nm]	90	65	45	32	22
Lg [nm]	37	25	18	13	9
EOT [nm]	1.2	0.9	0.7	0.6	0.5
Vdd [V]	1.2	1.1	1.0	0.9	0.8

1.1.3 Requirements for High-k Gate Dielectrics

The reason to thin down SiO_2 is to increase gate charges, which increases drain current. The capacitance C_i of gate dielectric at unit area is expressed with the following equation,

$$C_i = \frac{\varepsilon_0 k}{t} \qquad (1.1)$$

where ε_0 and k are vacuum and relative dielectric constant, respectively and t is the thickness of gate dielectrics. The value of vacuum dielectric constant is about 8.85×10^{-14} [F/cm] and relative dielectric constant of SiO_2 is 3.9. Thinning down SiO_2 used to be a simple and effective way to obtain high capacitance value as SiO_2 is greatly stable with silicon substrates as mentioned in former section. Now that the limit of SiO_2 is showing up, however, another way to increase the capacitance value is required. The answer for this requirement is to introduce new materials which have high dielectric constant. These materials are called high-k dielectrics. If one material which have a dielectric constant, k=7.8 (double compared to SiO_2) can be replaced instead of SiO_2, the capacitance value is maintained even though thickness of gate insulator become twice. If this replacement can be possible, that will be the answer enough to prevent direct tunneling effect taking place shown in Figure 1-4.

It is, however, not simple to replace SiO_2 to the high-k materials, because the high-k dielectrics must satisfy several conditions which determine the electrical properties of MOSFET. The requirements for high-k dielectrics are described in the pages that follow.

(1) High dielectric constant

As is already mentioned, the higher dielectric constant is, the thicker the gate insulator can be for same capacitance value. At the same time, however, the band gap which determines the barrier height against electrons and holes is roughly inversely proportional to the dielectric constant. Therefore, it is necessary for high-k dielectrics to be compatible with the band gap in order to suppress the leakage currents due to Schottky emission. Generally, it is considered that dielectric constant less than 50 is desirable.

(2) Stability at high thermal condition in contact with Si surface

There are some processes with thermal condition around 1000K in

LSI fabrication, such as activation after impurity doping. During such a thermal process, the formation of SiO_2 or $M_xSi_yO_z$ (silicate) may be grown at Si and high-k interface. These interfacial layers decrease the total dielectric constant enormously. Recently, however, lots of investigators have reported that these Silicon-like material such as silicate or SiO_2 layer produce good properties in terms of mobility or leakage current density and the attempt to use these layers positively is suggested.

Furthermore, micro-crystal growth in the films may also occur during the thermal process. That must be prevented because these condition increase leakage current tremendously.

(3)Low densities of interface state, fixed charge and High mobility

Mobility is one of the most important factors in properties of MOSFET because that directly affects the drain current. The key to obtain high mobility is the quality of the gate insulator. It is considered that Mobility is degraded by the carrier scattering effect caused by defects in the gate insulator such as fixed charges, which causes flat-band voltage shift, and higher density of interface states induce Coulomb scattering. These defects in high-k films, hence, must be suppressed at a low level.

From the mentioned above, the choice of high-k materials is exceedingly important and difficult as well. The representative materials of high-k dielectrics for gate insulator will be described in next section.

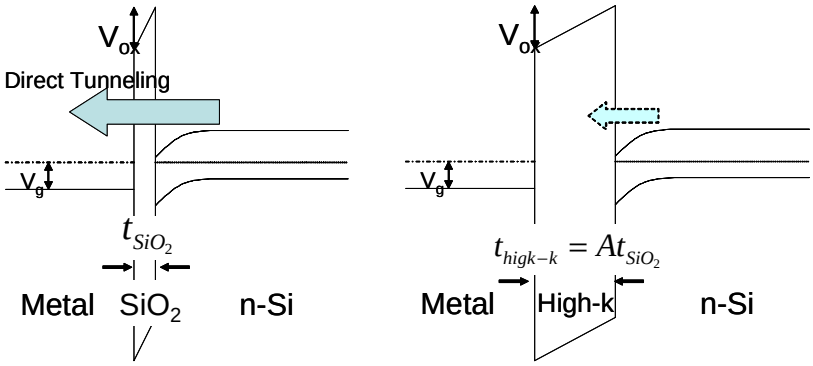

$$\varepsilon_{SiO_2} = 3.9 \qquad \varepsilon_{high-k} = A\varepsilon_{SiO_2}$$

$$C_{SiO_2} = \frac{\varepsilon_{SiO_2}}{t_{SiO_2}} \qquad C_{high-k} = \frac{\varepsilon_{high-k}}{t_{high-k}} = \frac{A\varepsilon_{SiO_2}}{At_{SiO_2}} = C_{SiO_2}$$

$$EOT = \frac{\varepsilon_{SiO_2}}{C_{SiO_2}} = t_{SiO_2} \qquad EOT = \frac{\varepsilon_{SiO_2}}{C_{high-k}} = \frac{\varepsilon_{SiO_2}}{C_{SiO_2}} = t_{SiO_2}$$

Figure 1-4: Advantage of high-k materials to SiO_2 as gate insulator

1.2 Rare Earth Oxides as the Candidates of High-k Dielectrics and Their Properties

In order to overcome the limits of SiO_2 explained in previous section, several promising materials have been investigated in recent years by a large number of researchers. The elements which can be the candidates of the alternative insulator are quite limited because of the reaction failure with Silicon or radioactivity as shown in Figure 1-5. Under these restricted conditions, metal oxides (MO_x) like Al_2O_3, ZrO_2, HfO_2 and recently N, Si, or Al doped HfO_2 gate dielectrics such as HfSiON, $HfAl_x$, HfON and rare earth oxides have been studied eagerly for the next generation gate dielectric materials.

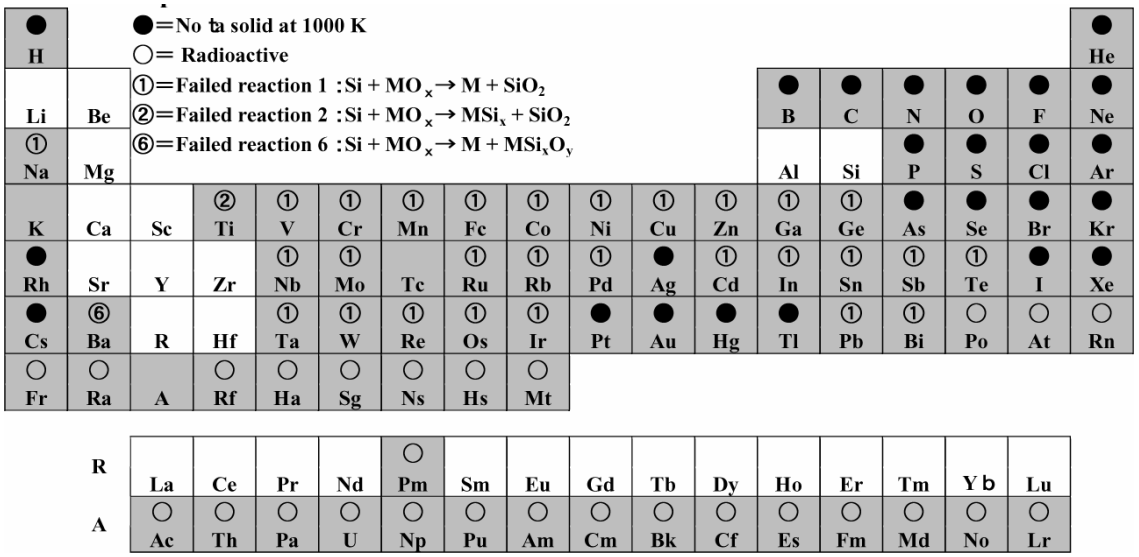

Figure 1-5: Candidates of the elements which have possibility to be utilized as high-k gate insulators

Table 1-4 shows the properties of the major candidate. SiO_2 has the biggest band gap and the highest barrier for electrons and holes, and remains amorphous in thermal condition through the LSI fabrication processes. Moreover, the contact stability with Silicon is completely excellent. Al_2O_3 has relatively higher band gap and remains amorphous against thermal processes. The dielectric constant, however, is considerably lower than other high-k candidates. ZrO_2 and HfO_2 used to be investigated much widely and zealously owing to their higher dielectric constant. As the investigation steps ahead, however, several problems are showing up. One of them is the formation of interfacial layer, which makes EOT hugely increased, through the post deposition annealing processes. Another one is the crystallization at around 700°C, which increases the leakage current tremendously. From these background, N, Si, or Al doped HfO_2 silicates have been reported frequently in very recent years.

Rare earth oxides are considered as one of the most promising high-k materials because most of the rare earth oxides have the higher dielectric constant on a level with ZrO_2 or HfO_2 and these metal oxides are relatively stable at the Silicon interface during the thermal process and it is reported to remain amorphous. Excellent results under EOT of 0.5 nm with lower leakage current using rare earth oxides have also been reported.

Table 1-4: Properties of major high-k materials

Materials	SiO_2	Al_2O_3	**La_2O_3**	**Pr_2O_3**	**Gd_2O_3**	HfO_2	ZrO_2
EOT (nm)	0.8	1.5	**0.48**	**1.4**	**1.5**	0.8	0.8
Contact stability with Si (kJ/mol) $Si+MO_x \rightarrow M+SiO_2$	Stable	+63.4	**+98.5**	**+105.8**	**+101.5**	+47.6	+42.3
Lattice energy (kJ/mol)	13125	15916	**12687**	**12938**	**13330**		11188
Bandgap (eV)	9	6 – 8	**5.4**	**3.9**	**5.4**	5.7	5.2 – 7.8
Structure	Amorphous	Amorphous	**Amorphous**	**Crystal T>700°C**	**Crystal T>400°C**	Crystal T>700°C	Crystal T>400 - 800°C
κ	3.9	8.5 – 10	**27**	**13**	**17**	24	11 – 18.5

A. Chin et al., Symp. on VLSI Tech., pp. 16 - 17 (2000)

Figure 1-6 shows the candidates of rare earth materials for gate insulators and their physical properties. Figure 1-6 (a) shows the value of band gap for rare earth oxides. This figure describes that each element has utterly different value and La_2O_3, Gd_2O_3 and Lu_2O_3 has the highest band gap of 5.4 eV. And most of rare earth oxides have the enough value of band gap around 5 eV. Figure 1-6 (b) shows the value lattice energy for rare earth oxides. Lattice energy means the energy which is required to separate single atom from the state of a crystal, namely the oxides having large lattice energy tend to show easy crystallization. As shown in Figure 1-6 (b), the lattice energy of rare earth oxides become larger with an atomic number.

Unfortunately, rare earth metal oxides also have several problems to be a alternative replacement as the gate insulator. One of them is the positive fixed charge in the rare earth oxides. This charge would make the flat band voltage (V_{FB}) shift to negative side and degrade the mobility owing to Coulomb scattering as explained in former section. This unacceptable problem must be solved in order to replace SiO_2 for sub 100nm CMOS technology.

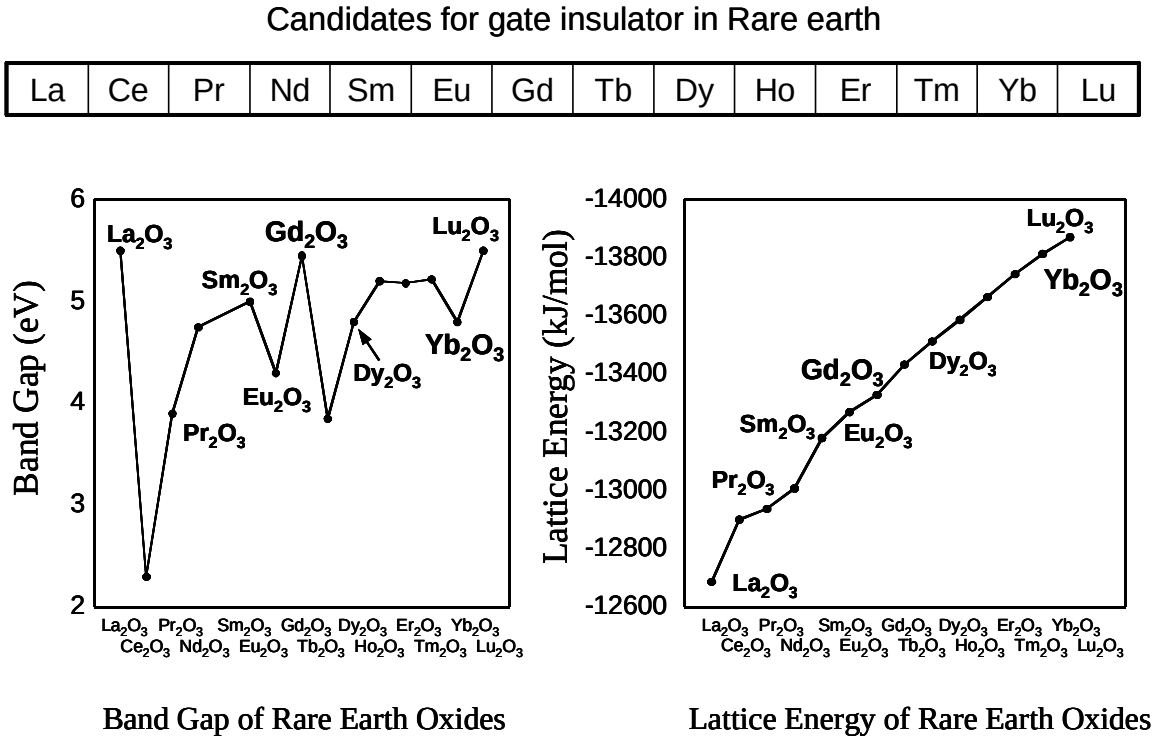

Figure 1-6: Physical Properties of Rare Earth Oxides
(a) Band Gap of Rare Earth Oxide (b) Lattice Energy of Rare Earth Oxides

1.3 Purpose of My Study

It is considered and concerned that one of the serious problems in all of high-k materials is the degradation of mobility. And one of the reasons why using high-k material degrades mobility is the fixed charges in high-k films as explained in former section. The fixed charges, moreover, would make V_{FB} shift and this effect would bring serious problems to electrical characteristics on MOSFET.

Figure 1-7 shows that the C-V characteristics for MIS capacitor with La_2O_3 films fabricated by post deposition annealing (PDA) and as-deposition (no annealing), and I_D-V_D characteristics for MOSFET with La_2O_3 films fabricated by PDA process. From C-V characteristics shown in Figure 1-7 (a), V_{FB} shift toward negative side around -0.7V was observed despite of as-deposition. This result means that formed La_2O_3 thin films contain positive fixed charges in the state of as-deposition. Moreover, although the annealing process has a role as the improvement in electrical characteristics, a huge V_{FB} shift more than 1V toward negative side was observed after PDA process. And it was also confirmed from I_D-V_D characteristics that MOSFET with La_2O_3 thin films fabricated by PDA process has normally-on characteristics resulting from that enormous V_{FB} shift. Normally-on characteristics on MOSFET would prevent from realizing the low power consumption.

From the aforementioned, this thesis focuses on the problem about V_{FB} shift, and will report the results of another way of annealing, post metallization annealing (PMA), and its optimization for rare earth oxides, mainly La_2O_3 thin films for the purpose of the suppression of V_{FB} shift.

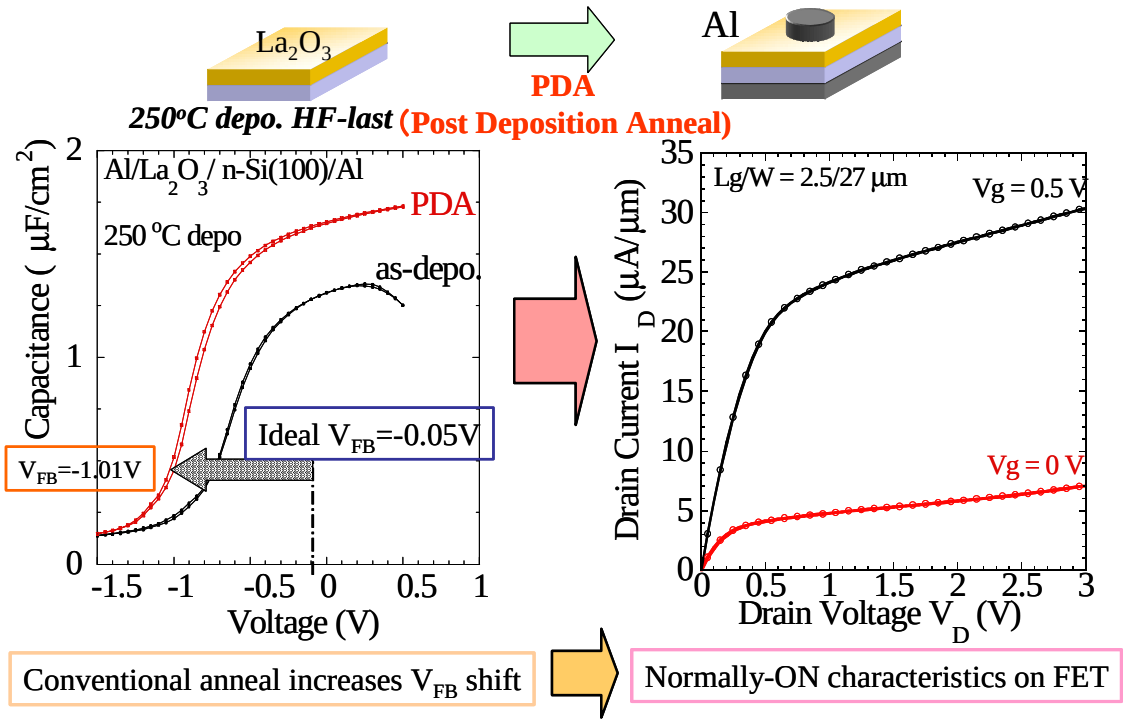

Figure 1-7: (a) C-V characteristics for Al/La_2O_3/n-Si(100)/Al MIS structures fabricated by PDA process

(b) I_D-V_D characteristics for MOSFET with La_2O_3 thin films fabricated by PDA process

Chapter 2

Fabrication And Characterization Methods

2.1 Fabrication Methods

The electrical characteristics of rare earth oxide thin films were evaluated by manufacturing Metal-Insulator-Semiconductor (MIS) capacitor. The fabrication flow of MIS capacitors is shown in Figure 2-1. In this investigation, two type of the annealing method were examined. One is Post Deposition Annealing (PDA) and another is Post Metallization Annealing (PMA). In the pages that follow, each process will be described in detail.

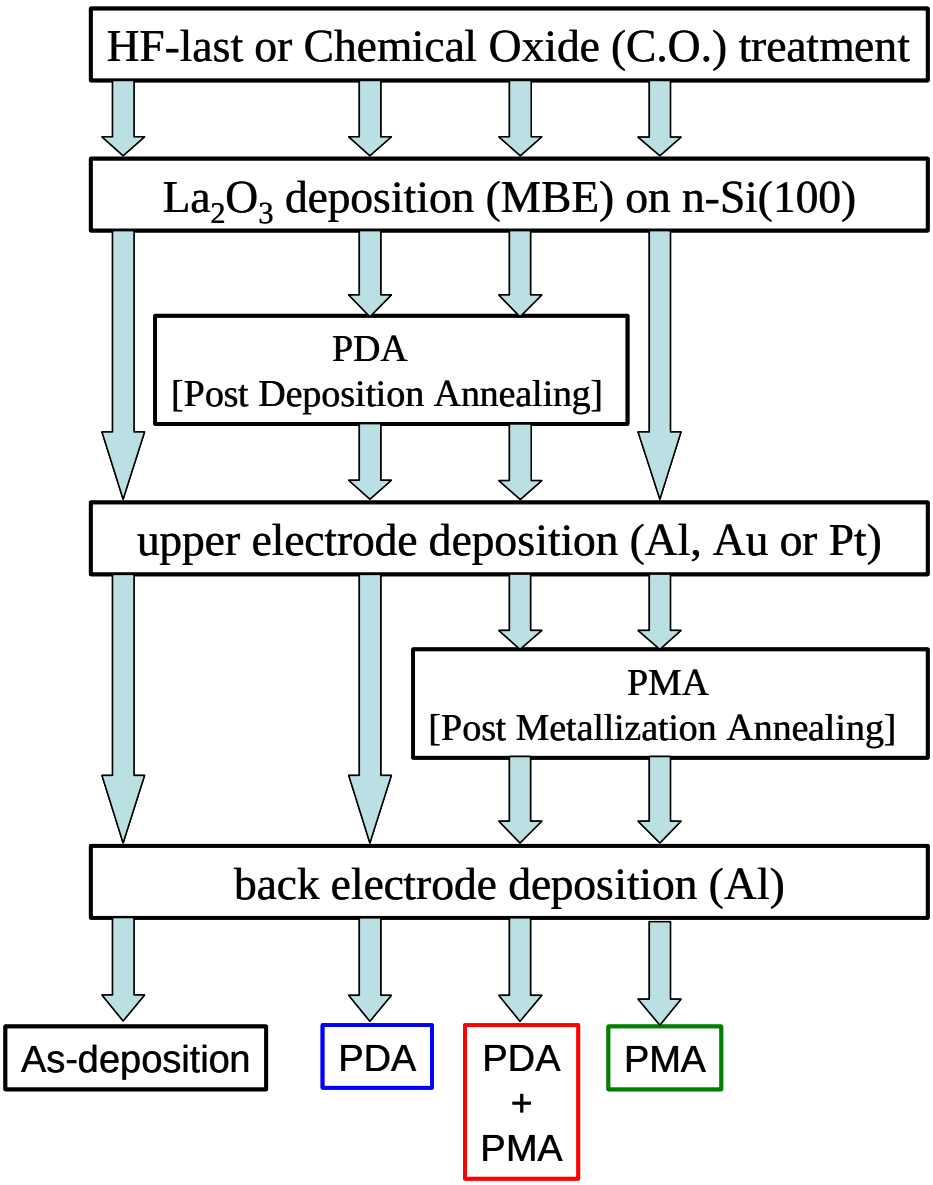

Figure 2-1: Fabrication Flow of MIS capacitors

2.1.1 Wet Cleaning Method of Silicon Substrates

It is well known that semiconductor science is highly sensitive to contaminations or particles. These factors exert exceedingly on electrical characteristics. Therefore, every process should be done with thorough care. On the basis of this fact, DI (de-ionized) water had been used through the cleaning of silicon substrates. DI water highly purified and filtered to remove all of ionic, particulate and bacterial contamination. The theoretical resistivity of pure water at 25°C is 18.25 MΩcm. Ultra-pure water (UPW) systems used in this investigation provided UPW with more than 18.2 MΩcm resistivity.

The substrates were basically cleaned by RCA cleaning process proposed by W. kern et al in 1970. This is the wet cleaning method mainly using H_2O_2 and some chemical liquid. Figure 2-2 shows the steps used in my investigations. Firstly, SPM cleaning was performed in order to remove organic materials and metal contaminations. SPM were made by mixing 96% sulfuric acid (H_2SO_4) and 30% hydrogen peroxide (H_2O_2) and their ratio was H_2SO_4:H_2O_2=4:1. And then, the native and/or chemical oxides were removed by 1% hydrofluoric acid (HF). Finally, the cleaned substrates were dipped in DI water for an instant. The surfaces of substrates result in hydrogen-terminated which are hydrophobic and tolerant of oxidations because Si-H protect oxygen absorption. This cleaning is called HF-last.

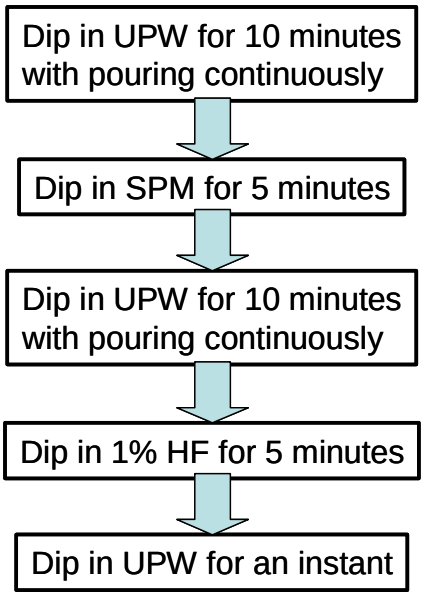

Figure 2-2: Wet cleaning of silicon substrates

2.1.2 Chemical Oxidation Treatment

Chemical oxidation treatment on silicon surface is considered as the fine way to obtain the good surface condition and suppress the leakage current. In order to compare with HF-last and investigate the effects of them, some of substrates were chemically oxidized by the following process as shown in Figure 2-3.

After HF-last treatment, some of substrates were dipped in H_2O_2 and dipped in UPW for an instant.

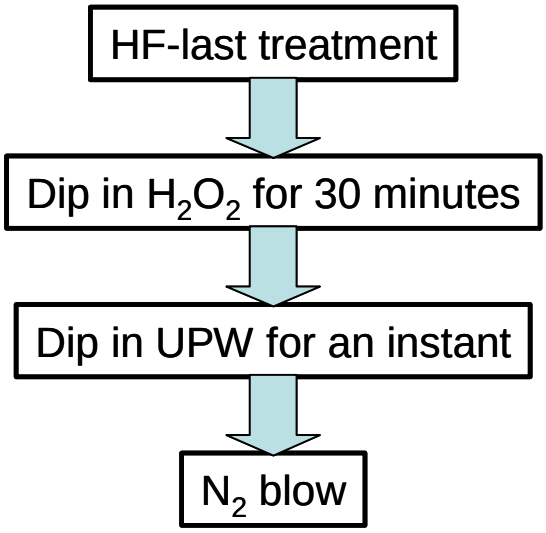

Figure 2-3: Chemical oxidation treatment

2.1.3 Molecular Beam Deposition (MBD) Method

In this investigation, MBD method using molecular beam epitaxy (MBE) equipment is introduced for rare earth oxides deposition. Depositions of rare earth oxides thin films were performed on silicon substrates by using E-beam. The pressure in the MBE chamber during depositions was 10^{-7}~10^{-5} Pa (10^{-9}~10^{-7} Torr). Molecular beam is the only method for the deposition in ultra high vacuum. MBD method has the advantage of the lower contaminations and damage than other method such as sputtering or Chemical Vapor Deposition (CVD). Accordingly, it can be said that MBD method is suitable for research in basic characteristics of thin films.

Figure 2-4 shows the schematic illustration of MBE equipment used in this investigation. There are two vacuum chambers. One is loading chamber where cleaned silicon substrates were loaded and growth chamber. There are four pumps, Turbo-Molecular Pump (TMP) and Rotary Pump (RP) in loading chamber, Titanium Sublimation Pump (TSP) and Ion Pump (IP) in growth chamber. There are also four E-guns and targets, and two power supplies in order to be capable to evaporate two materials in the same time. E-gun acceleration of -5 kV were used in this investigation. The purity of 99.999% La_2O_3 target was used in this investigation. The silicon substrates were rotated during the deposition for the purpose of uniformity of film thickness. The film thickness during deposition was monitored with the Inficon crystal oscillator sensor. In-situ RHEED system was equipped for crystallinity analysis at the silicon surface, and quadrupole gas analyzer was also equipped for the analysis of the gas in the growth chamber. The measurement of this gas detection is based on the mass spectrometry and some peaks are usually observed at 2, 18, 28, 44 of molecule mass. These peaks are considered to indicate H_2, H_2O, N_2 and CO_2. And the intensity ratio was about 50:1:3:1. During the heating Silicon substrates, the intensity of H_2O was slightly higher than that of CO_2 and during deposition, this magnitude relation were reversed.

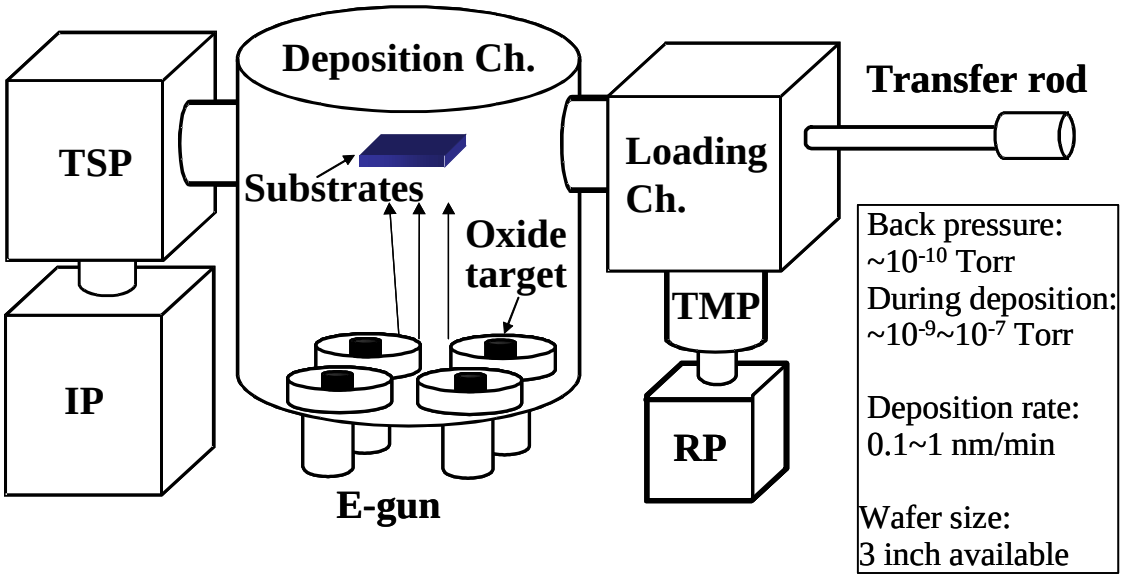

Figure 2-4: The schematic illustration of MBE equipment

2.1.4 Rapid Thermal Annealing (RTA) Method

In order to obtain high quality films, annealing process after deposition is required. The annealing after deposition is considered to bring the suppression of leakage current because of the defects in the films and surface roughness. And this thermal process also exerts an influence on hysteresis and flat band voltage (V_{FB}).

The equipment for annealing used in this investigation was MILA-3000 (ULVAC Co. Ltd). Figure 2-5 shows the schematic illustration of RTA equipment. The annealing was performed by four infrared lamps surrounding the sample stage which were made of carbon and coated by SiC. The heating temperature was controlled by thermocouple feedback. The rate of raising temperature was performed at 400°C per a minute for all samples in my investigation. As the ambience during the annealing, nitrogen, oxygen and forming gas (F/G) in atmospheric pressure were investigated respectively. And in order to remove the atmospheric impurity and improve the purity of the annealing ambience, the displacement of the gas ambience was performed by rotations of two processes, filling up and exhausting mutually five times each annealing as shown in Figure 2-6. Exhausting process was performed by rotary pump vacuuming for 30 seconds at each time. The gas was flowing throughout the annealing with the rate of 1.2 little per minute.

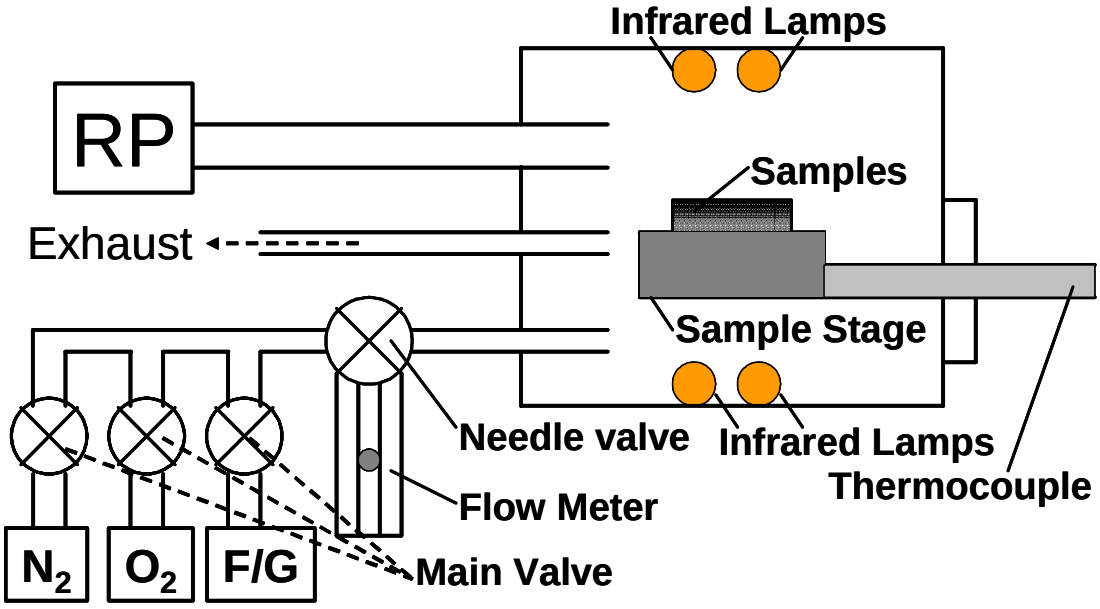

Figure 2-5: RTA equipment

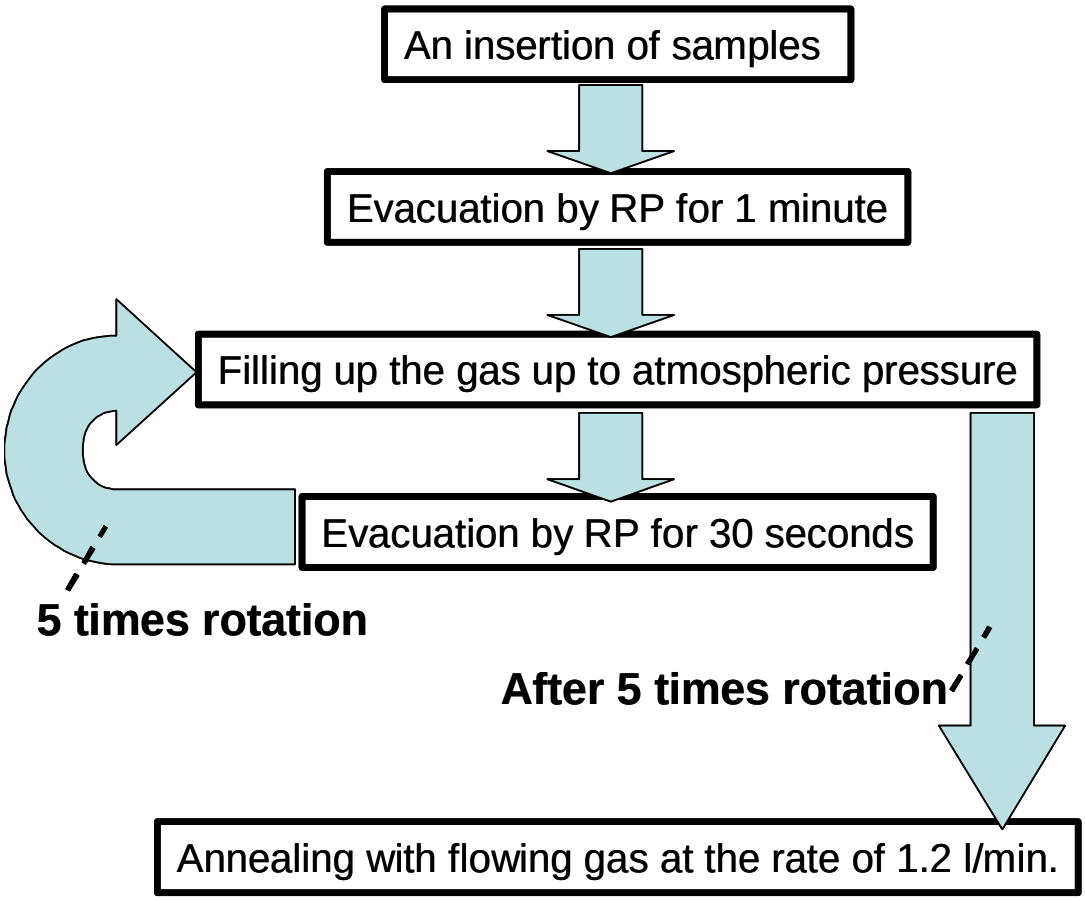

Figure 2-6: The procedure of RTA

2.1.5 Vacuum Evaporation Method

Aluminum, gold and platinum upper electrodes and backside aluminum electrodes were deposited by vacuum evaporation equipment. The advantage of this method is the simplicity and the quickness of evaporation as compared with sputtering.

Figure 2-7 shows the illustration of the vacuum evaporation equipment. In high vacuum chamber approximately 10^{-5} Torr, metal source was deposited on the samples through the metal shadow mask by thermal heating with high voltage regarding to aluminum and gold upper electrodes. In the case the deposition of platinum upper electrodes, E-gun beam was used for evaporation because of its higher melting point. The melting points of aluminum, gold and platinum melting are about 660°C, 1063°C, 1776°C respectively. The size of upper electrodes was about 110 μm in diameter. With regard to backside electrodes, aluminum was deposited without the mask after removing the native oxide on the silicon surface at backside.

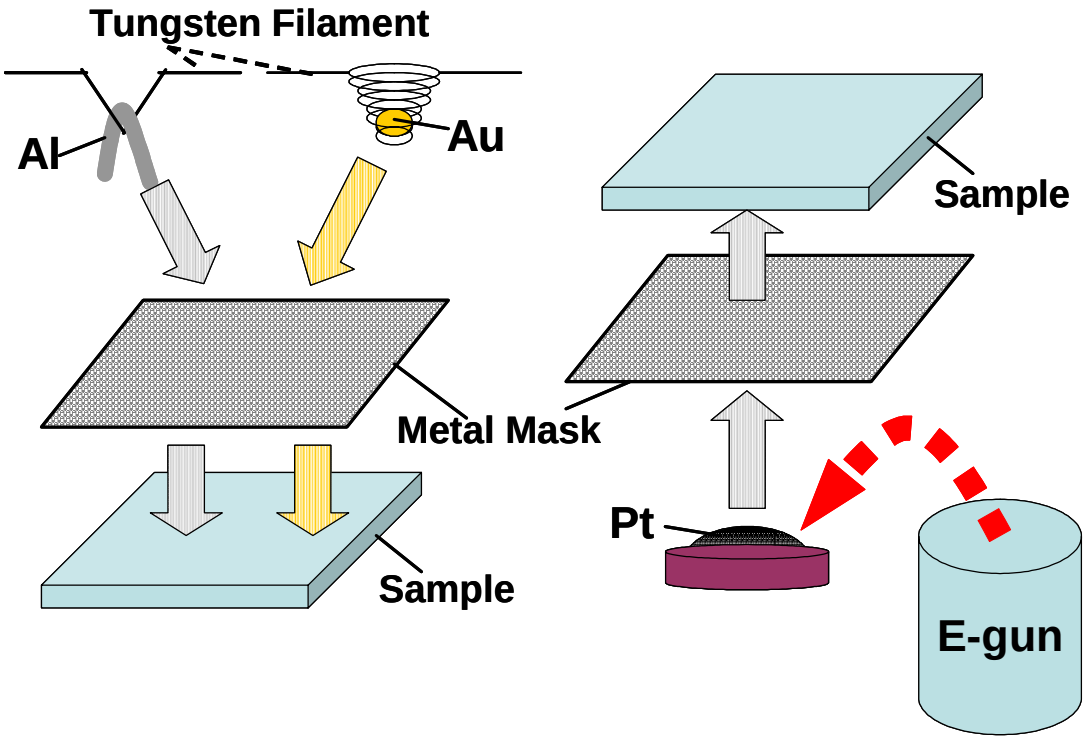

Figure 2-7: Vacuum evaporation method

2.2 Characterization Methods

In this section, the methods for characterization of MIS capacitors will be described in pages that follow.

2.2.1 Capacitance-Voltage (C-V) Characteristics

C-V characteristics were obtained by using Precision LCR Meter (HP 4284A, Agilent) to measure the MIS capacitor's impedance as RC series circuit. The high-frequency from 10 kHz to 1MHz voltage, whose amplitude was 20 mV, was applied on the d.c. voltage for bias.

Figure 2-8 shows the ideal high-frequency C-V characteristics of n-type Si MIS capacitor. The ideal equivalent circuit is composed of a series capacitance of insulator component, $C_{insulator}$ and silicon surface component, C_s. When positive bias is applied to the metal side, it is called accumulation region. There is no current flow in the structure in the case of an ideal MIS capacitor. Therefore, voltage causes band bending at silicon surface and accumulation of majority carriers (electrons). This is the reason that this case is called accumulation. Total capacitance in unit area of C is independent on applied voltage and given by

$$C = C_{insulator} = \frac{\varepsilon_0 \varepsilon_r}{t}, \qquad (2.1)$$

where ε_0 and ε_r are vacuum and relative dielectric constant, respectively and t is the thickness of the insulator. The value of vacuum dielectric constant is about 8.85×10^{-14} [F/cm]. C decreases near zero bias because broadening of accumulation charge causes series capacitance.

When zero bias is applied and surface potential is zero, MIS capacitor is in flat band condition. Silicon surface capacitance of C_s is not zero and given by

$$C_{sfb} = q\sqrt{\frac{\varepsilon_0 \varepsilon_r N_d}{kT}}, \qquad (2.2)$$

where $q = 1.6\times10^{-19} C$ is the electronic charge, $k = 1.38\times10^{-23} J/K$ is Boltzmann's constant, T is the absolute temperature and N_d is the density of ionized donors. From these equations, flat band capacitance of C_{fb} is obtained as following equation,

$$\frac{1}{C_{fb}} = \frac{1}{C_{insulator}} + \frac{1}{C_{sfb}} = \frac{t}{\varepsilon_0 \varepsilon_r} + \frac{1}{q}\sqrt{\frac{kT}{\varepsilon_0 \varepsilon_r N_d}} \,. \qquad (2.3)$$

When a small negative voltage is applied, surface band bend upward and apart from Felmi level. This is the state of depletion because majority carriers are depleted at the silicon surface. C keeps decreasing because depletion region act as a dielectric in series with the insulator.

When a larger negative voltage is applied, the bands bend even more upward such that the intrinsic level at the surface crosses over the Felmi level. At this point, the number of holes (minority carriers) at surface is larger than that of holes, in other words, surface is inverted. Consequently, this state is called inversion. The total capacitance gets to a minimum because of following two reasons. Firstly, the recombination and generation rates of holes can not catch up with higher frequency signals. From empirical knowledge, it is possible for Metal-SiO_2-Si MOS capacitor to increase total capacitance up to the insulator capacitance again at the low frequency between 5 and 100 Hz. Secondly, once strong inversion occurs, the depletion layer width reaches a maximum because the semiconductor is effectively shielded by further penetration of electric field by the inversion layer. Accordingly, the maximum width, W_m, of the surface depletion region can be obtained as following equation,

$$W_{dm} = \sqrt{\frac{4\varepsilon_o \varepsilon_r kT \ln(N_a / n_i)}{q^2 N_d}} \,, \qquad (2.4)$$

where n_i is intrinsic doping concentration. And the corresponding total capacitance is given by

$$C_{\min} = \frac{\varepsilon_o \varepsilon_r}{t} = \frac{\varepsilon_o \varepsilon_r}{W_m} \,. \qquad (2.5)$$

In fact, flat band voltage, V_{FB}, is not zero because there is the difference of work function between metal and semiconductor.

In a practical MOS capacitor, interface traps and oxide charges exist and these affect the ideal MOS characteristics. The influence of these charges in the SiO_2 and at SiO_2/Si interface has been investigated extensively. It has not been understood at present if these theories can apply to high-k films. Here, only two type of factors, charges and traps is considered now. Charges in the dielectrics are called the fixed charge Q_f, and it can not be

charged or discharged over a wide variation of applied gate voltage. The fixed charge density Q_f is located near the high-k/Si interface and its origin is considered as excess silicon (trivalent silicon) or a loss of electrons from excess oxygen centers (non-bridging oxygen) near the high-k/Si interface. This positive Q_f causes the C-V curve to shift toward negative side from the ideal C-V curve for both n-type and p-type substrates. The magnitude of the shift is generally evaluated by the difference between experimental V_{FB} and ideal V_{FB}.

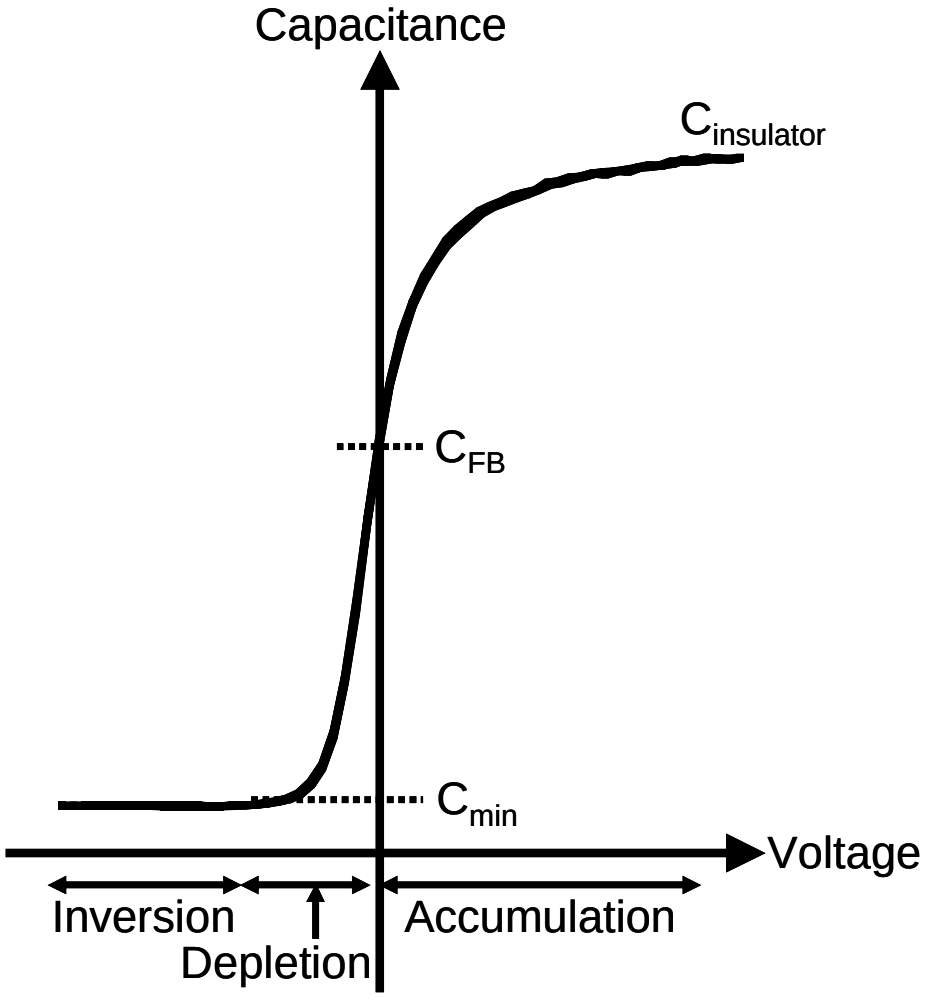

Figure 2-8: The ideal high-frequency C-V curve of n-type Si MIS capacitor.

In C-V curve, the two type of hysteresis exists in dependence on its direction. One is the charge injection type, and another is mobile ion type as shown in Figure 2-9 and 2-10 respecticely. Verifying the type of hysteresis is greatly important to understand the conditions of films.

At a Silicon surface, there are some located states of energy in the forbidden energy gap of silicon because the lattice of bulk silicon and all the properties associated with its periodicity result in a termination. These interface states capture some charges when the surface potential bend upward in the case of n-type silicon, and these interface states are located under the Felmi level. The amount of trapped charges is consequently varied by the applied voltage. The C-V curve, hence, does not shift to parallel direction compared to the ideal C-V curve. Trapped charges depend on the measured frequency because these trapping or releasing can not follow the ac voltage swing. These trapped charges affect not only C-V characteristics, but also MISFET characteristics. Surface states reduce the conduction current in MISFET. Furthermore, the trapped electrons and holes located at the interface can act as charged scattering centers for the mobile carriers in a surface channel, and thus that could lead lower mobility. Interface states can also act as localized generation-recombination centers. These could lead to generation-recombination leakage currents and affect the dielectric reliability.

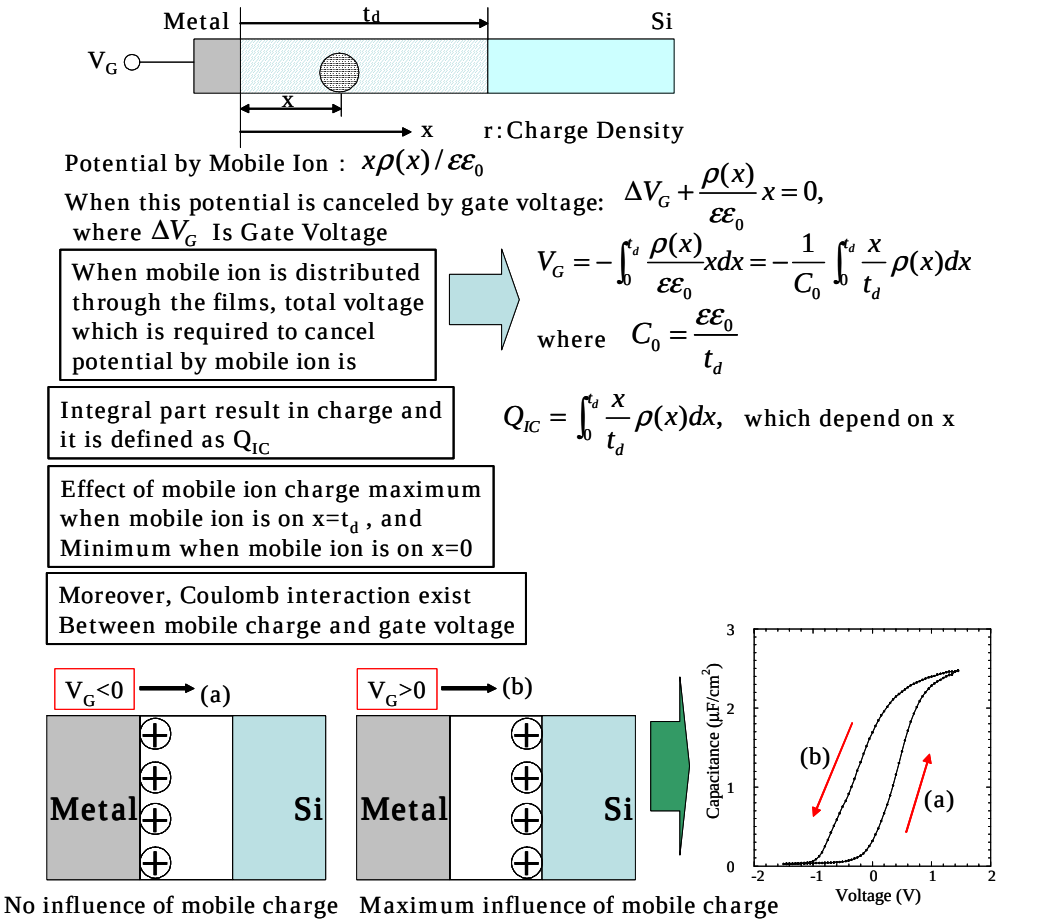

Figure 2-9: The mechanism of mobile-ion-type hysteresis

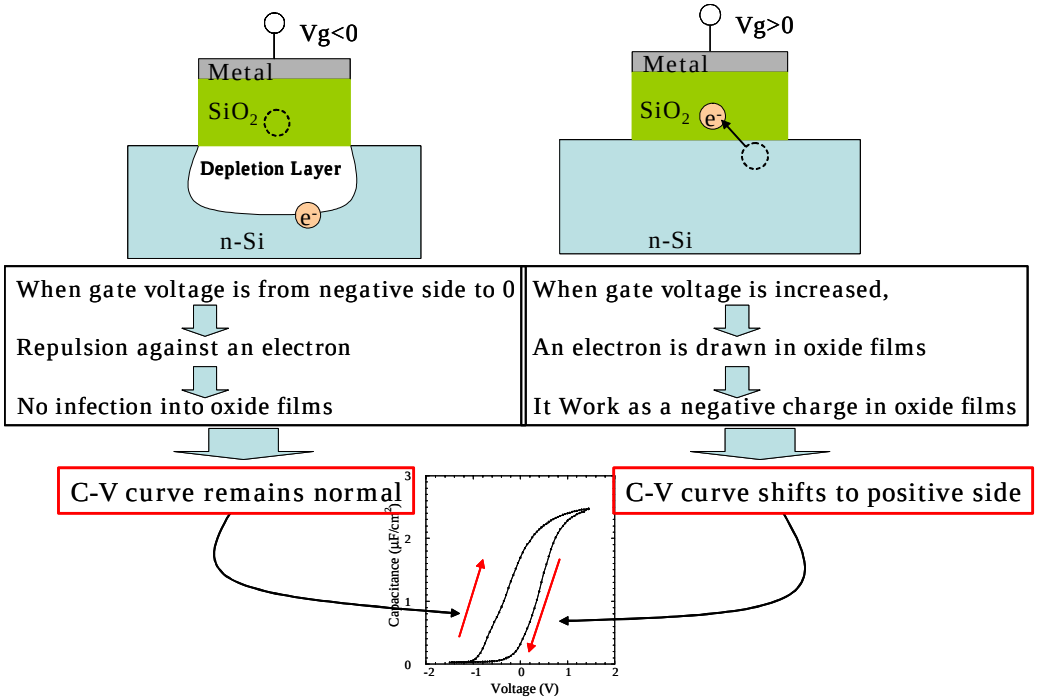

Figure 2-10: The mechanism of charge-injection-type hysteresis

2.2.2 Leakage Current Density-Voltage (J-V) Characteristics

J-V characteristics for MIS capacitor were measured by Precision Semiconductor Parameter Analyzer (HP4156C, Agilent). In the case of ideal MIS capacitor, the conductance of the insulator is supposed to be zero. In fact, however, practical insulators show the carrier conduction by electrons and holes when the electric field or temperature is sufficiently high. The two types of conduction models will be described here.

Firstly, Poole-Frenkel model is due to field-enhanced thermal excitation of trapped electrons into the conduction band as shown in Figure 2-11. This is called trap-assist conduction. The expression of Poole-Frenkel emission is given by

$$J = J_o \exp\left\{\frac{q\left(\beta_{PF}\sqrt{E} - \Phi_{PF}\right)}{kT}\right\}, \qquad (2.6)$$

where $J_0 (J_0 \sim E)$ is the low-field current density, Φ_{PF} is the barrier height for Poole-Frenkel mechanism and β_{PF} field lowering coefficients are given by

$$\beta_{PF} = \sqrt{\frac{q^3}{\pi\varepsilon_0\varepsilon_r}} \qquad (2.7)$$

A plot of ln(J/E) versus $E^{1/2}$ yields a straight line with a slope determined by dielectric constant of the insulator and the plot segment contains the information of the barrier height as trapped charge in the insulator. This conduction process also has temperature dependence and J versus 1/T also yields a straight line.

Secondly, Fowler-Nordheim model is one of the tunneling emissions caused by the tunneling of trapped electrons into the insulator conduction band as shown in Figure 2-12. The expression is given by

$$J_{FN} = \frac{q^3 {E_{ox}}^2}{16\pi^2\hbar\Phi_{FN}} \exp\left(-\frac{4\sqrt{2m^*}{\Phi_{FN}}^{3/2}}{3\hbar q E_{ox}}\right), \qquad (2.8)$$

where E_{ox} is the electric field in the insulator and Φ_{FN} is the barrier height for Fowler-Nordheim mechanism. Equation (2.8) shows that Fowler-Nordheim tunneling current is characterized by a straight line in a

plot of $\ln(J/E_{ox}^{2})$ versus $1/E_{ox}$. The Fowler-Nordheim tunneling emission has the strongest dependence on the applied voltage but is essentially independent on the temperature. These plots and/or temperature dependence thus decide the carrier transport type.

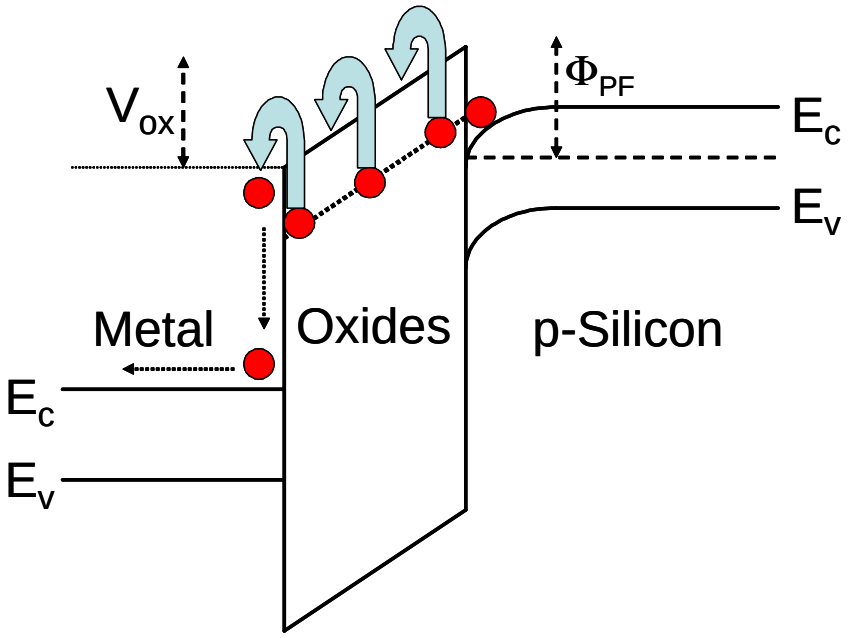

Figure 2-11: Poole-Frenkel mechanism

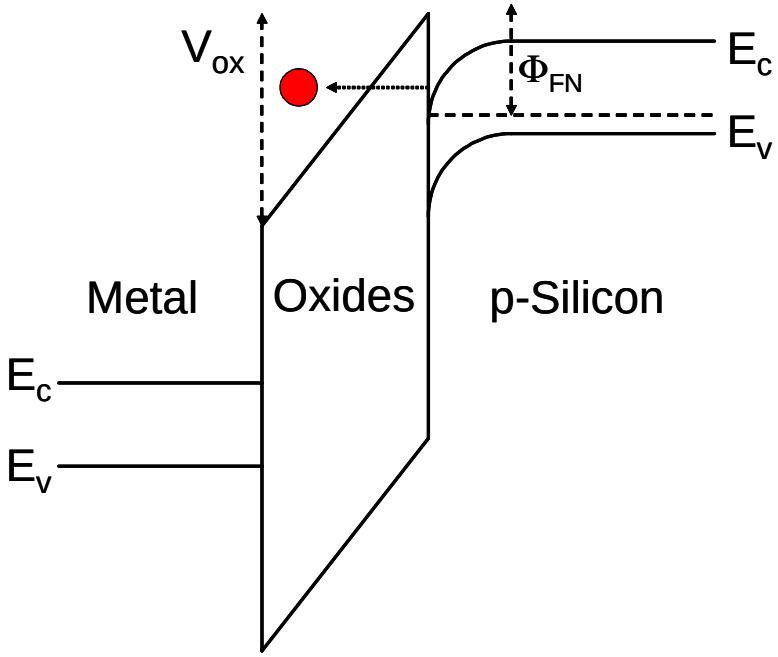

Figure 2-12: Fowler-Nordheim mechanism

2.2.3 Ellipsometry Method

Ellipsometry method was utilized for estimating the thickness of the deposited rare earth film. The principle of ellipsometry method is to make use of the difference of polarization before and after reflection. Figure 2-13 shows the plane-polarized light incident on a plane surface. The incident polarized light can be resolved into a component p, parallel to the plane of incidence and a component s, perpendicular to the plane of incidence. The light propagates as a fluctuation in electric and magnetic fields at right angles to the direction of propagation. The reflection coefficients

$$R_P = \frac{E_P(reflected)}{E_P(incident)} \qquad (2.9)$$

$$R_S = \frac{E_S(reflected)}{E_S(incident)} \qquad (2.10)$$

are not separately measurable. However, the complex reflection ratio ρ defined in terms of the reflection coefficients R_P and R_S or ellipsometric angles ψ and Δ,

$$\rho = \frac{R_P}{R_S} = \tan(\psi)e^{j\Delta} \qquad (2.11)$$

is measurable. Then, ψ and Δ are called ellipso parameter.

For the air (n_0)-thin film (n_1)-substrate (n_2-jk_2) system, where n_x is the index of refraction and k_x is the index of extinction coefficient. In the case of silicon substrate, n_2 and k_2 are known, then n_1 and film thickness can be calculated from the result of ψ and Δ measurement.

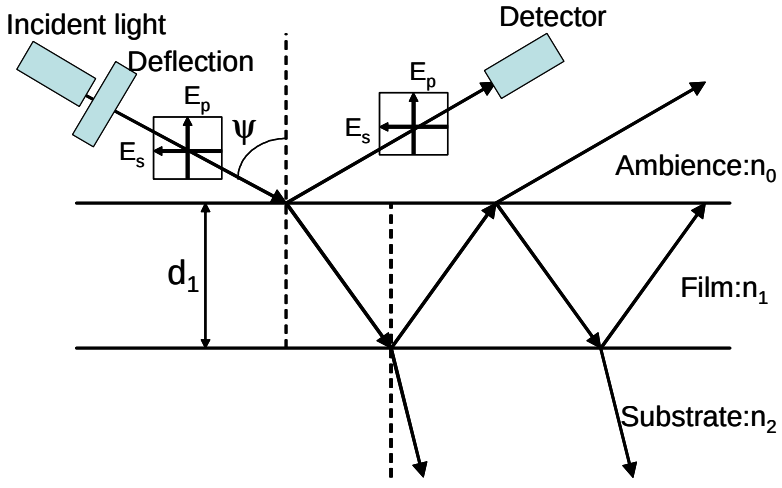

Figure 2-13 Principle of ellipsometry method

Chapter 3

Experimental Results

3.1 Introduction

In this chapter, the results of post metallization annealing (PMA) for lanthanum oxides (La_2O_3) with several upper metal electrodes for the purpose of the suppression of V_{FB} shift will be reported. As upper metal electrodes, aluminum, gold and platinum were investigated.

3.2 Experimental Procedure

Figure 3-1 shows experimental procedure for MIS capacitors. Rare earth metal oxides were deposited on n-Si(100) substrates by ultra high vacuum e-beam deposition method. The pressure in the MBE chamber during depositions was 10^{-7} – 10^{-5} Pa (10^{-9} – 10^{-7} Torr). E-beam deposition method has some advantages compared to conventional CVD or sputtering in terms of purity and damage in the deposited films, respectively.

Chemically cleaned N-type silicon (100) substrates were immediately loaded into the chamber. In this study, two surface pretreatments were investigated. One is HF-last treatment and another is chemical oxidations, which are explained in chapter 2 respectively.

Amorphous La_2O_3 thin films were deposited on silicon substrate by MBE system at 250^{o}C. The deposition rates of the films were 0.1-1.0 nm/min.

Some of the samples were annealed in N_2, O_2 or forming gas ambience from 0 second (spike) to 100 minutes by RTA (Rapid Thermal Annealing) system, before upper metal electrodes deposition. This annealing is named as post deposition annealing (PDA).

Upper electrodes were deposited through a metal hard mask. Some of the PDA samples and the other samples were annealed after the upper electrodes deposition. This annealing is named as post metallization annealing (PMA). In this study, aluminum, gold and platinum were investigated as upper metal electrodes for PMA.

Finally, back side Al electrodes were deposited for all the samples.

The ratio of rising annealing temperature was investigated in the case of 75^{o}C/minute and 400^{o}C/minute about aluminum upper electrodes, and gold and platinum were investigated at annealing ratio of 400^{o}C/minute.

Annealing temperature from 200°C to 450°C was investigated with regard to aluminum upper electrodes, from 300°C to 450°C was investigated with regard to gold upper electrodes and from 300°C to 600°C was investigated in regard with platinum upper electrodes respectively.

These fabricated MIS capacitors were characterized by C-V and J-V.

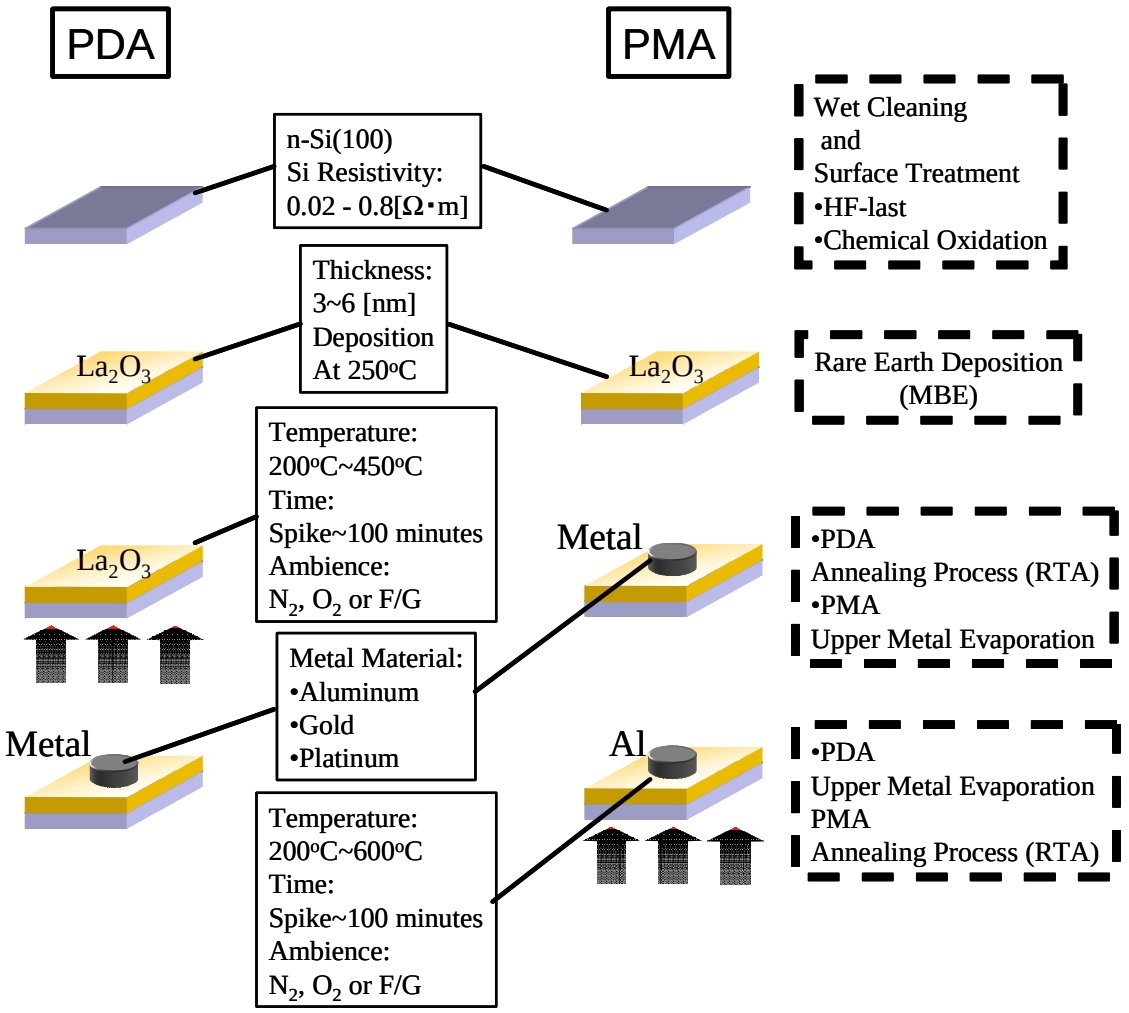

Figure 3-1: The Fabrication Process for MIS Capacitors

3.3 Electrical Characteristics in the case of PDA

Before the examinations of PMA, investigating the effects of PDA must be done beforehand. The following is the results of PDA.

3.3.1 Dependence on the Temperature of PDA

Figure 3-2 shows the C-V characteristics dependent on the temperature of PDA for La_2O_3 thin films. The surface treatment was HF-last and the annealing temperatures from 300°C to 450°C were examined respectively, and all of them were annealed for 10 minutes in nitrogen ambience and measured at 1 MHz.

The hysteresis was not observed both as-deposited samples and PDA samples. That means La_2O_3 films have good properties without mobile charges like K^+ or Na^+ ion and with few charge traps at the state of as-deposition. Moreover, it should be noted that the capacitance value increased with increase in the annealing temperature. This phenomenon suggests two effects. One of them is that La_2O_3 films were densified by the higher temperature annealing and their quality improved significantly. Another one is that high purity nitrogen ambient suppressed the growth of interfacial layer. On the other hand, however, it was found that the value of V_{FB} shift increased with increase in the annealing temperature.

Figure 3-3 shows the J-V characteristics dependence on the temperature of PDA for La_2O_3 thin films. The annealing temperatures from 300°C to 450°C were examined respectively. It was also found that leakage current decreased with increase in the annealing temperature. This result suggests that the higher temperature post deposition annealing decreased the defects in La_2O_3 films.

Figure 3-4 shows the frequency dependence on C-V characteristics of an as-deposited sample and PDA samples annealed at 300°C, 400°C and 450°C respectively. Ranges of frequency form 10 kHz to 1 MHz were measured. It was observed that the fluctuations of measuring value were almost completely suppressed by PDA at 450°C.

From the above mentioned, it can be concluded that post deposition annealing improved the electrical characteristics such as the capacitance value, leakage current, frequency dependence except for V_{FB} shift toward negative side.

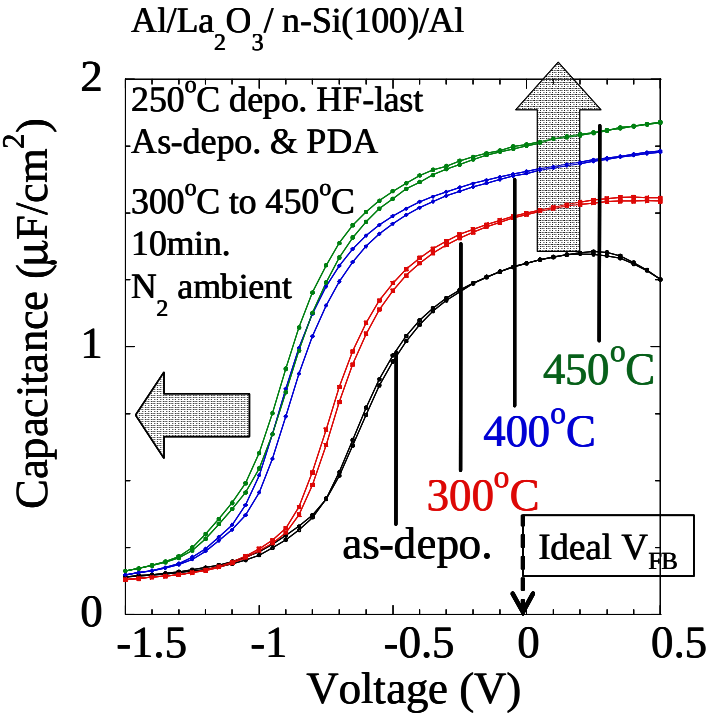

Figure 3-2: C-V characteristics dependent on temperature of PDA process

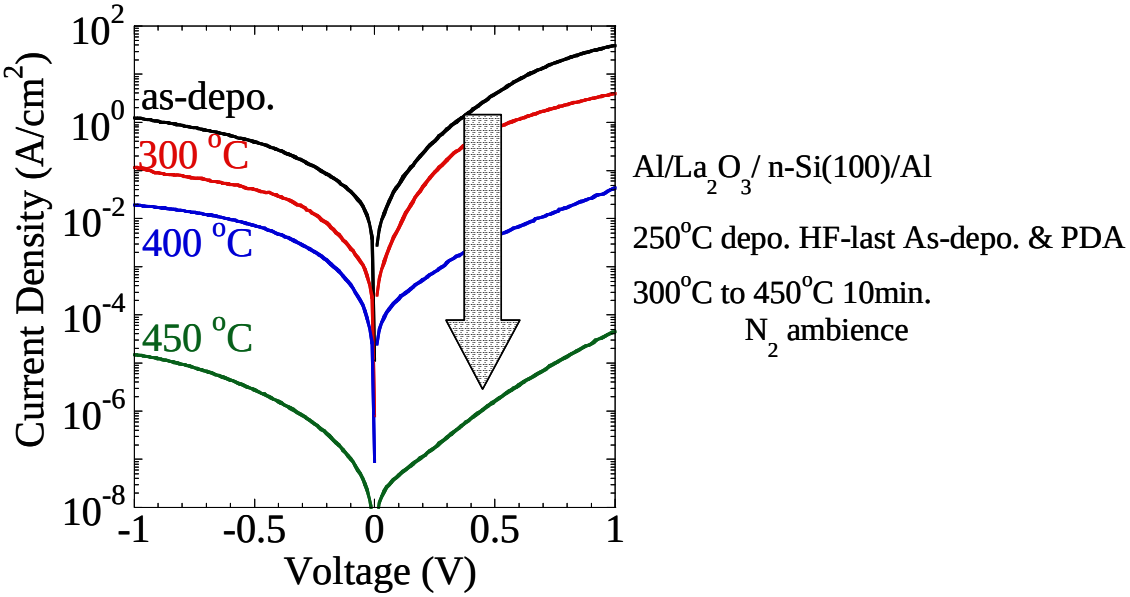

Figure 3-3: J-V characteristics dependent on temperature of PDA process

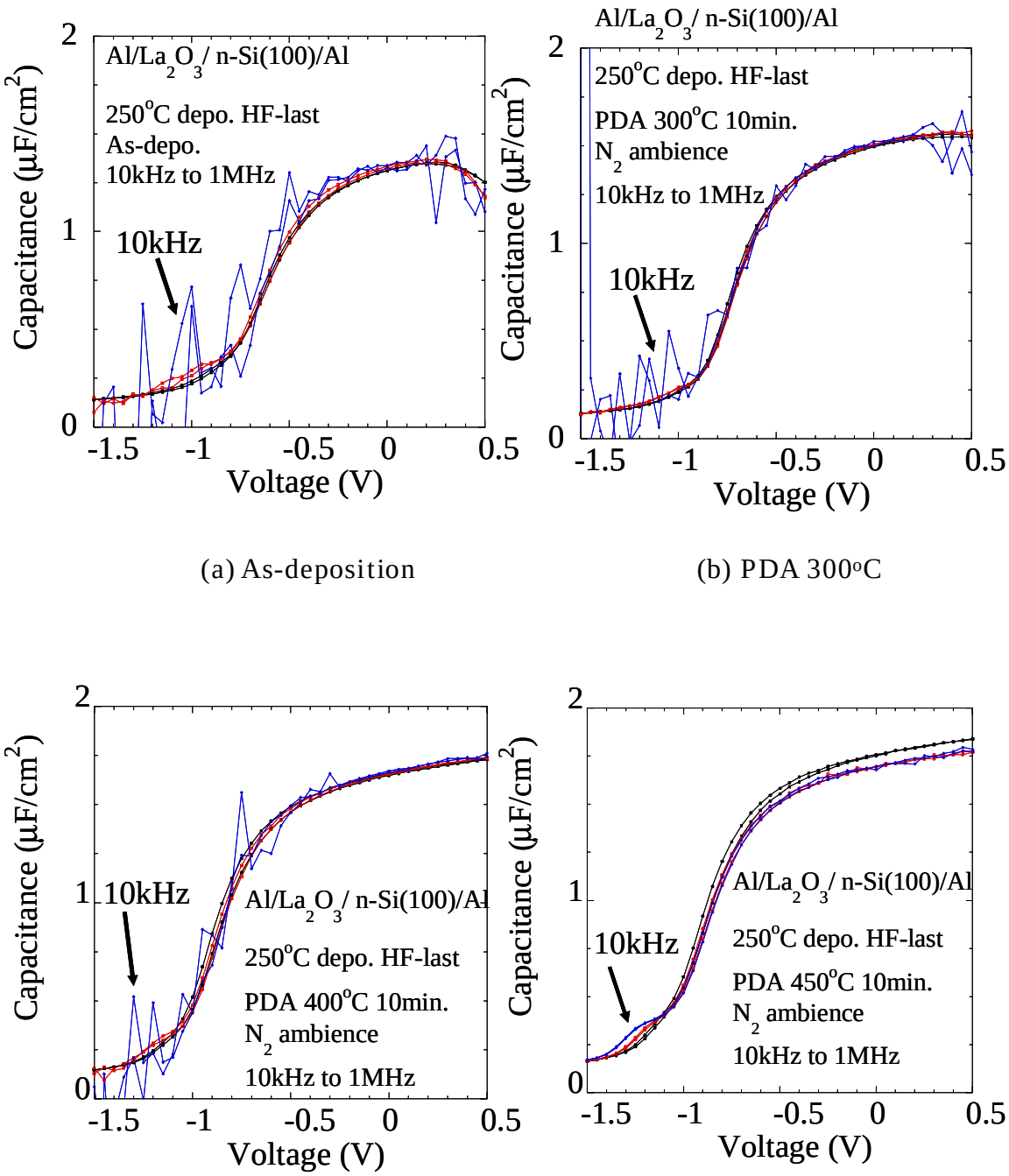

Figure 3-4: C-V characteristics of PDA samples with frequency dependence
(a) As-deposition (b) PDA 300°C
(c) PDA 400°C (d) PDA 450°C

Figure 3-5 shows the plots of EOT dependent on annealing temperature of PDA. It was observed that EOT decreased proportionally as the increase of annealing temperature. Moreover, leakage current also decreased with decrease in EOT as shown in Figure 3-6. These magnificent results demonstrate not only the improvement in quality of films by PDA, but also the latent faculties of La_2O_3 as high-k gate dielectrics.

Figure 3-7 shows the plots of V_{FB} shift dependent on the annealing temperature of PDA. Unfortunately, the value of V_{FB} shift increased abruptly from 300°C to 400°C of PDA and it seems quite difficult to recover the flat band voltage shift toward negative side by PDA. Figure 3-8 shows EOT versus V_{FB} shift plots. Although it is desirable to approach toward the lower right side in this graph, experimental plots were headed for the lower left side. This phenomenon indicates that there is trade-off relationship between EOT and V_{FB} shift, and that also means that it is so difficult to combine lower EOT and V_{FB} shift by only PDA process.

The dependence on the rising ratio, 75°C/minute and 400°C/minute, of PDA was examined. It was confirmed that in the case of PDA, there is almost no dependence on rising ratio as shown in Figure 3-9

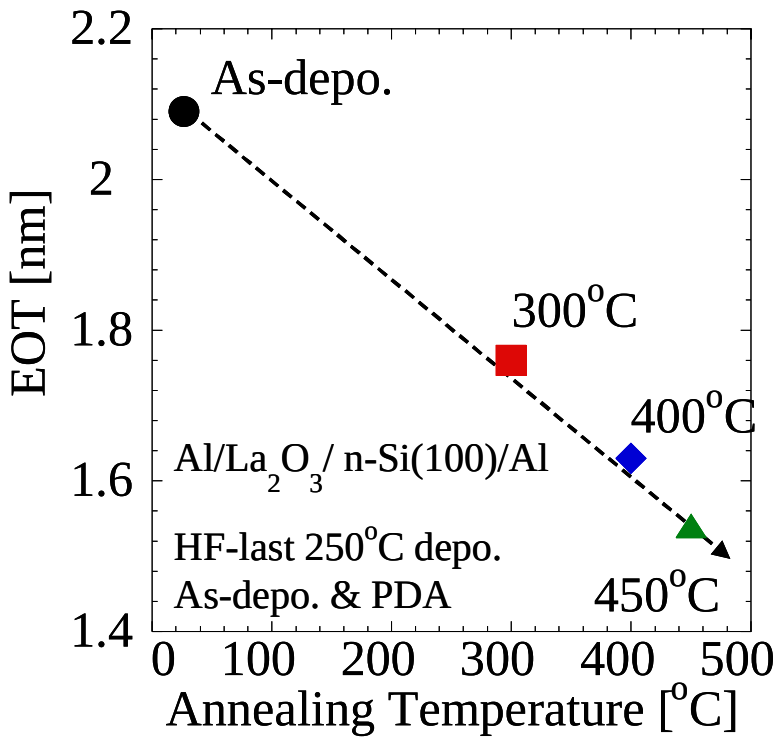

Figure 3-5: EOT plots dependent on annealing temperature.

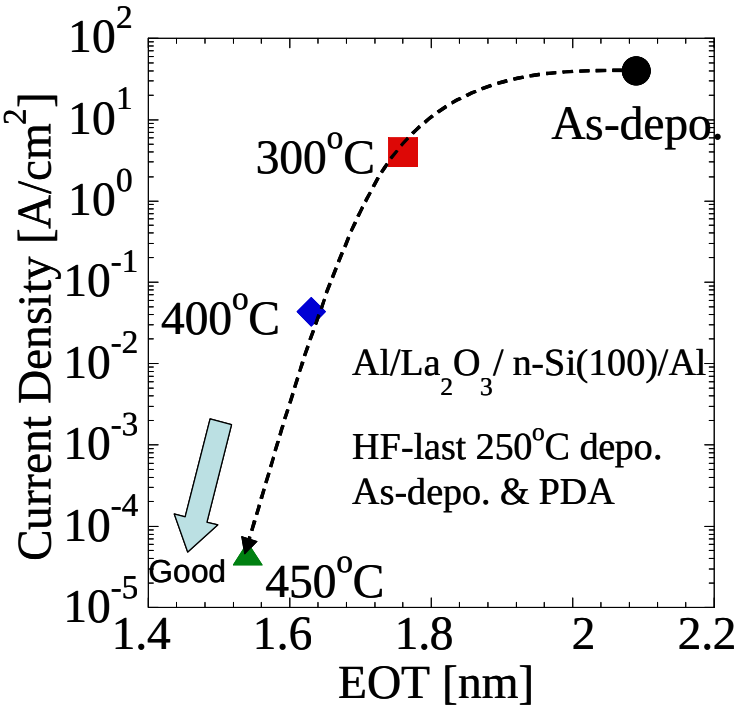

Figure 3-6: EOT – Leakage current density plots

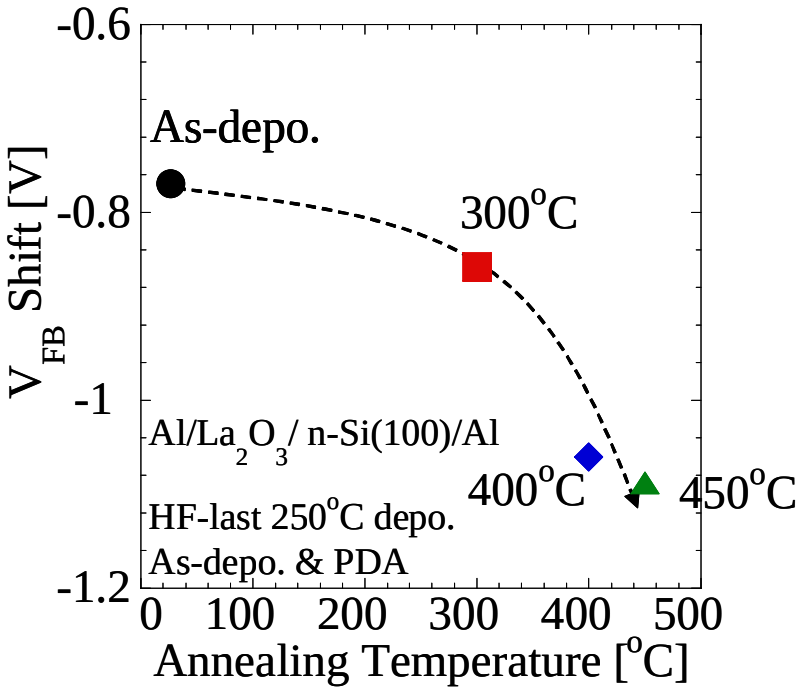

Figure 3-7: The value of V_{FB} shift dependent on annealing temperature.

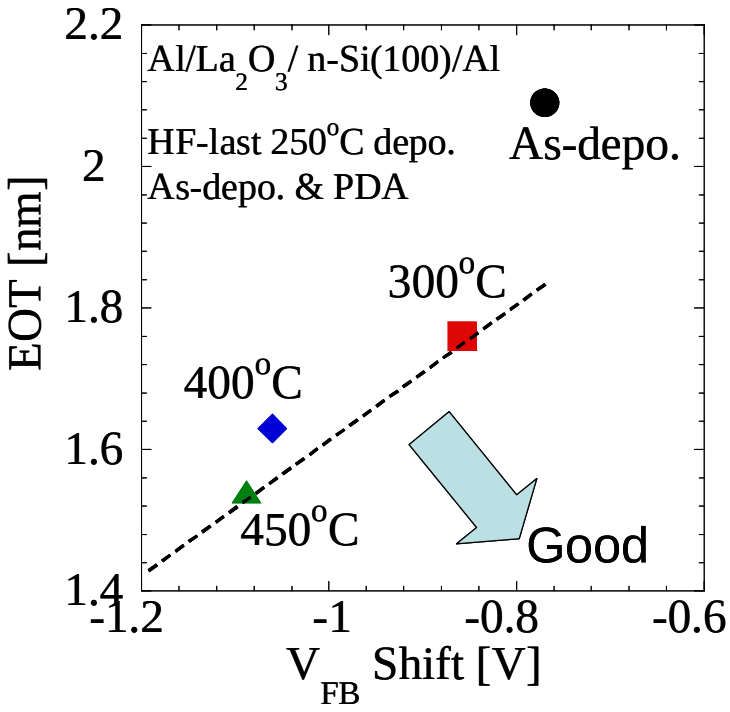

Figure 3-8: V_{FB} shift – EOT Plots

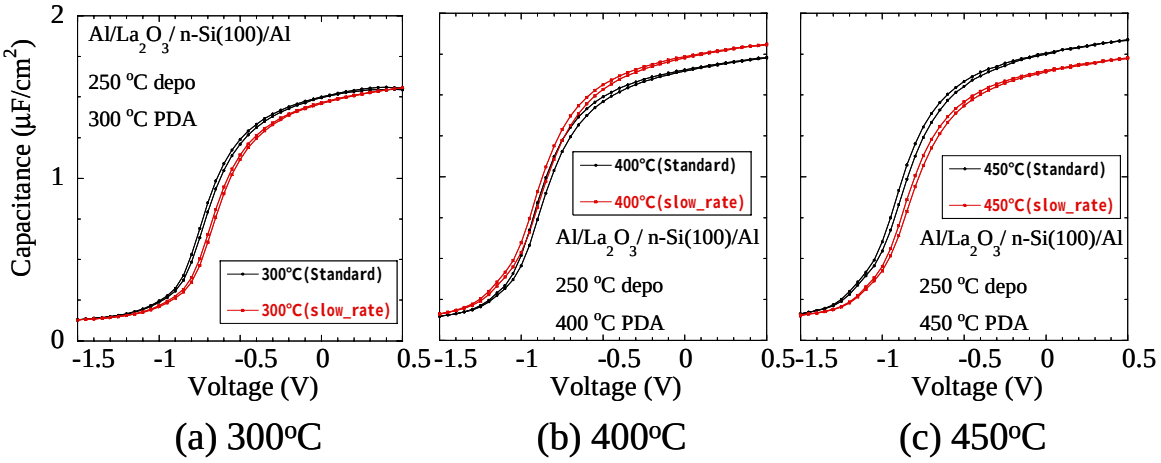

Figure 3-9: The C-V characteristics Dependent on the rising ratio of PMA at (a) 300°C (b) 400°C (c) 450°C

3.3.2 Effects of Chemical Oxidation Treatment for PDA

It is anticipated that Chemical oxidation treatment would bring the better characteristics in many ways because SiO_2 is magnificently stable at higher temperature, and also have larger band gap and good matching with silicon surface, which is the most important part in terms of electrical characteristics. Some excellent results have already been reported by using chemical oxidation. On the basis of the facts, the effect of chemical oxidation treatment for La_2O_3 thin film was examined.

Figure 3-10 shows the comparison of C-V characteristics between HF-last treatment and chemical oxidation treatment. It is observed that the capacitance value of the samples treated by chemical oxidation was maintained on a level with the samples treated by HF-last although extra layer having lower dielectric constant was inserted. Two reasons can be assumed for this phenomenon. One is owing to a formation of the good silicate layer. It is conceivable that La_2O_3 reacted with chemically formed SiO_2 through thermal process and this reaction would create the good silicate layer. Another one is a formation of thinner layer. Although these samples were fabricated by same deposition, there is a possibility that they have different thickness. The samples treated by HF-last were deposited on silicon substrates. On the other hand, however, the samples treated by chemical oxidation were deposited on SiO_2. The deposition rate might change on what La_2O_3 films were deposited.

Figure 3-11 shows the comparison of J-V characteristics between HF-last treatment and chemical oxidation treatment. It is confirmed that chemical oxidation treatment suppressed the leakage current about 2 orders of magnitude at +1 V as compared with HF-last treatment. Therefore, it seems proper that chemical oxidation treatment brought a formation of the good silicate layer and that led to the suppression of the leakage current with maintaining the capacitance value. From these results, It can be said that chemical oxidation treatment was quite effective for La_2O_3 thin films.

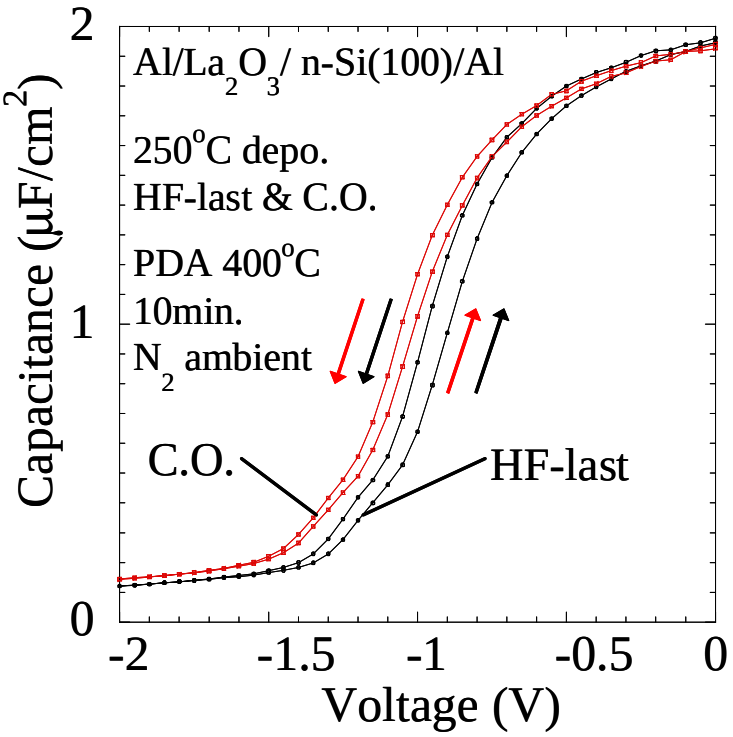

Figure 3-10: The comparison of C-V characteristics between HF-last treatment and chemical oxidation treatment

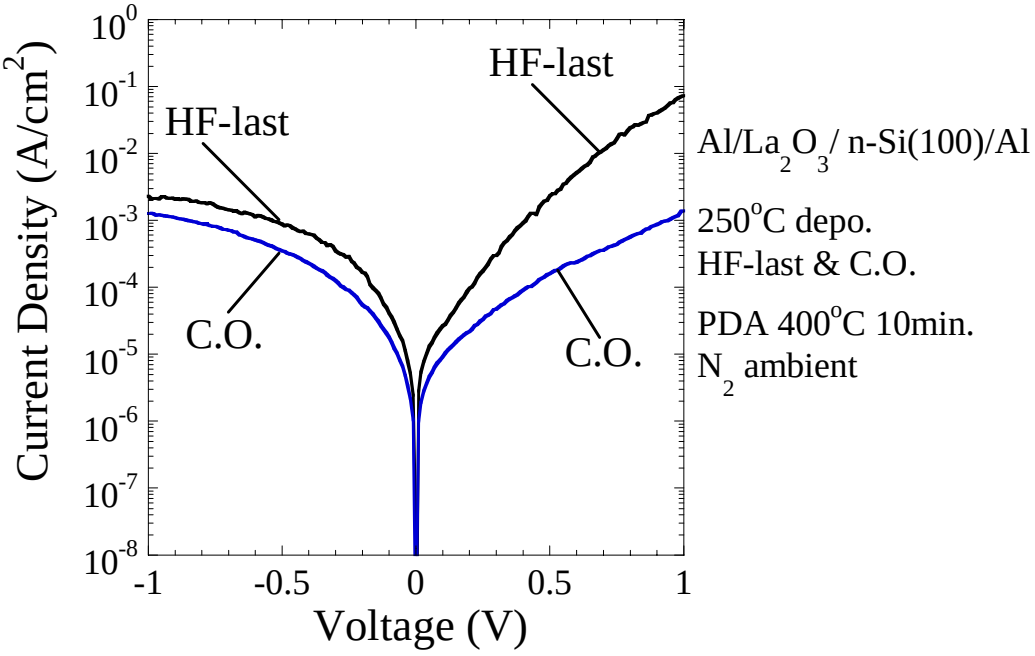

Figure 3-11: The comparison of J-V characteristics between HF-last treatment and chemical oxidation treatment

3.3.3 Dependence on the Annealing Time of PDA

The C-V characteristics dependent on annealing time was examined. It was confirmed that the longer time PDA still made the V_{FB} shifted to negative side although the capacitance values almost did not change as shown in Figure 3-12 and Figure 3-13.

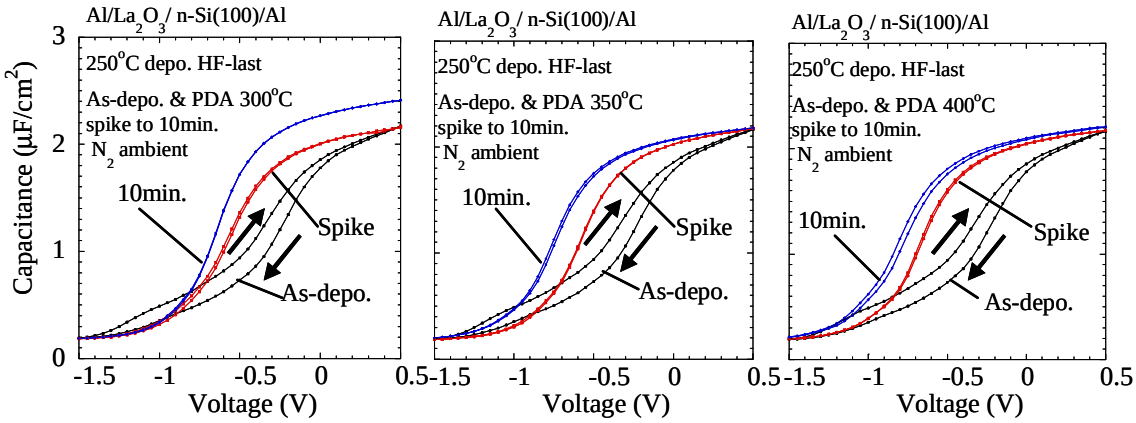

(a) PDA 300°C (b) PDA 350°C (c) PDA 400°C

Figure 3-12: The dependence of V_{FB} shift on the annealing time of (a) PDA 300°C (b) PDA 350°C (c) PDA 400°C

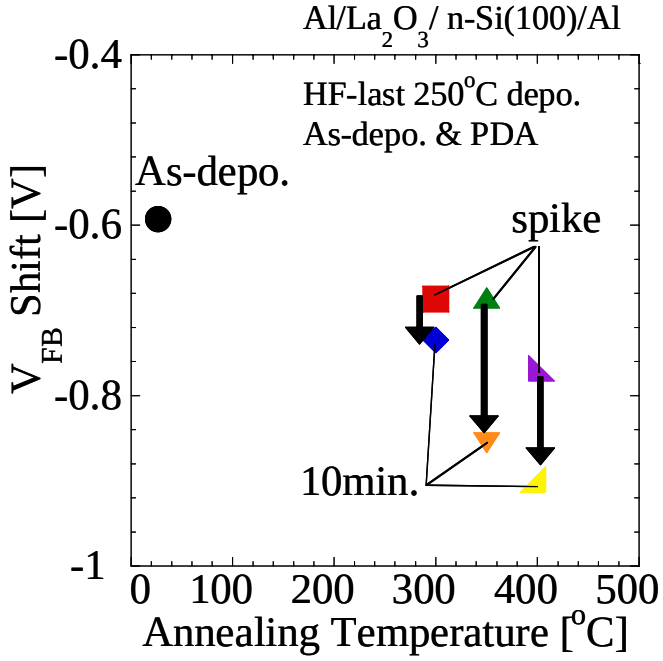

Figure 3-13: V_{FB} shift plots dependent on the PDA time.

3.3.4 Dependence on the Ambience of PDA

Finally, the dependence on the ambience of PDA was examined. Since films are exposed in the atmosphere during annealing, the influence of the atmosphere for PDA should be higher than one for PMA if there is some reaction between the ambience and films.

Figure 3-14 shows the comparison of PDA between annealing in nitrogen and oxygen ambience. It was confirmed that there was not any difference between nitrogen and oxygen ambience. However, it was observed that annealing in forming gas ambience slightly suppressed V_{FB} shift to negative side as compared with annealing in nitrogen ambience as shown in Figure 3-15. These results indicate that hydrogen might exert some influence on the cause of fixed charge.

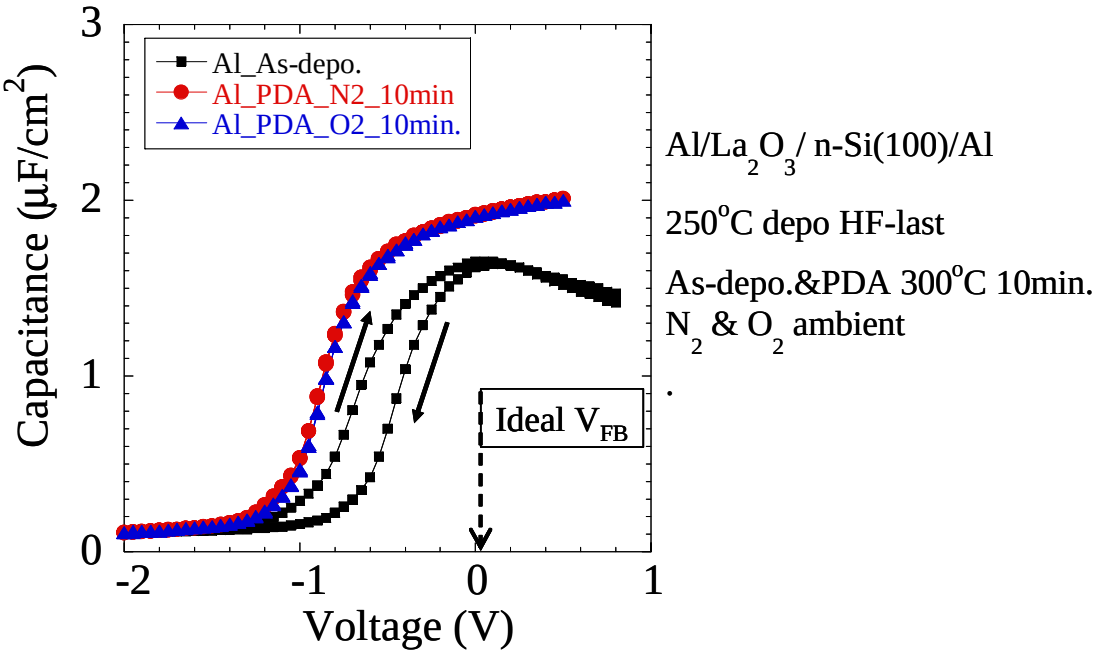

Figure 3-14: The comparison of PDA between the annealing in nitrogen and oxygen ambience

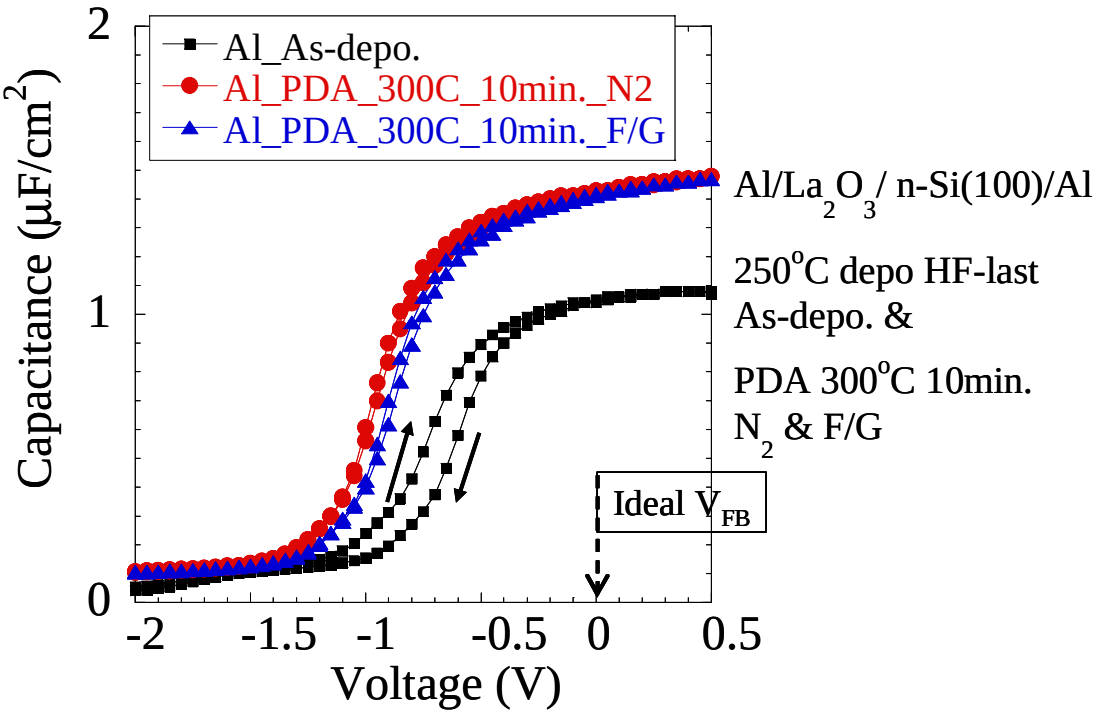

Figure: 3-15: The comparison of PDA between the annealing in nitrogen and forming gas ambience

3.4 Electrical Characteristics in the case of PMA

In the pages that follow, the result of post metallization annealing (PMA) will be mainly described. Especially, V_{FB} shift after annealing and comparison with PDA were focused.

3.4.1 Effects of PMA for Aluminum Upper Electrodes

For examination of PMA, a choice of upper electrodes material is quite significant because La_2O_3 films are supposed to be done staying contact with upper metal electrodes during thermal process and that might bring some reaction which affect electrical characteristics. In this sub-section, PMA with Aluminum upper electrodes were investigated.

3.4.1.1 Dependence on the Temperature of PMA with Aluminum Upper Electrodes

First, dependence on the temperature of PMA was investigated. Figure 3-16 shows the C-V characteristics dependent on the temperature of PMA for La_2O_3 thin films with Al electrodes. All of PMA samples were HF-last treatment and annealed in nitrogen ambience for 10 minutes. Annealing temperature from 200^{o}C to 450^{o}C was examined respectively. It was confirmed that PMA at 300^{o}C with aluminum upper electrodes made it possible to recover the negative V_{FB} shift. However, it was found that PMA with Aluminum electrodes in the case of temperature higher than 300^{o}C degraded electrical characteristics, causing such as an increase of hysteresis or a decrease of capacitance value. On the other hand, it was also found that PMA with Aluminum electrodes in the case of temperature lower than 300^{o}C did not make electrical characteristics improve sufficiently such as slight V_{FB} shift toward negative side or a drop of capacitance value in accumulation region.

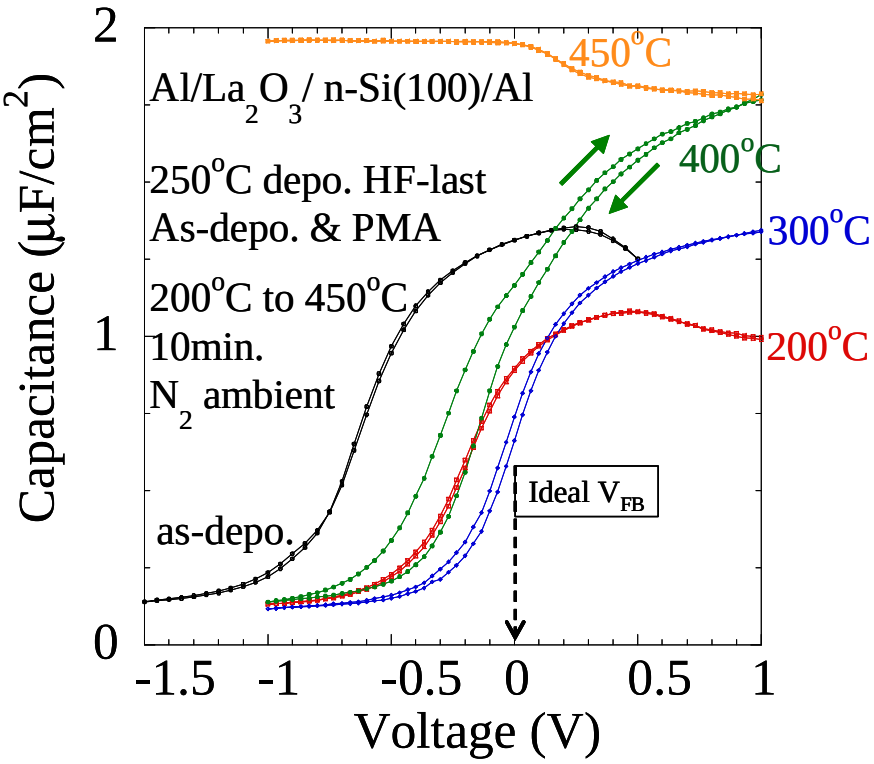

Figure 3-16: C-V characteristics dependent on temperature of PMA process

Figure 3-17 shows frequency dependence on C-V characteristics of PMA samples annealed from 200°C to 450°C respectively. It can be observed that frequency dependence at weak inversion became larger suddenly from PMA at 400°C. And, to make matters worse, C-V characteristics could not maintain its figure in the case of PMA at 450°C. This result indicates that PMA at higher temperature increased the interface state density. At the same time, it also indicates that some reactions took place by PMA with aluminum and that reactions seriously affected the electrical characteristics. The consideration about this reaction will come up later. Figure 3-18 shows the J-V characteristics dependent on temperature of PMA. Temperature from 200°C to 450°C as-deposited samples was examined. It was confirmed that leakage current increased with increase of annealing temperature as it were the substantiation of an increase of the interface state density. However, low leakage current was maintained by PMA at 300°C. And it was also confirmed PMA at 200°C was not a sufficient temperature to suppress the leakage current.

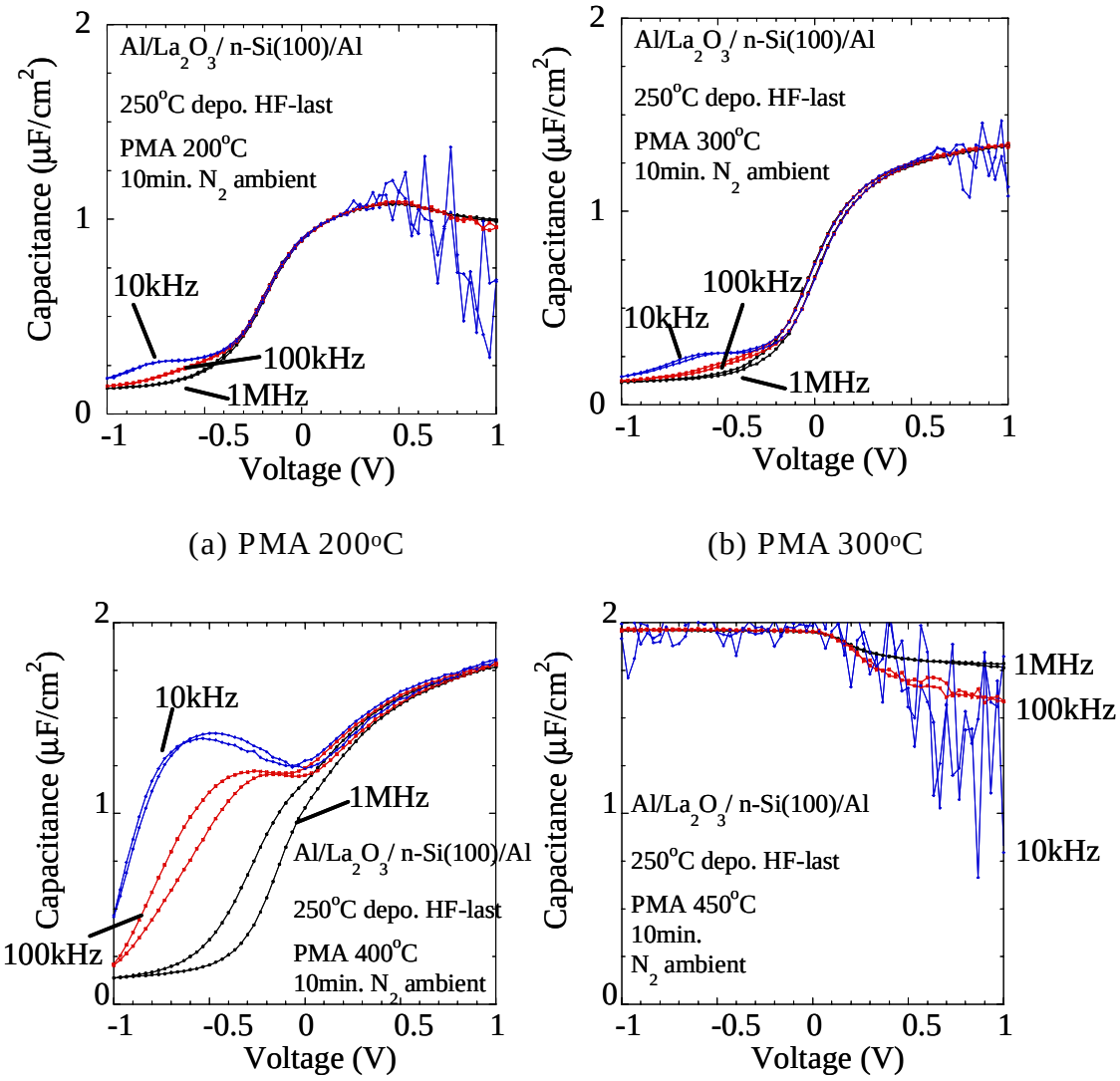

(a) PMA 200°C (b) PMA 300°C

(c) PMA 400°C (d) PMA 450°C

Figure 3-17 Frequency dependence on C-V characteristics of PMA at (a) 200°C (b) 300°C (c) 400°C (d) 450°C

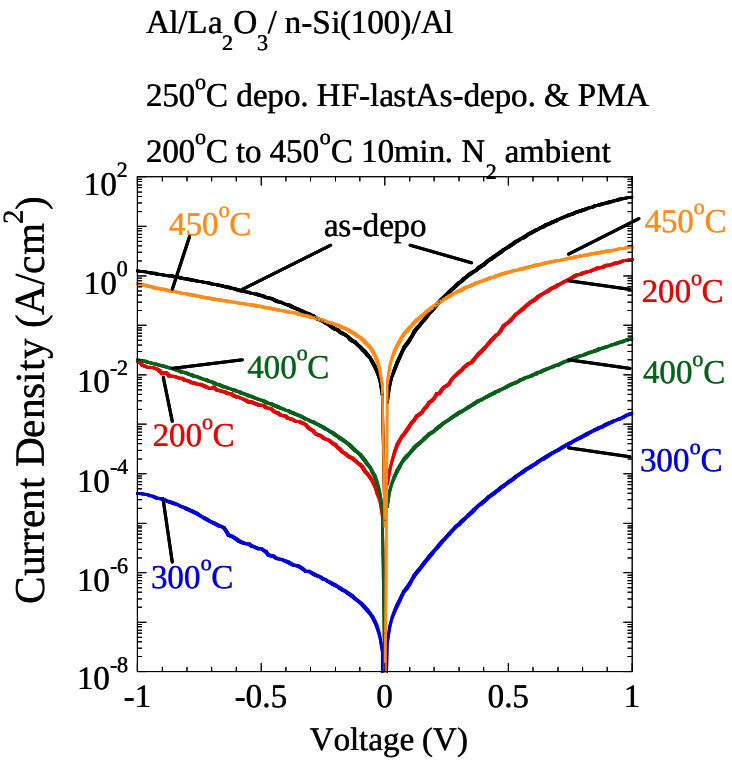

Figure 3-18: The J-V characteristics dependent on temperature of PMA

Finally, the dependence on the rising ratio, 75°C/minute and 400°C/minute, of the PMA temperature was examined same as PDA. In contradistinction to the case of PDA, It was confirmed that the slow rising ratio of the PMA temperature made the capacitance value decreased as shown in Figure 3-19. Moreover, it was also confirmed that the slow ratio of the PMA temperature made the leakage current increased as shown in Figure 3-20. These results indicate that PMA with aluminum electrodes is considerably sensitive to the annealing condition rather than PDA.

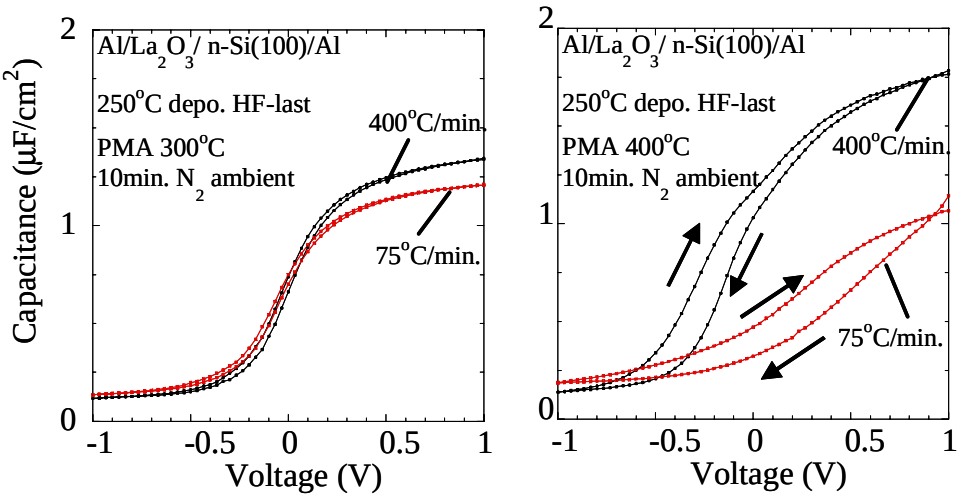

(a) PMA 300°C (b) PMA 400°C

Figure 3-19: The C-V characteristics Dependent on the rising ratio of PMA at (a) 300°C (b) 400°C

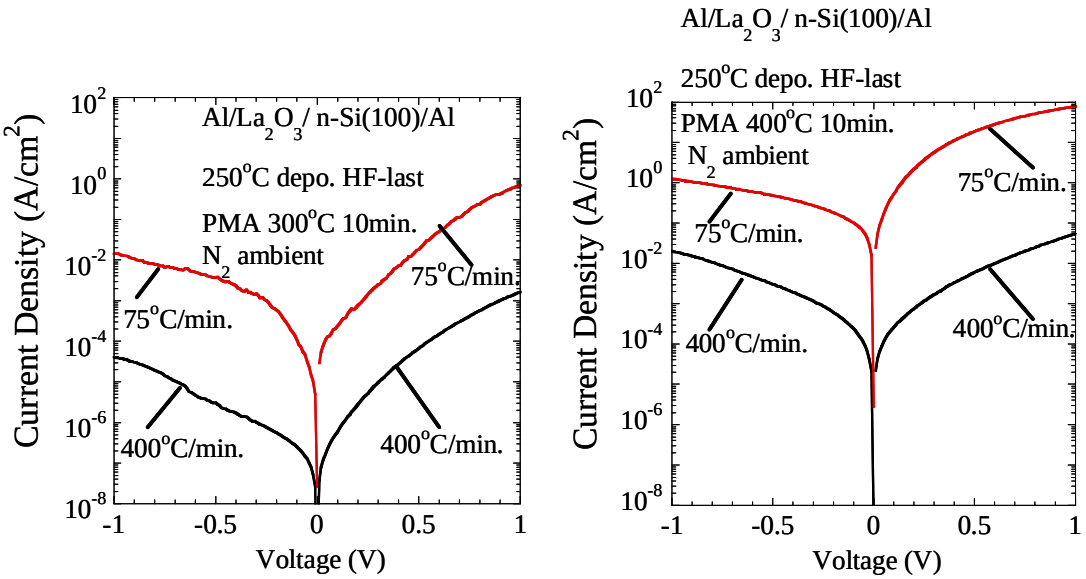

(a) PMA 300°C (b) PMA 400°C

Figure 3-20: The J-V characteristics Dependent on the rising ratio of PMA at (a) 300°C (b) 400°C

As the summary of this sub-section, the dependence on the temperature of PMA, the comparison between PDA and PMA at 300°C was showed in the pages that follow. Figure 3-21 shows the comparison of C-V characteristics between PDA and PMA at 300°C. Each sample was annealed in nitrogen ambience for 10minutes. It was observed that V_{FB} shift was only -0.1 V from the theoretical V_{FB} value without surface fixed charge in the case of PMA, and increase of hysteresis was suppressed under 0.03 V. On the other hand, the V_{FB} shift was -0.80 V in the case of PDA. Furthermore, PMA suppressed the leakage current more than 3 orders of magnitude as compared with PDA as shown in Figure 3-22. From the above, it can be presumed that the fittest temperature of PMA is around 300°C under the condition of nitrogen ambience and 10 minutes annealing.

However, some faults of PMA were also confirmed from these results. One of them is the increase of EOT. Figure 3-23 shows leakage current as a function of EOT. It was found that PMA had higher value of EOT as compared with one of PDA. Moreover, PMA would increase the interface state density. Figure 3-24 shows the comparison of frequency dependence on C-V characteristics between PDA and PMA. It was observed that there was no frequency dependence in the case of PDA. On the other hand, however, it was observed that there was frequency dependence at weak inversion region in the case of PMA. Although the fixed charge density dramatically decreased by the PMA at 300°C, interface state density seems to increase. Further study to reduce the interface state density will be required.

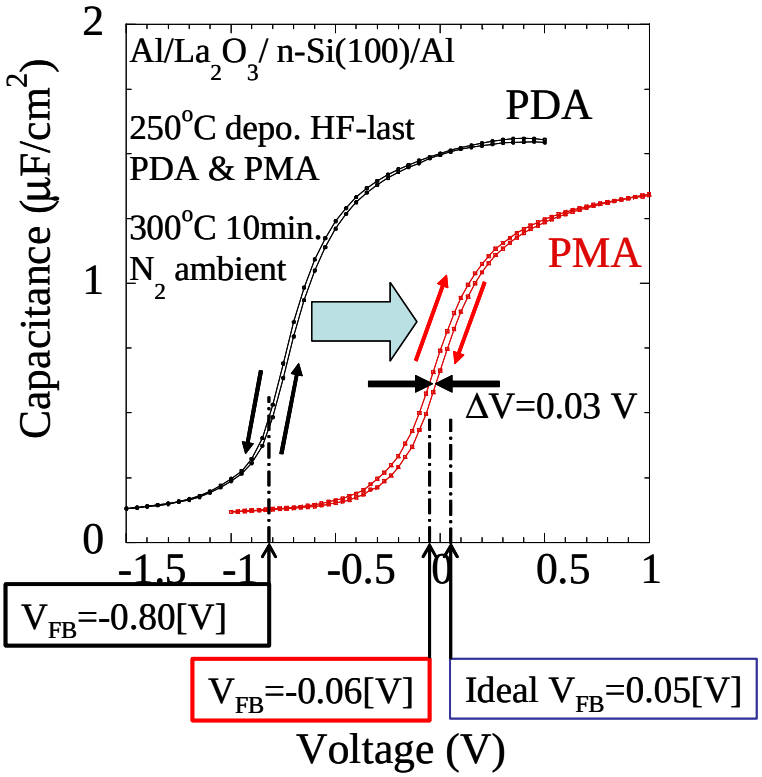

Figure 3-21: The comparison of C-V characteristics between PDA and PMA.

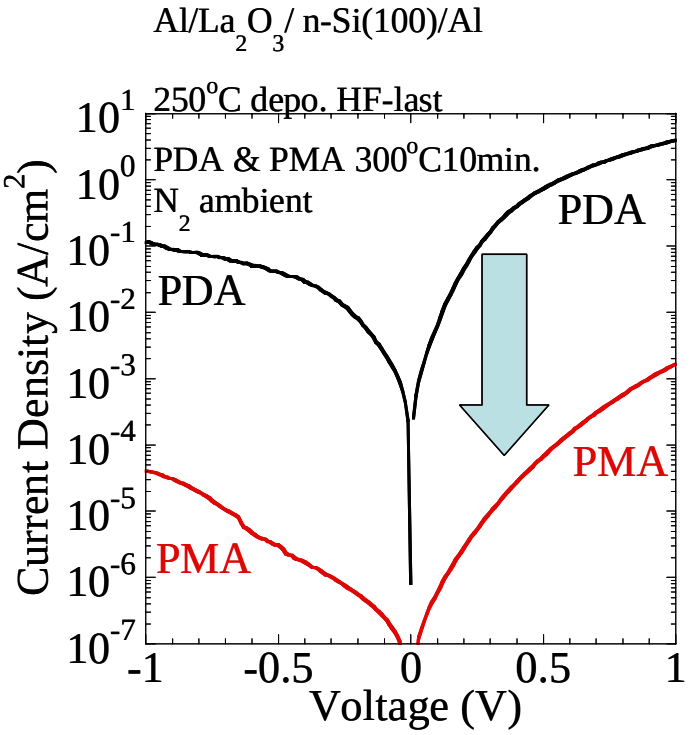

Figure 3-22: The comparison of J-V characteristics between PDA and PMA

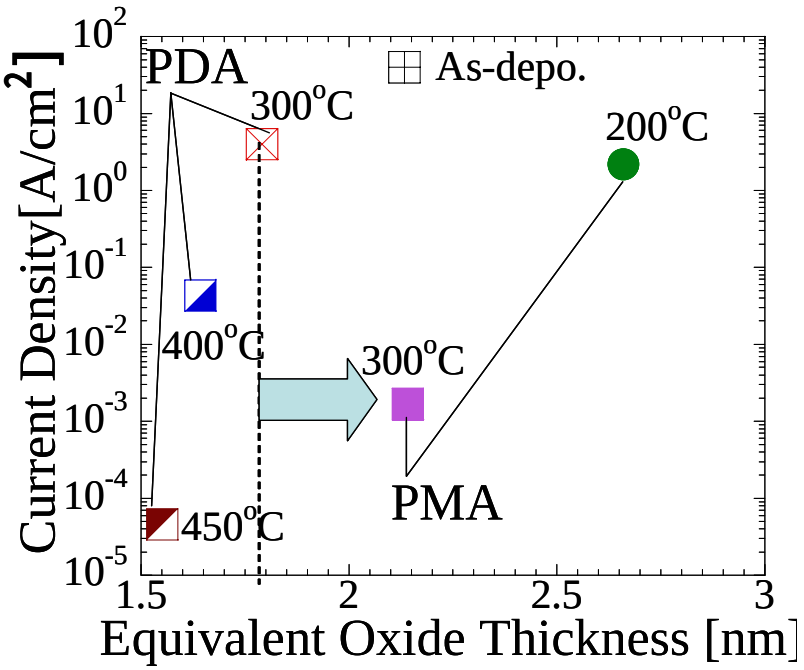

Figure 3-23: EOT-J plots

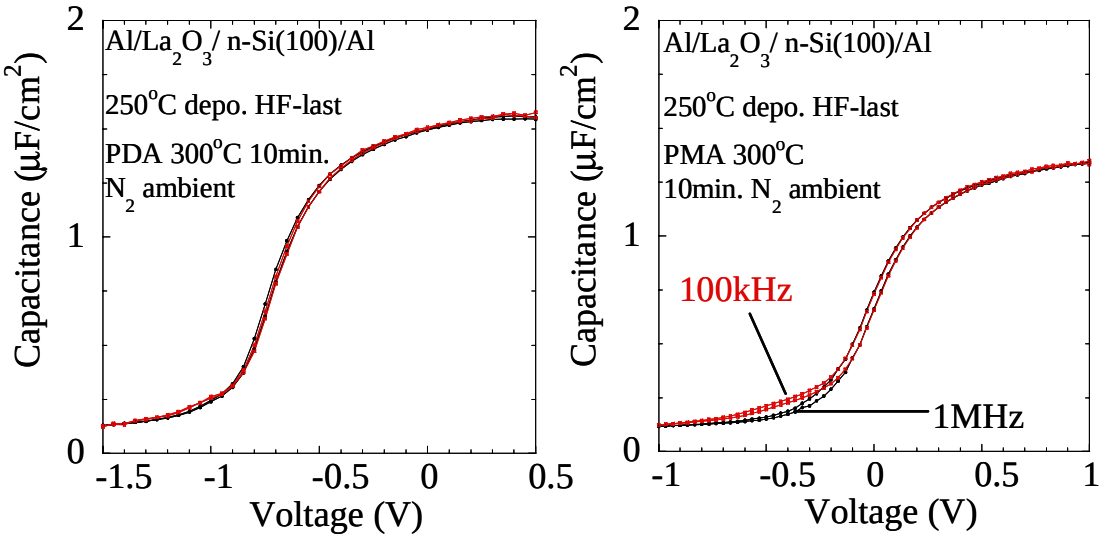

(a) PDA 300°C (b) PMA 300°C

Figure 3-24: Comparison of Frequency dependence on C-V characteristics of (a) PDA 300°C (b) PMA 300°C

3.4.1.2 Effects of Chemical Oxidation Treatment for PMA with Aluminum Upper Electrodes

Chemical oxidation treatment was anticipated that electrical characteristics were improved same as the case of PDA. Figure 3-25 shows the C-V characteristics of PMA dependent on the annealing temperature in the case of HF-last treatment (Figure 3-25 (a)) and chemical oxidation treatment (Figure 3-25 (b)) respectively. From rough view, the tendency for the effect of PMA appeared on chemical oxidation treatment. To be precise, chemical oxidation treatment decreased EOT and increased the width of hysteresis at 300°C as compared with HF-last treatment as shown in Figure 3-26. And in the case of HF-last, V_{FB} was shifted abruptly with increase in the temperature of PMA as compared with chemical oxidation treatment as shown in Figure3-27. However, almost the theoretical value of V_{FB} was obtained by PMA at 300°C in both treatments as shown in same figure.

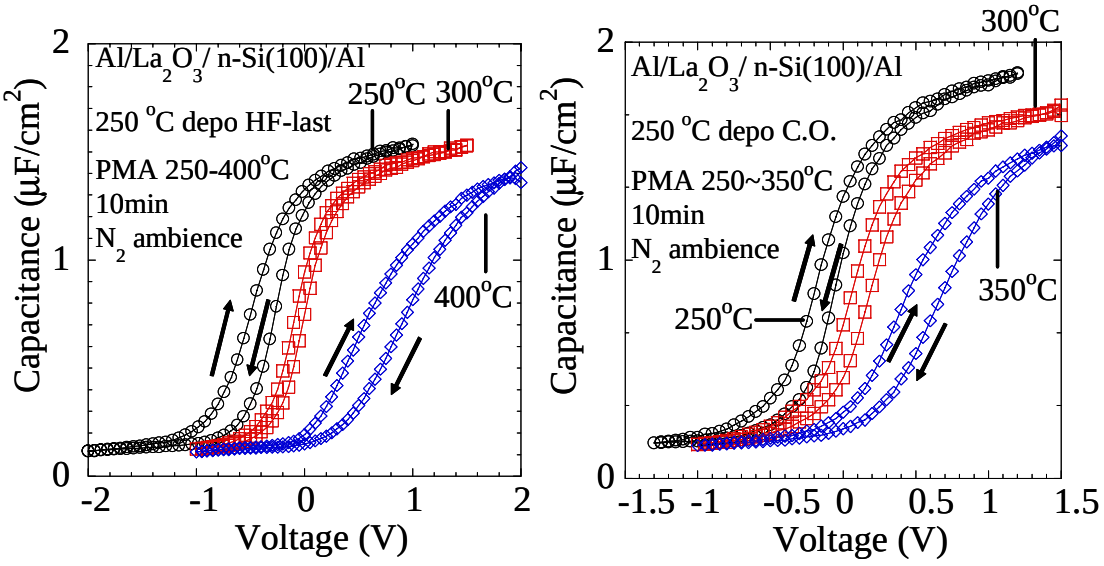

(a) HF-last (b) Chemical oxidation

Figure 3-25: the C-V characteristics of PMA dependent on the annealing temperature in the case of (a) HF-last treatment (b) chemical oxidation treatment

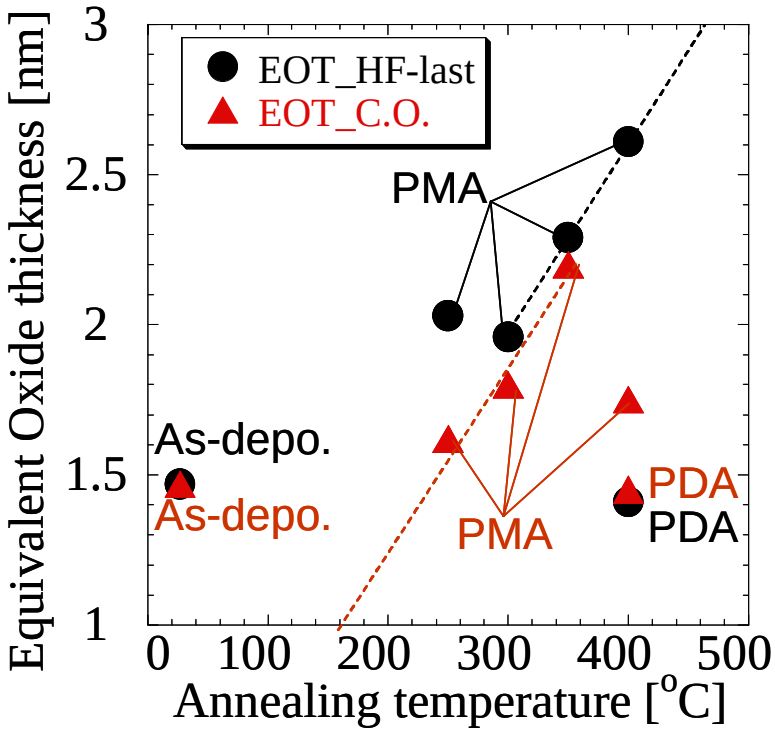

Figure 3-26: Plots of EOT dependent on the temperature of PMA

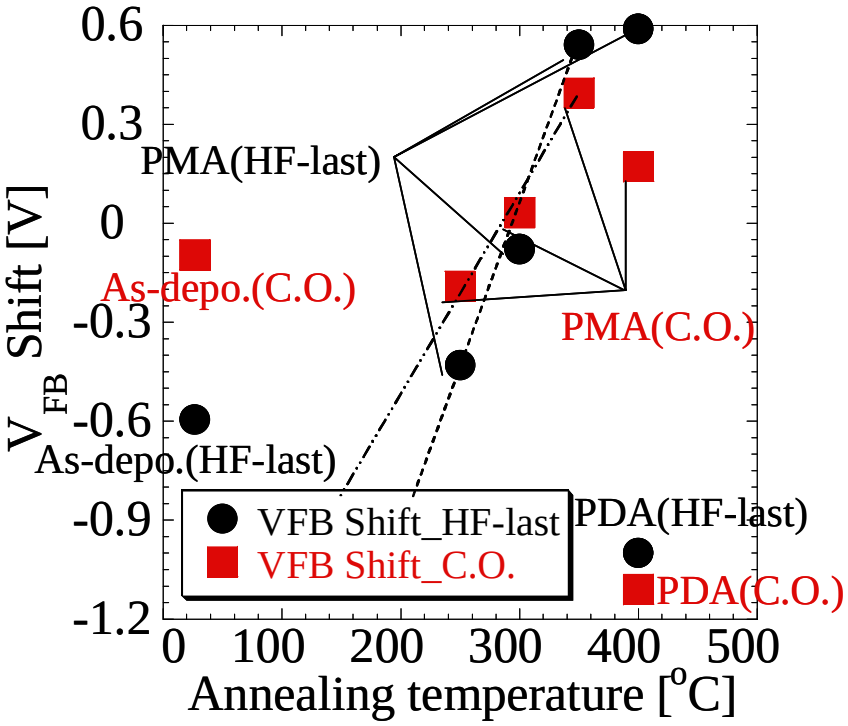

Figure 3-27: Plots of V_{FB} shift dependent on the temperature of PMA

3.4.1.3 Dependence on the Annealing Time of PMA with Aluminum Upper Electrodes

Thus far, the time of PMA was fixed on 10 minutes. The time of annealing temperature should affect V_{FB} same as the case of PDA as described in section 3.3.3, and also should be optimized. The dependence of PMA on annealing time from 0 second (spike) to 100 minutes was investigated. Here, the temperature of PMA was fixed on 300°C and annealing ambience was fixed on nitrogen as well taking the results of the dependence on the temperature described in section 3.1.1.1 into account. Figure 3-28 shows the C-V characteristics dependent on the time of PMA. It was confirmed that V_{FB} shift was recovered to positive side as the annealing time. However, hysteresis still remained slightly in each samples. This result indicates that PMA could not eliminate the defects in films and that led to the type of charge injected hysteresis. Moreover, to make matters worse, the width of hysteresis was expanded widely in the case of PMA for 100 minutes.

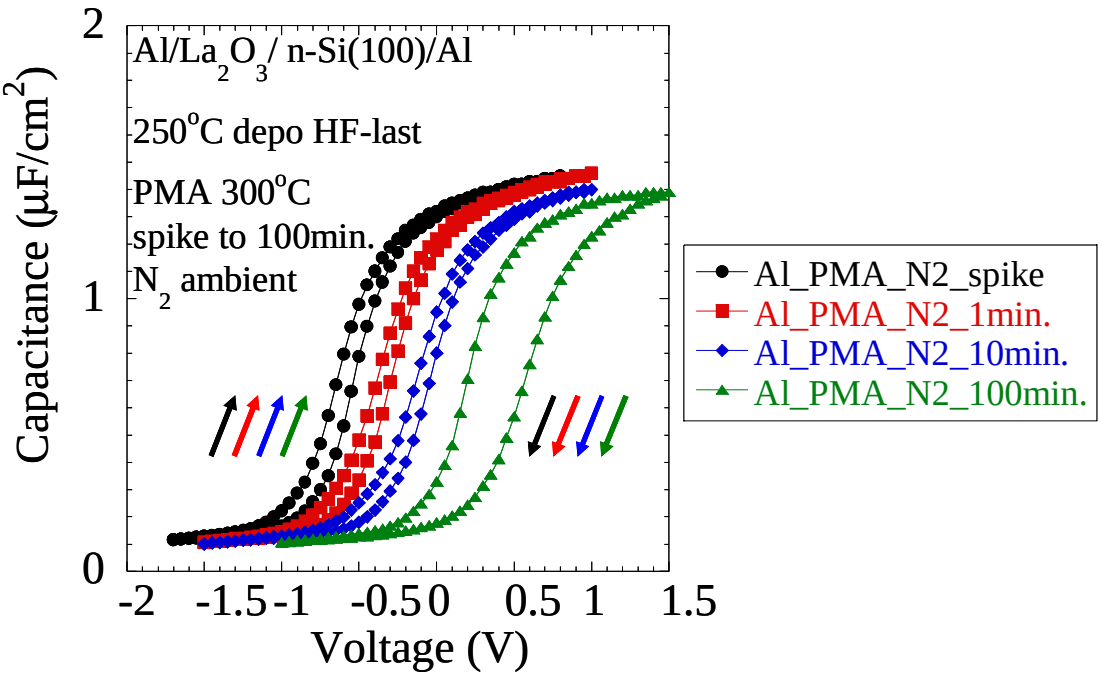

Figure 3-28: The C-V characteristics dependent on the time of PMA

Figure 3-29 shows the plots of V_{FB} shift dependent on the time of PMA. This graph also contains the plots of As-deposited and PDA samples deposited simultaneously. It is confirmed that PMA for aluminum upper electrodes made V_{FB} exponentially shifted to positive side dependent on the time of PMA. And it was also confirmed that the dependence of the time of PMA is much higher than one of PDA as shown in Figure 3-29. As a summary, it can be suggested that the appropriate time of PMA with aluminum upper electrodes for La_2O_3 thin films is around 10minutes and the value V_{FB} shift could be controlled precisely by adjusting the time of PMA.

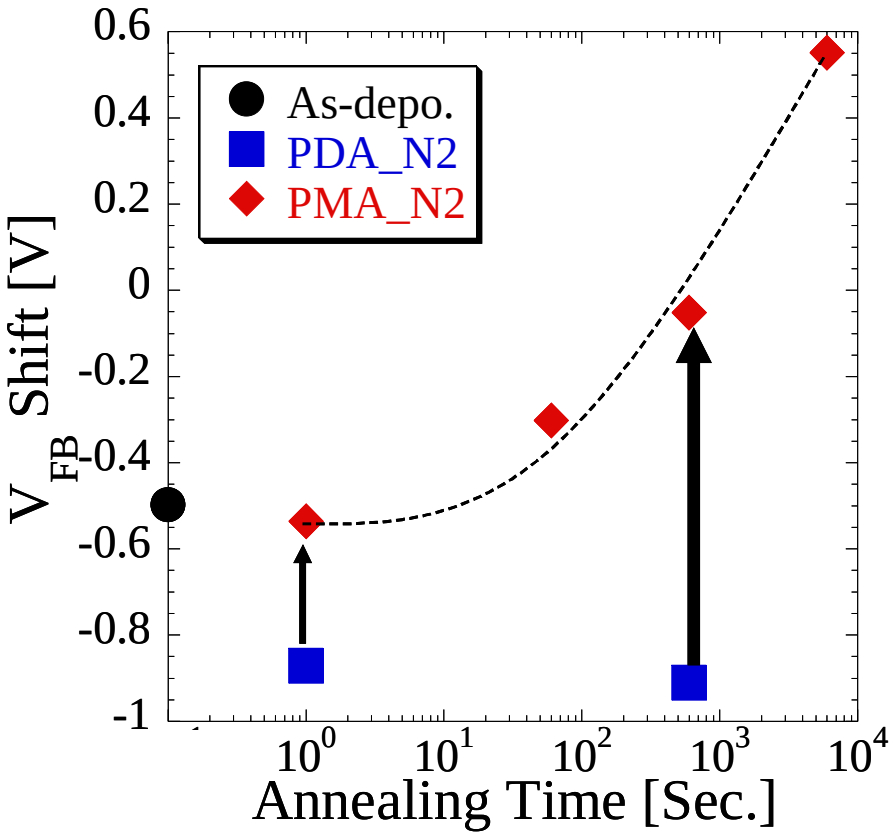

Figure 3-29: The plots of V_{FB} shift dependent on the time of PMA

Figure 3-30 shows the plots of EOT dependent on the time of PMA. This graph also contains the plots of As-deposited and PDA sample deposited simultaneously. It was found that the value of EOT almost did not change dependent on the time of PMA until 10minutes. When the annealing time reached 100 minutes, a slight increase of EOT was observed same as a increase of hysteresis as already mentioned. However, it was also observed that the value of EOT severely increased as compared with one of PDA. From a large number of experiments, it is found that the rate of the increase of EOT after PMA compared to PDA is not same for each deposition on our experiment. The rate of the increase of EOT were about 20 ~ 50 % from EOT of PDA. From this fact, it is conceivable that the same quality of La_2O_3 thin films could not have been deposited in our present experimental system. From empirical knowledge, it is also found that the electrical characteristics practically tend to become better as the same La_2O_3 source was used for long term. The considerations of the reason why PMA with aluminum increases EOT will be explained later.

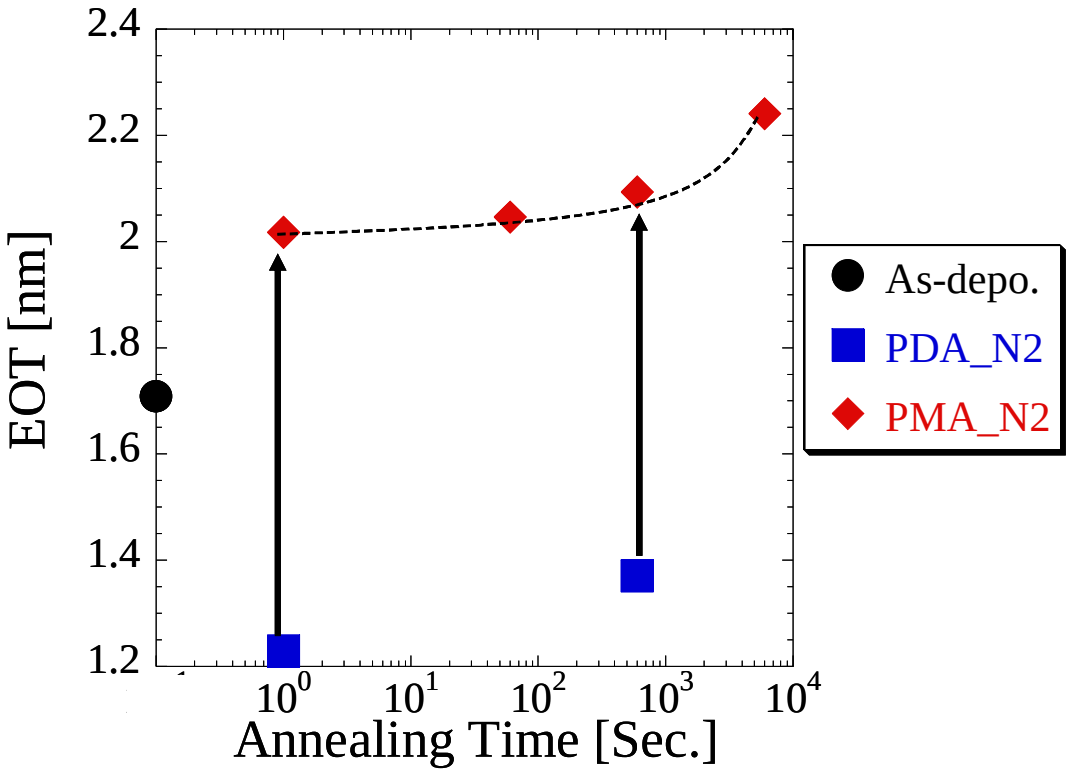

Figure 3-30: The plots of EOT dependent on the time of PMA

3.4.1.4 Dependence on the Ambience of PMA with Aluminum Upper Electrodes

The influence of annealing ambience on the electrical characteristics of PDA was already described. And up to this point, all of experiments in terms of PMA were done fixed to nitrogen ambience. Then, the influence of the annealing ambience through PMA was examined same as PDA. Figure 3-31 shows the C-V characteristics annealed in nitrogen, oxygen and forming gas ambience respectively. The any difference from nitrogen ambience, however, was not observed in the case of PMA. Figure 3-32 shows the comparison of the C-V characteristics of PMA between nitrogen and oxygen ambience on each annealing time from 0 second (spike) to 100 minutes. It is confirmed that there was, roughly speaking, nothing different between nitrogen and oxygen ambience. It can be considered that it is difficult for PMA samples to affect the ambience during the annealing because La_2O_3 thin films are always covered with upper electrodes in the case of PMA, in other words, La_2O_3 films are not supposed to expose the atmosphere directly during annealing. This fact would make it difficult to exert an influence on the electrical characteristics. Finally, the plots of V_{FB} shift and EOT were shown, as the supplements to Figure 3-29 and 3-30, in Figure 3-33 and Figure 3-34 respectively. From these Figures, it was found that there was no influence on V_{FB} and EOT owing to the annealing ambience and both ambience showed similar tendency.

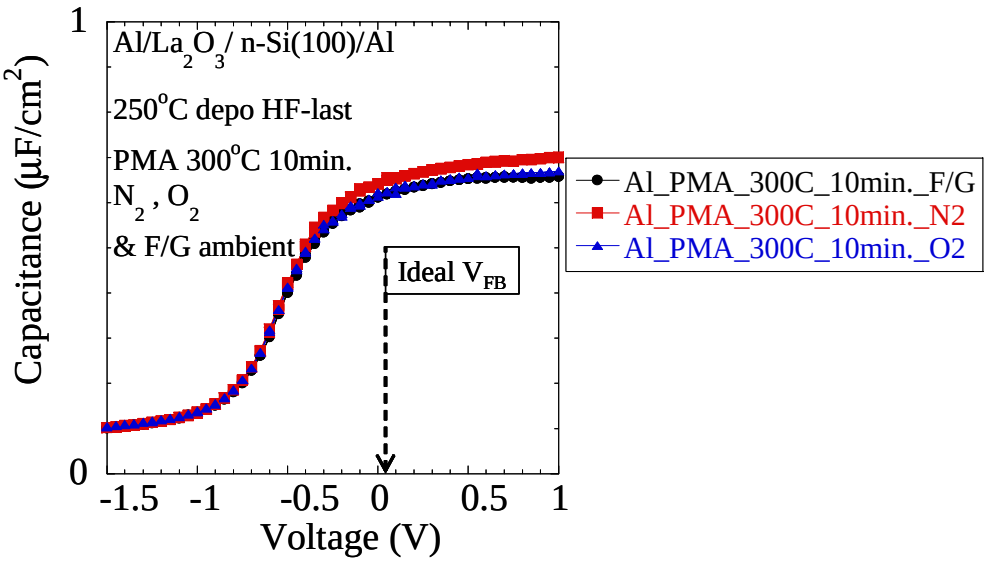

Figure 3.31: The C-V characteristics annealed in N_2, O_2 and F/G ambience

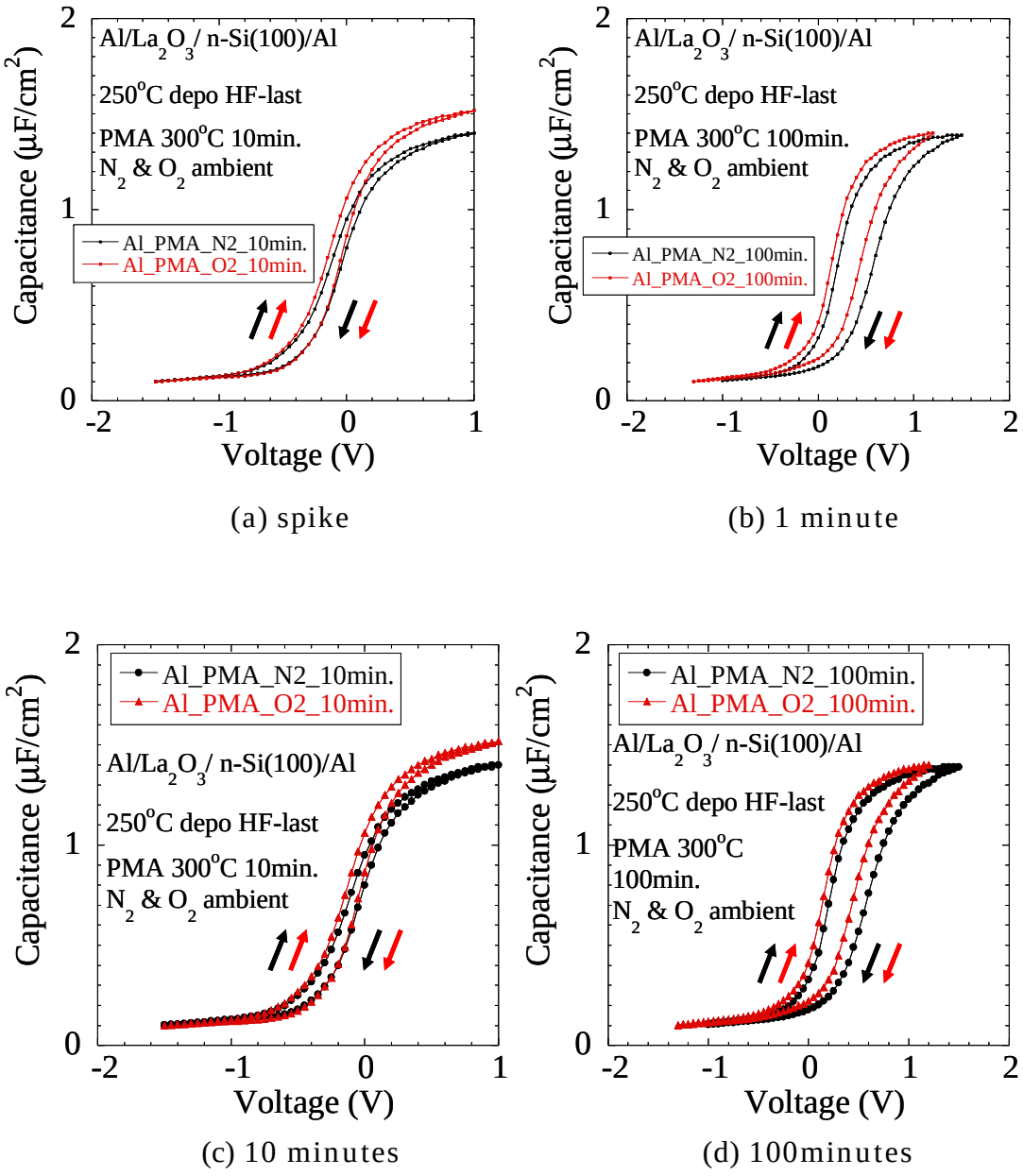

Figure 3-32: The comparison of the C-V characteristics of PMA between nitrogen and oxygen ambience on each annealing time from 0 second to 100 minutes

(a) 0 second (spike) (b) 1minute

(c) 10minutes (d) 100minutes

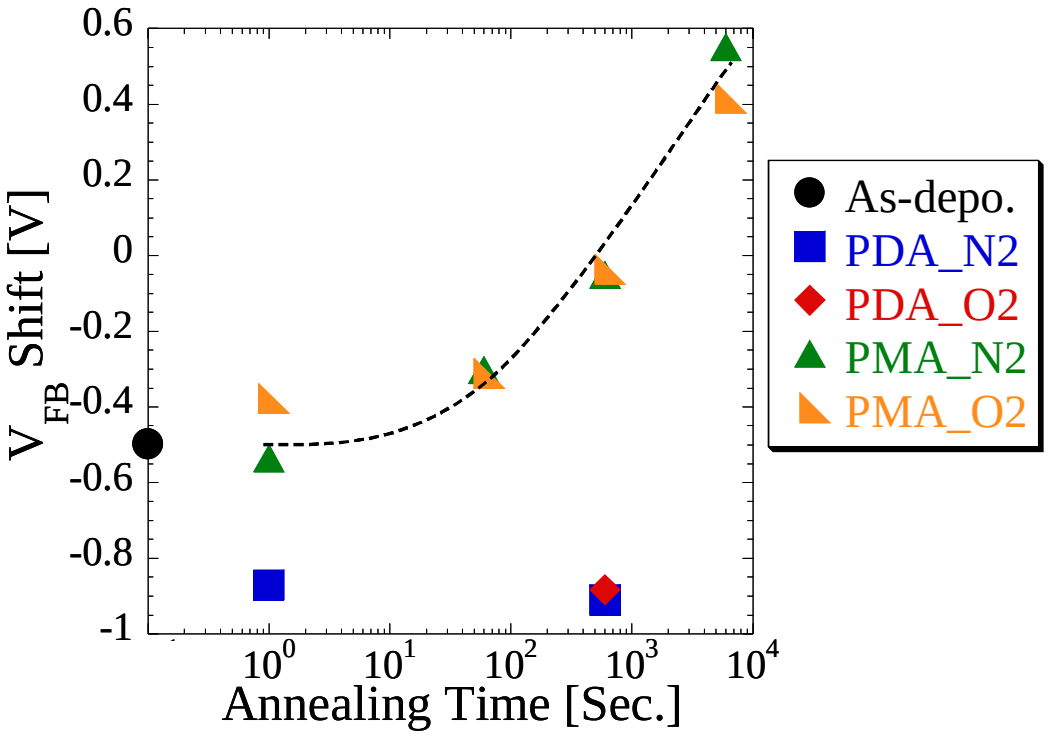

Figure 3-33: The plots of V_{FB} shift in the case of nitrogen and oxygen ambience

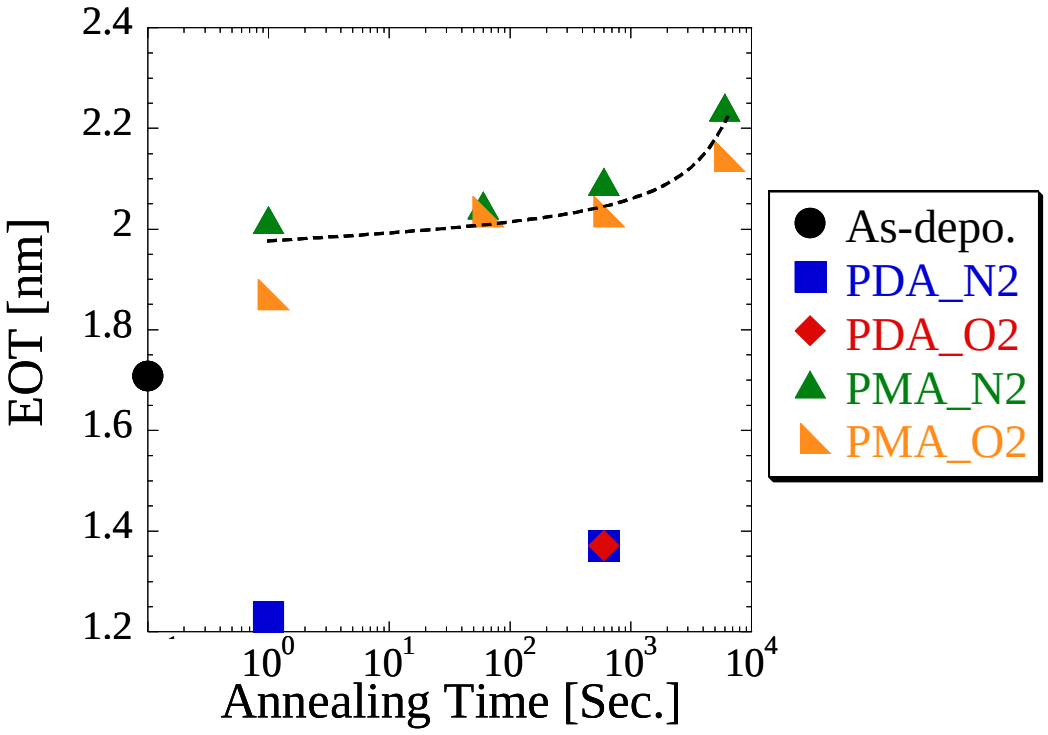

Figure 3-34: The plots of EOT in the case of nitrogen and oxygen ambience

3.4.1.5 The Combination of PDA and PMA

Thus far, the electrical characteristics by various conditions of PDA and PMA with aluminum upper electrodes were examined for their optimization. As a result, it was found that in the case of aluminum upper electrodes, negative V_{FB} shift was enlarged by PDA, while all the other characteristics such as EOT, leakage current or interface state density were improved. On the other hand, it was found that the V_{FB} shift was almost completely recovered by PMA at 300°C. However, PMA with Al upper electrodes decreased the capacitance value. Also PMA was not sufficient to decrease the leakage current, and even increased the interface state density. From these results, it is natural to consider that combining PDA and PMA could bring good characteristics owing to the counterbalance by each merit.

Figure 3-35 shows the C-V characteristics in the case of the combination of PDA and PMA compared to only PDA or PMA treatment, and their dependence on the time of PMA from 0 sec (spike) to 10 minutes. The temperature of PDA was 300°C and the temperatures of PMA were 250°C and 300°C respectively. All of samples were annealed in nitrogen ambience. In the case of spiked PMA at 250°C, any effects of the suppression of the V_{FB} shift did not appear as shown in Figure 3-35 (a). However, when the time of PMA lengthened up to 10 minutes, the V_{FB} shift was recovered on a level with PMA-only treatment without any degradation of electrical characteristics as shown in Figure 3-35 (c). On the other hand, in the case of spiked PMA at 300°C, the V_{FB} shift was recovered on a level with PMA at 250°C for 10 minutes despite of spiked PMA as shown in Figure 3-35 (d). However, when the time of PMA lengthened up to 10 minutes, some degradation of electrical characteristics such as a decrease of capacitance value or an increase of hysteresis width appeared, although the V_{FB} shift was recovered on a level with PMA-only treatment as shown in Figure 3-35 (f).

From these results, it was found that the combination of PDA and PMA was considerably effective in the suppression of V_{FB} shift with maintaining the capacitance value. However, it was also found that PMA for aluminum upper electrodes were highly sensitive to the combination of the annealing temperature and time, therefore it is anticipated that optimizing the condition of the combination of PDA and PMA could make it possible to suppress the V_{FB} shift with remaining high capacitance value.

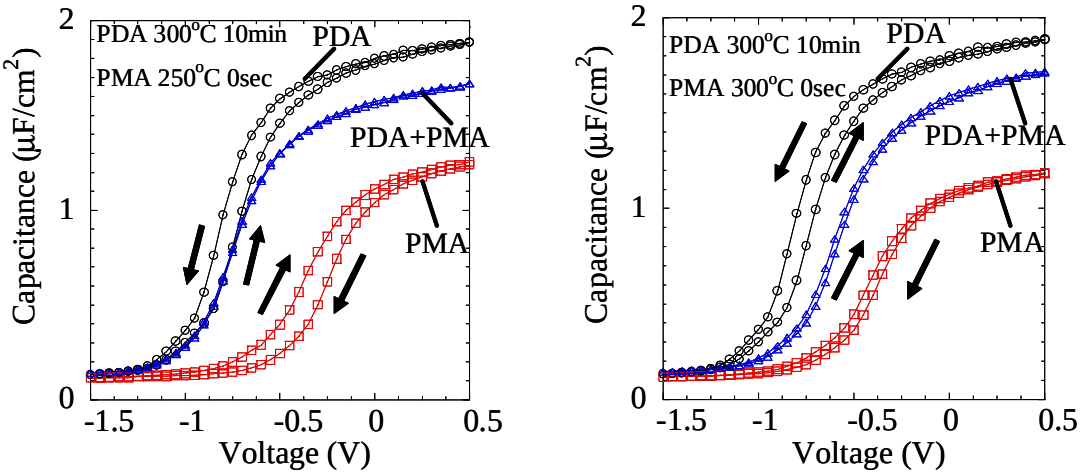

(a) 250°C spike

(d) 300°C spike

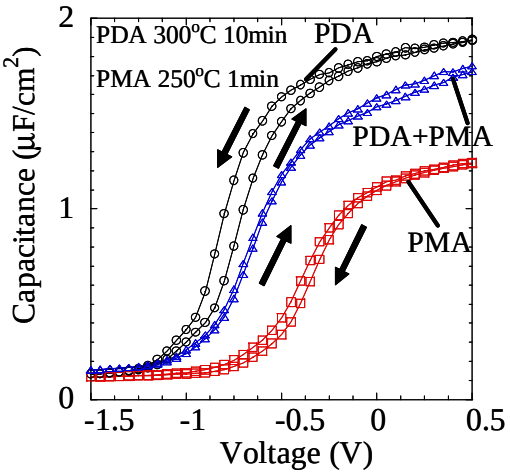

(b) 250°C 1 minute

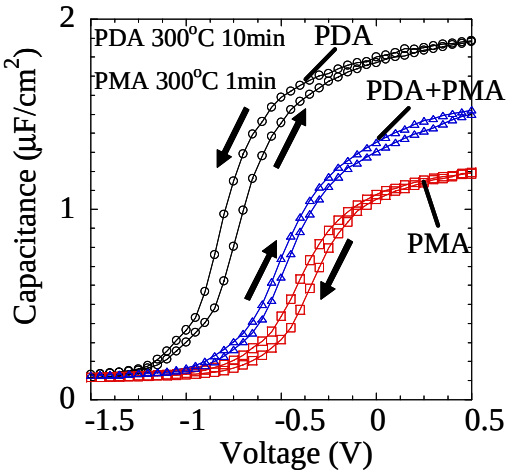

(e) 300°C 1 minute

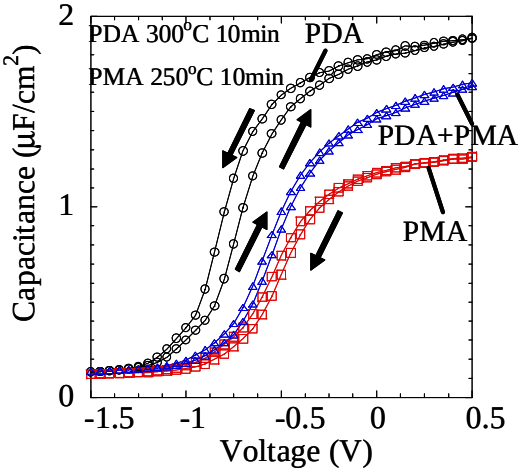

(c) 250°C 10 minute

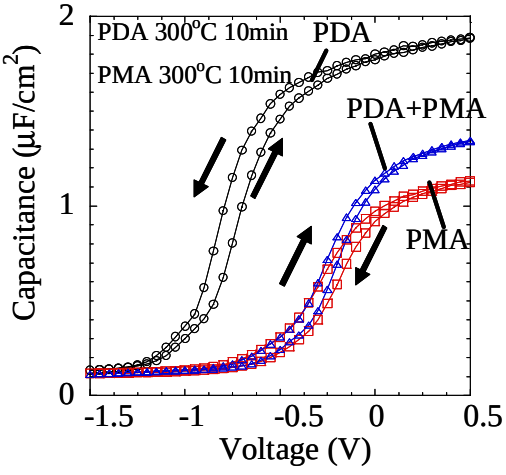

(f) 300°C 10 minute

Figure 3-35: The C-V characteristics in the case of the combination of PDA and PMA compared to only PDA or PMA treatment, and their dependence on the time of PMA from 0 sec (spike) to 10 minutes

3.4.2 Effects of PMA for Gold Upper Electrodes

From the investigation of PMA with aluminum upper electrodes for La_2O_3 thin films, it was found that V_{FB} was recovered to positive side by PMA. However, it was not clear that the reasons of that recovery of V_{FB} was owing to the PMA itself, covering La_2O_3 thin films with metal electrodes during thermal process, or some reactions between La_2O_3 and aluminum as a result of annealing with contact one another. Hence, PMA with another upper electrode should be investigated.

In order to clarify the mechanism of the effect of PMA, PMA with gold upper electrodes was investigated.

3.4.2.1 Dependence on the Temperature of PMA with Gold Upper Electrodes

Firstly, dependence on the temperature of PMA with gold upper electrodes for La_2O_3 thin films was investigated. Figure 3-36 shows the C-V characteristics dependent on the temperature of PMA for La_2O_3 thin films with gold upper electrodes. Here, all of samples were HF-last treatment and annealed in nitrogen ambience for 10 minutes. Annealing temperature from 300^{o}C to 450^{o}C was examined respectively. It was observed that PMA with gold upper electrodes increased the capacitance value with increase in the annealing temperature, but also increased V_{FB} shift to negative side with increase in annealing temperature in contrast with the case of PMA with aluminum upper electrodes.

Figure 3.37 shows the values of EOT versus annealing temperature plot for La_2O_3 thin films with gold upper electrodes. Here, the results of As-deposition and PDA were shown in same graph. It was found that a decrease of EOT caused by PMA was proportional to the annealing temperature in the case of gold upper electrodes.

Figure 3.38 shows the values of the V_{FB} shift versus annealing temperature plot for La_2O_3 thin films with gold upper electrodes. It was found that variations of the V_{FB} shift caused by PMA were proportional to the annealing temperature to negative side in the case of gold upper electrodes. And a range of the V_{FB} shift cause by PMA was less than the

case of aluminum electrodes as compared with Figure 3-27.

Figure 3.39 shows EOT versus J (leakage current) plot for La_2O_3 MIS capacitor with gold upper electrodes fabricated by as-deposition, PDA and PMA. In this graph, the leakage currents for all samples were compared at +1V. From this graph, the universal tendency for leakage current to be dependent on EOT was confirmed in the case of gold upper electrodes.

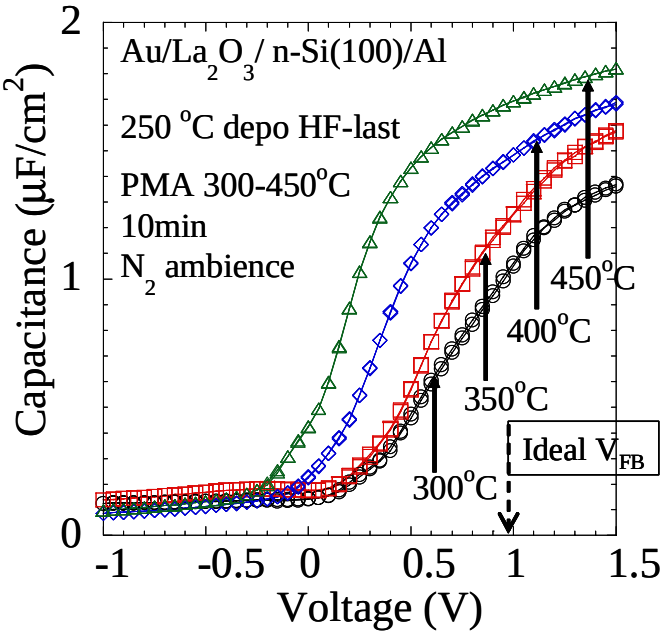

Figure 3-36: The C-V characteristics dependent on the temperature of PMA treated by HF-last

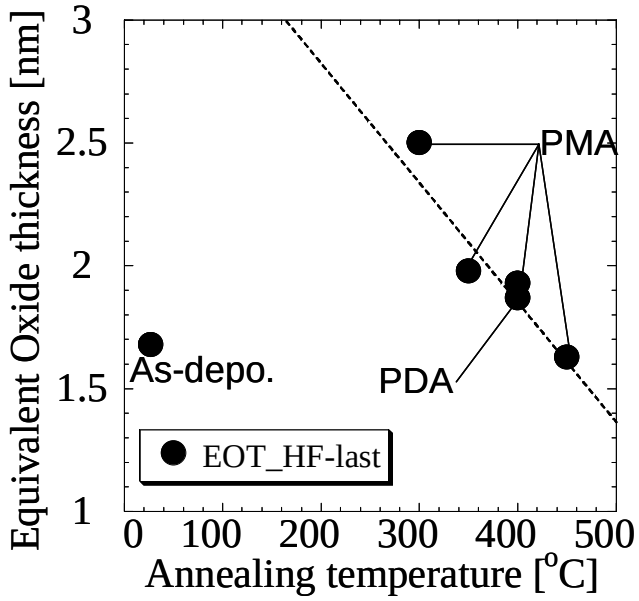

Figure 3-37: The values of the EOT shift versus annealing temperature plot

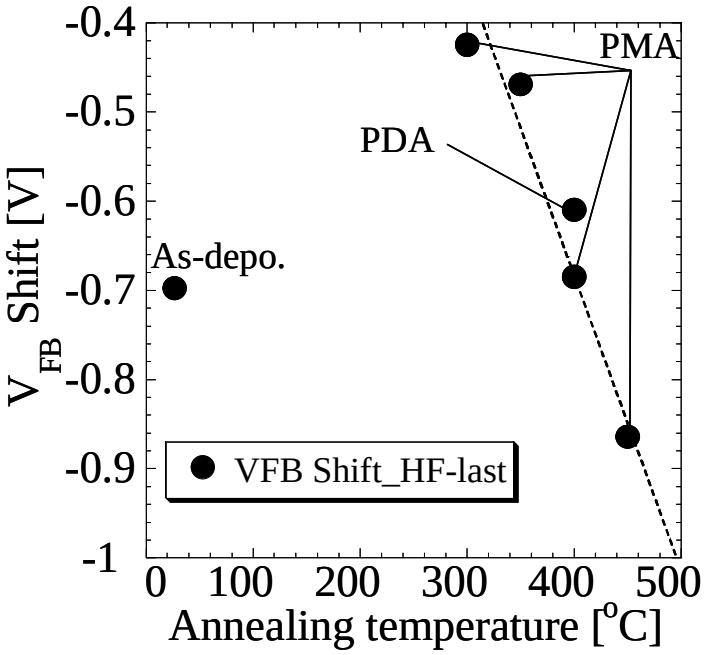

Figure 3-38: The values of the V_{FB} shift versus annealing temperature plot

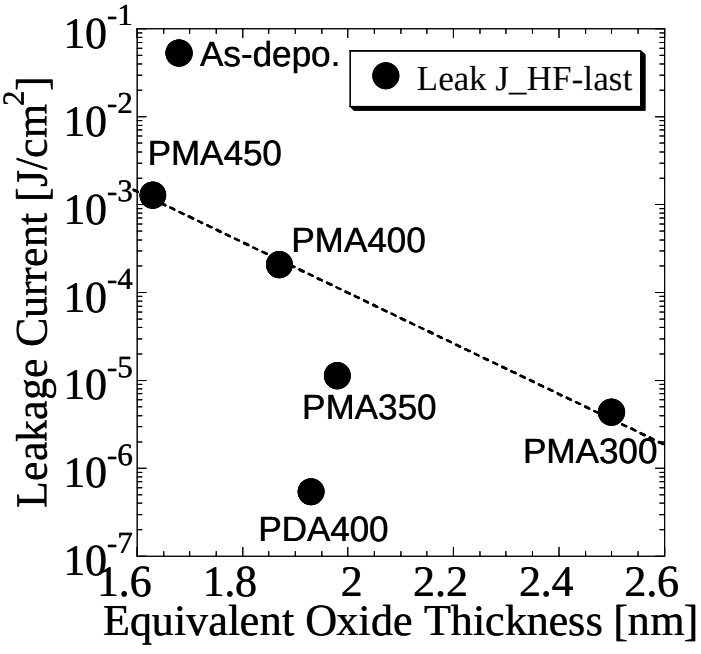

Figure 3-39: EOT versus leakage current plot

3.4.2.2 Effects of Chemical Oxidation Treatment for PMA with Gold Upper Electrodes

The effects of chemical oxidation treatment for PMA with gold upper electrodes were investigated same as the case of PMA with aluminum upper electrodes. Figure 3-40 shows the C-V characteristics of PMA dependent on the annealing temperature in the case of chemical oxidation treatment. From rough view, the tendency for the effect of PMA appeared on chemical oxidation treatment same as in the case of PMA with aluminum upper electrodes, namely, an increase of the capacitance value with increase in the annealing temperature, and an increase of V_{FB} shift to negative side with increase in annealing temperature as well. To be precise, some effects of chemical oxidation treatment were found from the comparison with HF-last treatment. Figure 3-41 shows the values of the EOT versus annealing temperature plot for La_2O_3 thin films with gold upper electrodes as the supplement to Figure 3-37. It was found that chemical oxidation treatment slightly decrease the value of EOT as compared to the ones of HF-last treatment, but also a decrease of EOT was almost proportional to annealing temperature. Figure 3-42 shows the values of the V_{FB} shift versus annealing temperature plot for La_2O_3 thin films with gold upper electrodes as the supplement to Figure 3-38. This graph indicates that chemical oxidation treatment for PMA with gold upper electrodes slightly enlarged the V_{FB} shift toward negative side for same annealing temperature, but also V_{FB} was almost proportional to the temperature of PMA. Figure 3-43 shows EOT versus J plot for La_2O_3 MIS capacitor with gold upper electrodes fabricated by as-deposition, PDA and PMA as the supplement to Figure 3-39. It was found that chemical oxidation treatment decreased leakage current approximately 1 to 2 orders of magnitude as compared to HF-last treatment, and universal relation between EOT and leakage current was also observed same as the case of HF-last treatment.

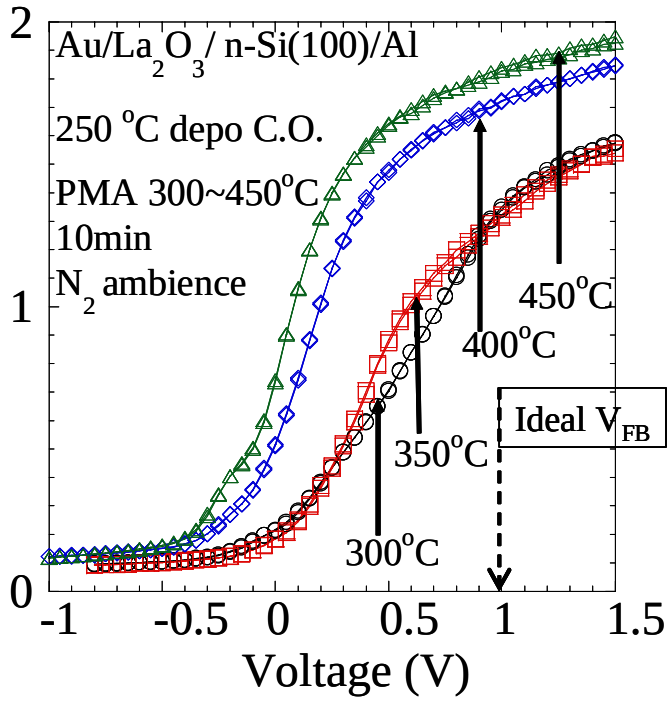

Figure 3-40: The C-V characteristics dependent on the temperature of PMA treated by chemical oxidation

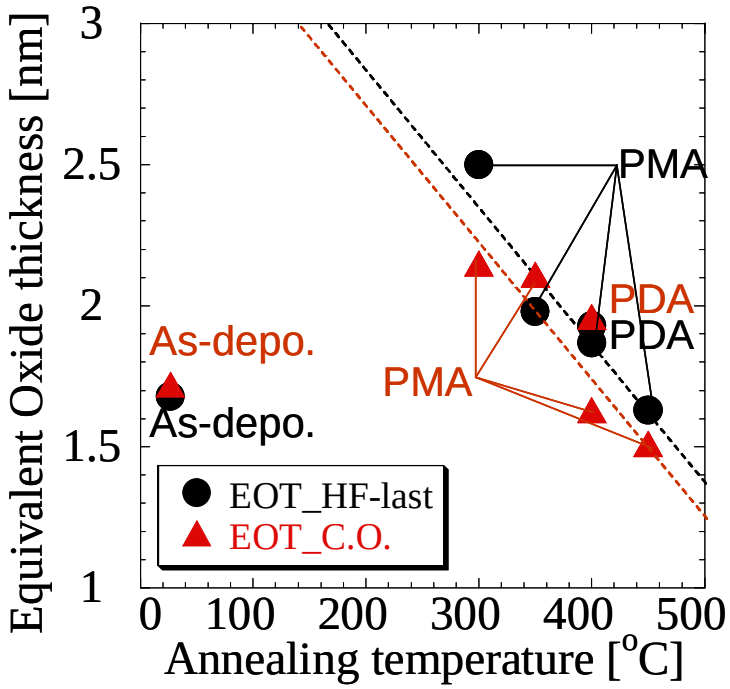

Figure 3-41: The values of the V_{FB} shift versus annealing temperature plot

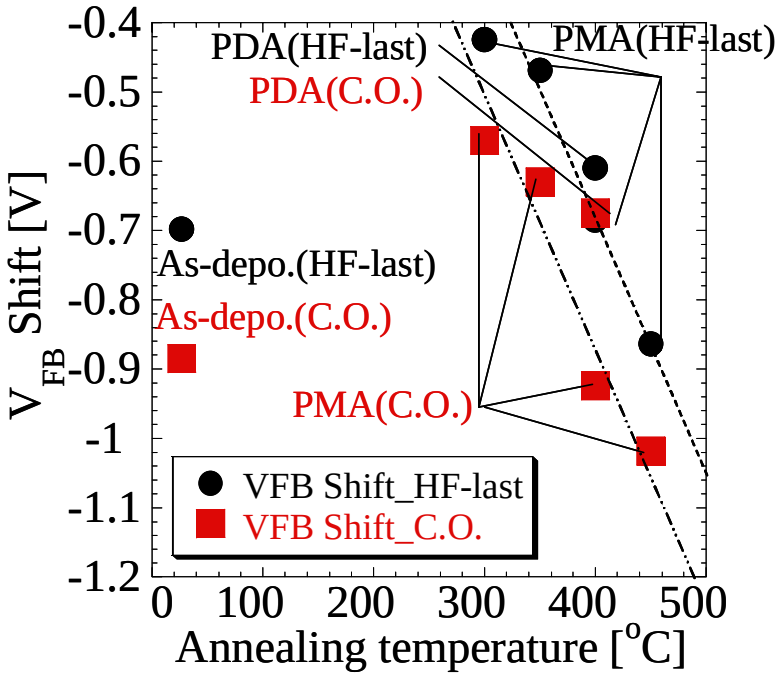

Figure 3-42: The values of the V_{FB} shift versus annealing temperature plot

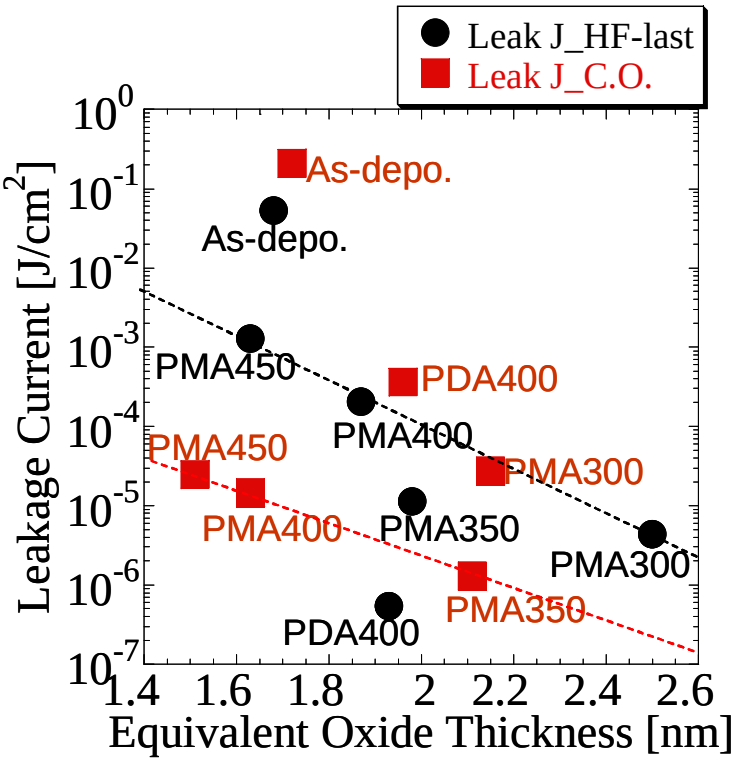

Figure 3-39: EOT versus leakage current plot

3.4.2.3 Dependence on the Annealing Time of PMA with Gold Upper Electrodes

The influence of the time of PMA with gold upper electrodes was already described in section 3.4.1.3. It is conceivable that annealing time would exert any influence on any electrical characteristics in the case of PMA with gold upper electrodes same as the case of aluminum upper electrodes. Accordingly, the dependence on the annealing time for PMA with gold upper electrodes was investigated. Figure 3-44 shows the C-V characteristics dependent the time of PMA with gold upper electrodes. Annealing time was examined from 0 sec to 100 minutes. The results of As-deposition and PDA samples were shown in same graph as well. In contrast with the case of PMA with aluminum upper electrodes, it was found that there was almost no difference in electrical characteristics by variety of annealing time in the case of PMA with gold upper electrodes. To be precise, the value of EOT slightly decreased with decrease in annealing time as shown in Figure 3-45. And it was also found that the value of EOT considerably increased when annealing time became longer from 0 second to 10 minutes. However, the dependence of V_{FB} shift on annealing time was not confirmed in the case of PMA with gold upper electrodes as shown in Figure 3-46.

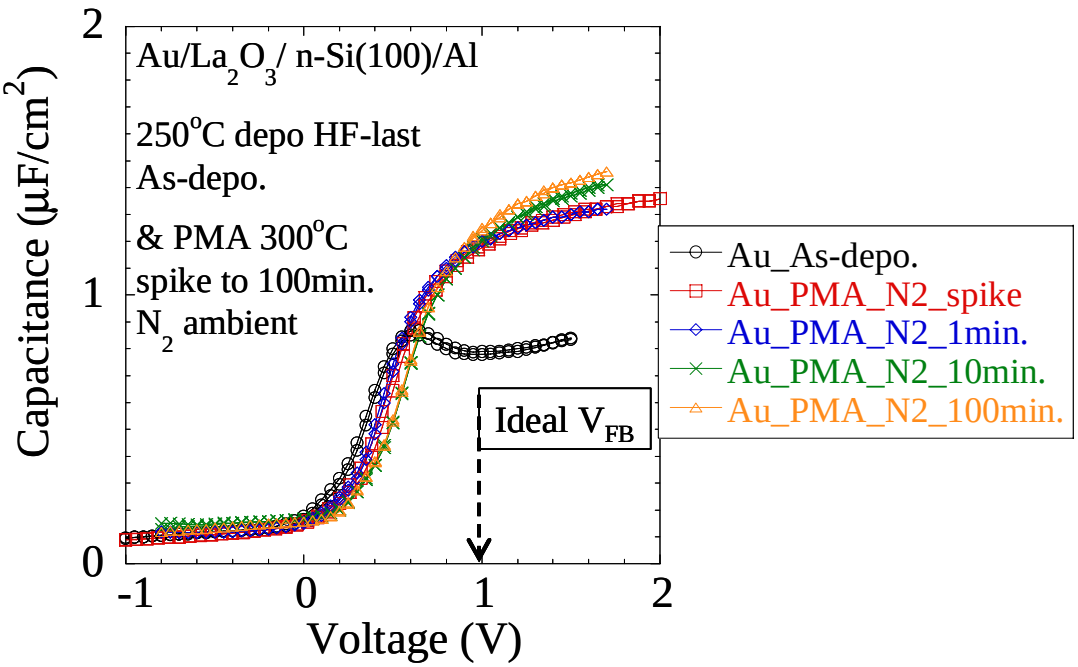

Figure 3-44: The C-V characteristics dependent the time of PMA with gold upper electrodes

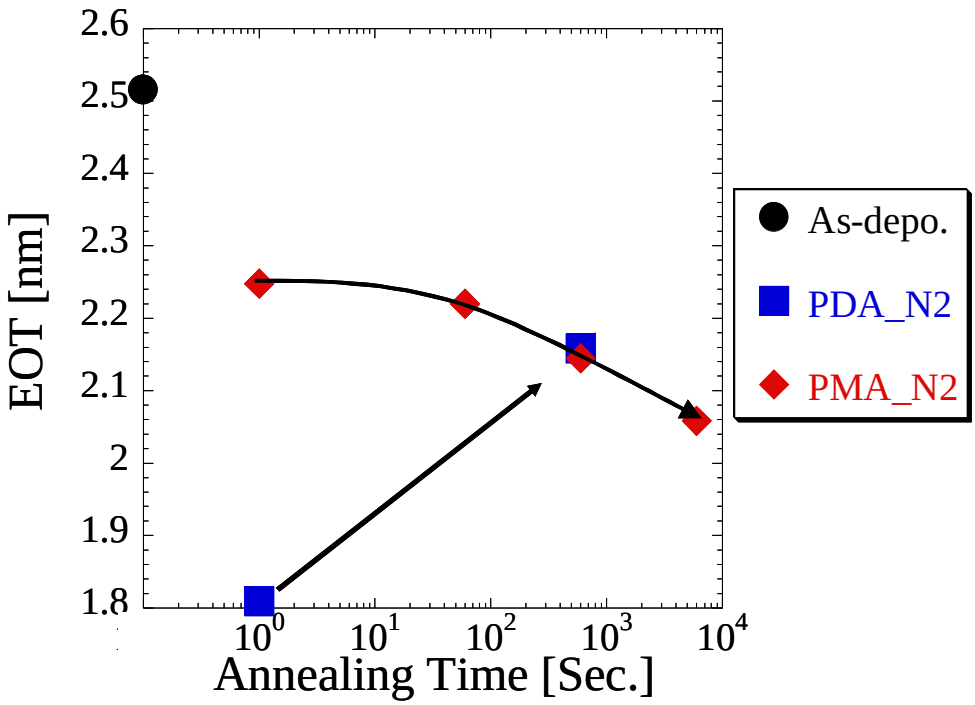

Figure 3-45: The value of EOT dependent on annealing time

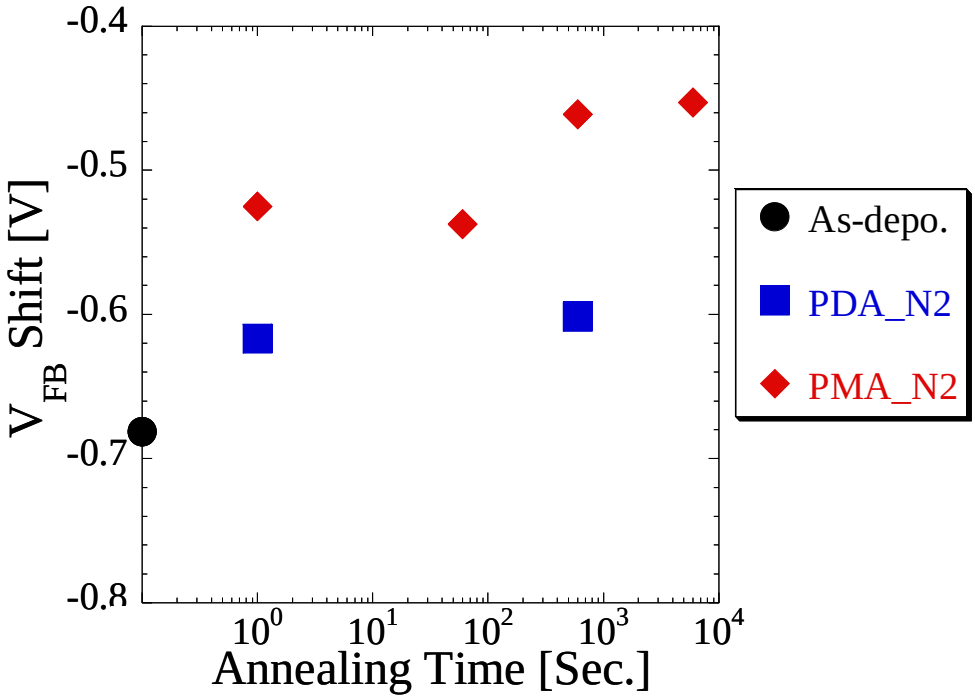

Figure 3-46: The value of V_{FB} shift dependent on annealing time

3.4.2.4 Dependence on the Ambience of PMA with Gold Upper Electrodes

The influence of annealing ambience on the electrical characteristics after PMA with aluminum upper electrodes, almost no dependence on annealing ambience, was already described in section 3.4.1.4. And up to this point, all of experiments in terms of PMA with gold upper electrodes were done fixed to nitrogen ambience. Then, the influence of the annealing ambience through PMA was examined same as PMA with the case of aluminum upper electrodes.

Figure 3-47 shows the comparison of the C-V characteristics of PMA between nitrogen and oxygen ambience on each annealing time from 0 second (spike) to 100 minutes. It was confirmed that there was, roughly speaking, nothing different between nitrogen and oxygen ambience in terms of V_{FB} shift. However, the higher capacitance value was observed in the case of annealing in oxygen ambience. To be precise, the value of EOT in the case of annealing in oxygen ambience was decreased about 0.2 ~ 0.3 nm compared to the one in the case of annealing in nitrogen ambience although the value of EOT was not almost changed dependent on annealing ambience in the case of PDA as shown in Figure 3-48 in which plots of the result of annealing in oxygen ambience are added to Figure 3-45. And it was also found that variations of EOT were almost proportional to the time of PMA and a degree of variation slope was sharper than the one in the case of nitrogen ambience. However, the tendency dependent on annealing time was not observed in terms of V_{FB} same as in the case of nitrogen ambience as shown in Figure 3-49 in which plots of the result of annealing in oxygen ambience are added to Figure 3-46.

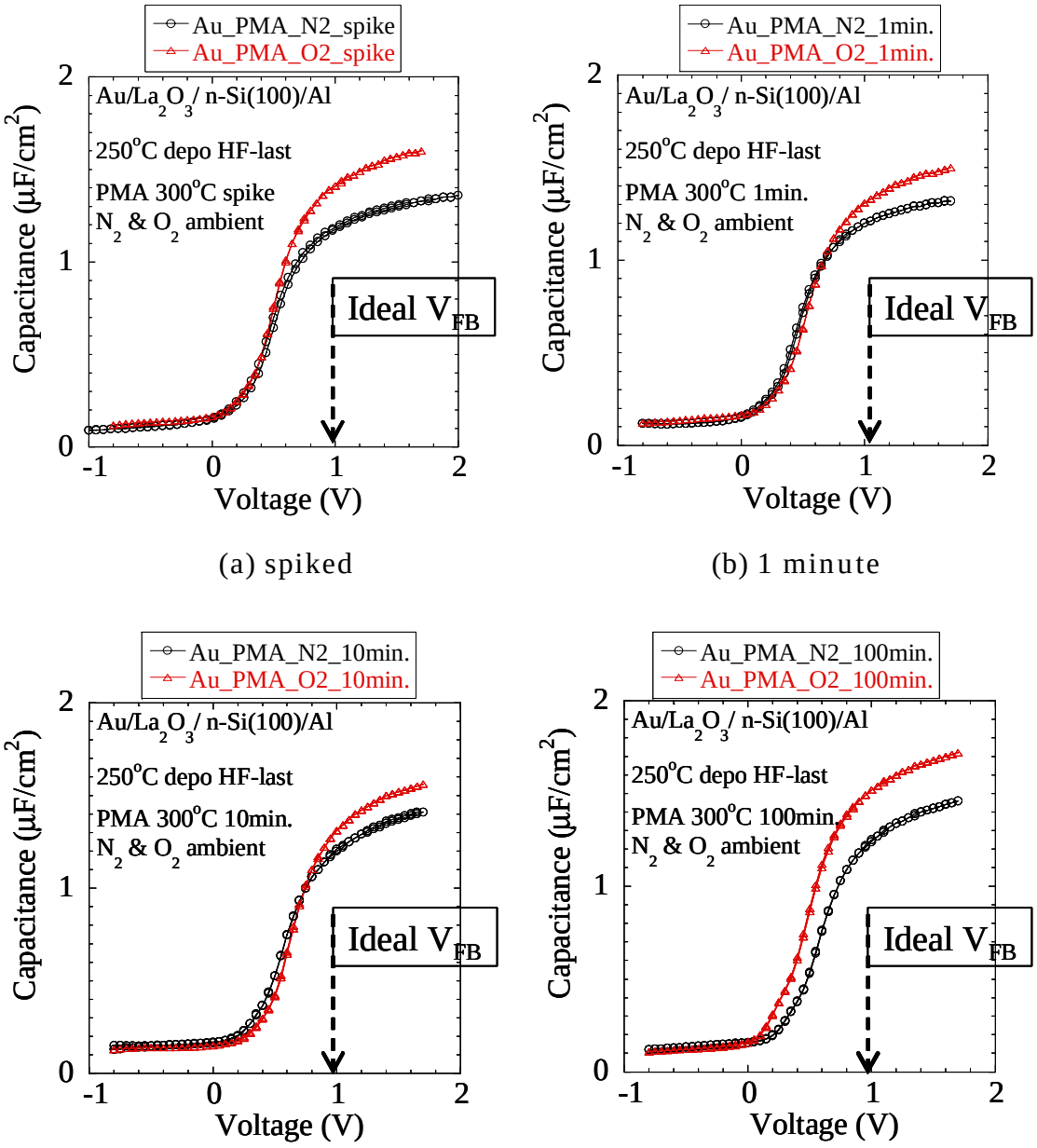

Figure 3-47: The comparison of the C-V characteristics of PMA between nitrogen and oxygen ambience on each annealing time from 0 second to 100 minutes
(a) 0 second (spike) (b) 1minute
(c) 10minutes (d) 100minutes

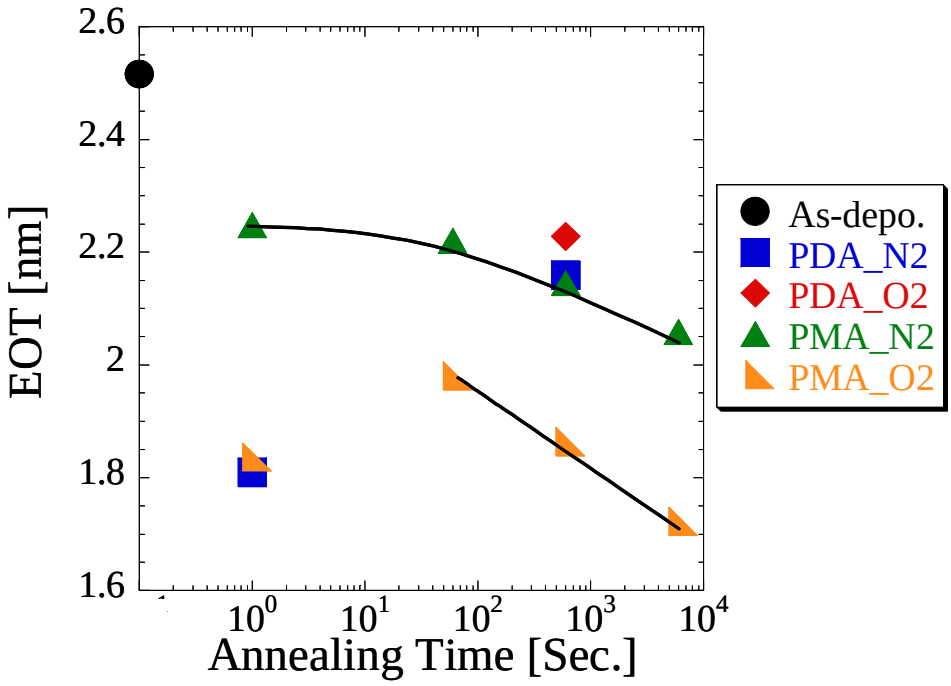

Figure 3-48: The plots of EOT dependent on annealing temperature in the case of nitrogen and oxygen ambience

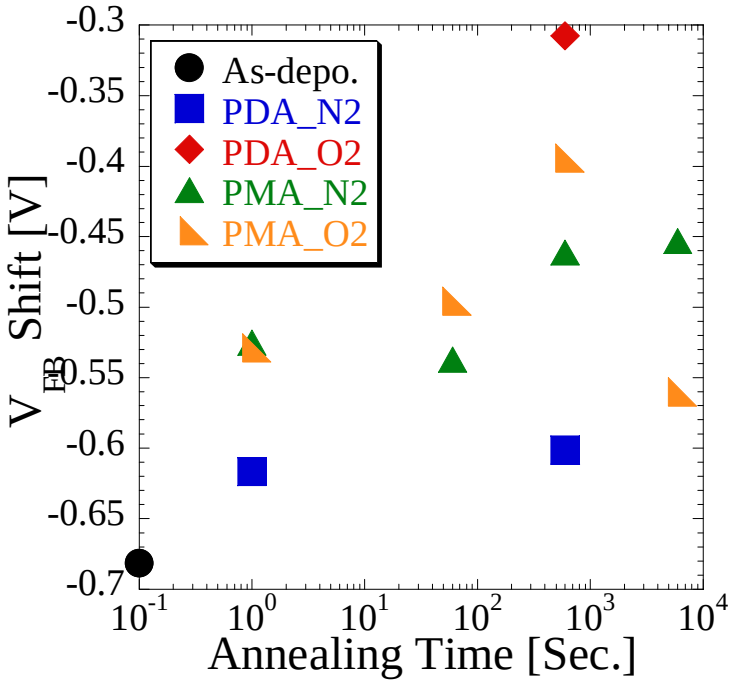

Figure 3-49: The plots of V_{FB} shift in the case of nitrogen and oxygen ambience

3.4.2.5 The comparison with the case of Aluminum Electrodes

As a summary of PMA with gold upper electrodes, the difference of behavior after thermal process was described. The C-V characteristics after PDA/PMA compared to As-deposition are shown in Figure 3-50 and Figure 3-51 respectively. It should be noted that although PDA with aluminum upper electrodes yielded a huge V_{FB} shift toward negative side, PDA with gold upper electrodes almost did not yield any V_{FB} shift. This result indicates that La_2O_3 thin films might react with aluminum upper electrodes the moment both came into contact. In the same way, although PMA with aluminum upper electrodes yielded a recovery of the V_{FB} shift but also a decrease of the capacitance value, PMA with gold upper electrodes yielded just a little V_{FB} shift and, on the contrary, an increase of the capacitance value. From these phenomena, it can be suggested that the choice of metal upper electrodes would exert an enormous influence on the electrical characteristics regardless of PDA or PMA, and the key of the solution of a matter of grave concern with the electrical characteristics of La_2O_3 would be included in this reaction which recovers V_{FB} shift, but also decrease the capacitance value.

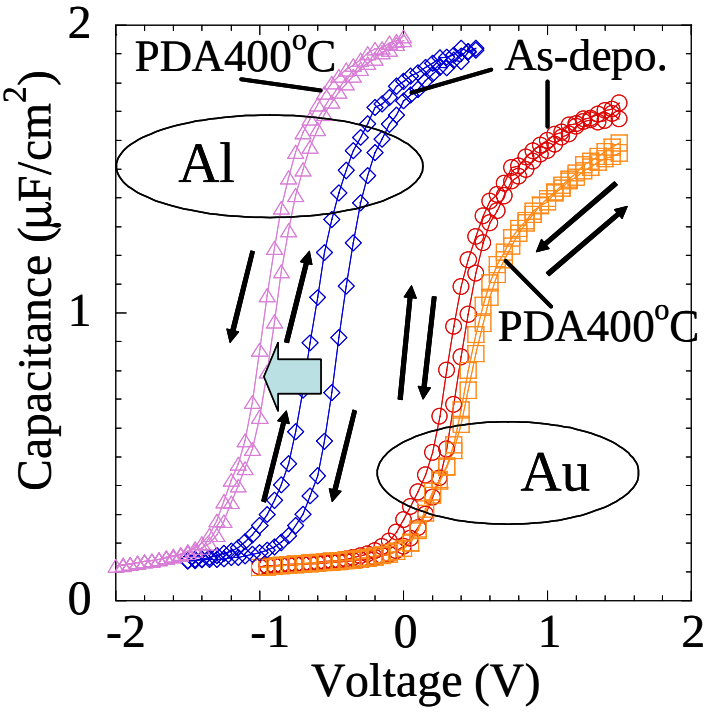

Figure 3-50: The comparison of electrical behavior after PDA between gold and aluminum upper electrodes.

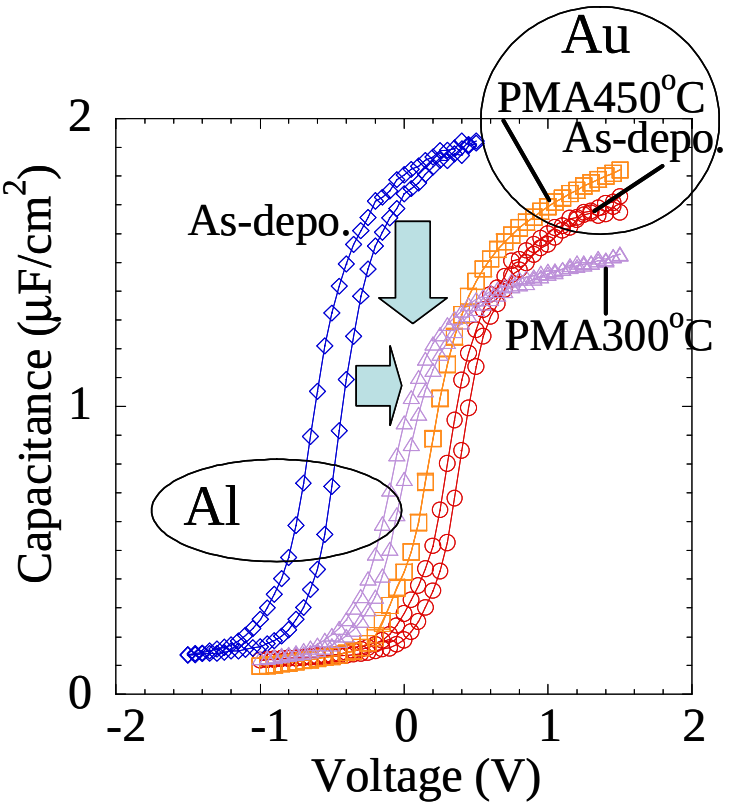

Figure 3-51: The comparison of electrical behavior after PMA between gold and aluminum upper electrodes.

3.4.3 Effects of PMA for Platinum Upper Electrodes

In former section, PMA with gold upper electrodes were investigated in order to be compared with PMA with aluminum upper electrodes. Consequently, PMA with these two metal electrodes showed quite different behavior after PMA, and also PDA. And although V_{FB} was recovered almost completely by PMA at 300°C for 10 minutes in nitrogen ambience in the case of aluminum upper electrodes, a recovery of V_{FB} shift was not realized by any annealing in the case of gold upper electrodes. From these results, it is conceivable that some reaction between aluminum and La_2O_3 would lead to the recovery of V_{FB} shift, and also a decrease of capacitance value. In order to corroborate this supposition, another metal electrode except aluminum should be examined. In my study, PMA with platinum upper electrodes were investigated and these results will be described the following pages.

3.4.3.1 Dependence on the Temperature of PMA with Platinum Upper Electrodes

Firstly, dependence on the temperature of PMA with platinum upper electrodes for La_2O_3 thin films was investigated same as other metal electrodes. Figure 3-52 shows the C-V characteristics dependent on the temperature of PMA for La_2O_3 thin films with platinum electrodes. Here, all of samples were HF-last treatment and annealed in nitrogen ambience for 10 minutes. Annealing temperature from 300°C to 600°C was examined respectively. It was observed that the excellent C-V characteristic without any hysteresis and much V_{FB} shift was observed by PMA at 300°C. However, the degradation of the C-V characteristics such as an appearance of hysteresis classified into charge infection type or a decrease of capacitance value were also observed with increase in the temperature of PMA with platinum upper electrodes.

Figure 3.37 shows the values of EOT versus annealing temperature plot for La_2O_3 thin films with platinum upper electrodes. Here, the results of as-deposition and PDA were shown in same graph. It was found that PMA with platinum upper electrodes increased the value of EOT with increase in annealing temperature even though the value of EOT in the case

of PMA at 300°C was maintained on a level with the one of as-deposition. And it was also found that the value of EOT in the case of PDA with platinum upper electrodes became lower as compared with PMA at same condition likewise for the results of aluminum upper electrodes.

Figure 3.54 shows the values of the V_{FB} shift versus annealing temperature plot for La_2O_3 thin films with platinum upper electrodes. It was found that variations of V_{FB} shift by PMA tended to recover up to 300°C. However, it was observed that the V_{FB} shifted toward negative side by PMA from 400°C to 600°C. And it was also observed that the V_{FB} resulting from PDA shifted toward negative side from the one of as-deposition likewise for the results of aluminum upper electrodes.

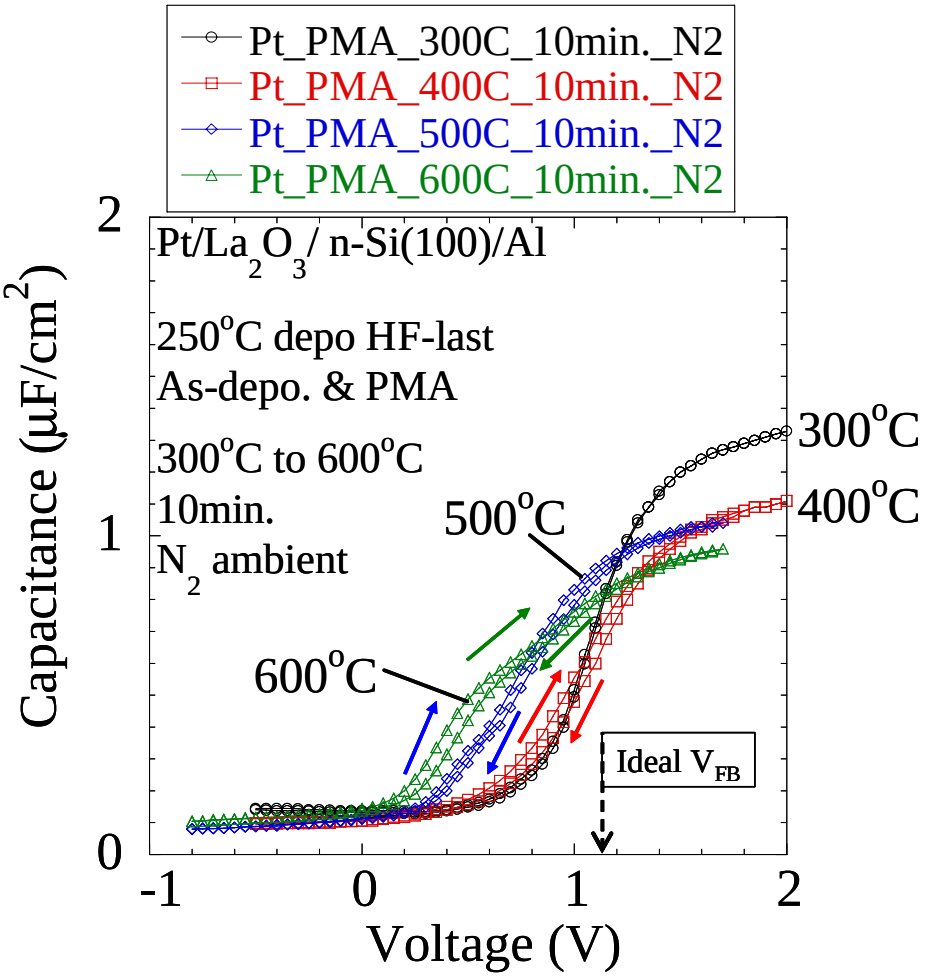

Figure 3-52: The C-V characteristics dependent on the temperature of PMA

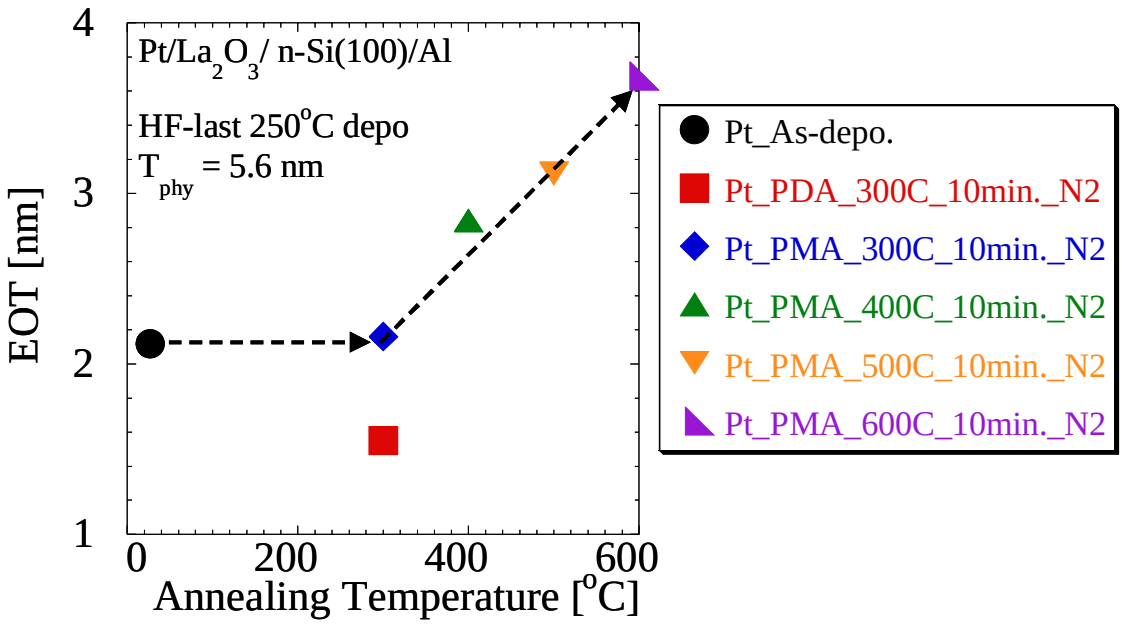

Figure 3-53: The values of the EOT shift versus annealing temperature plot

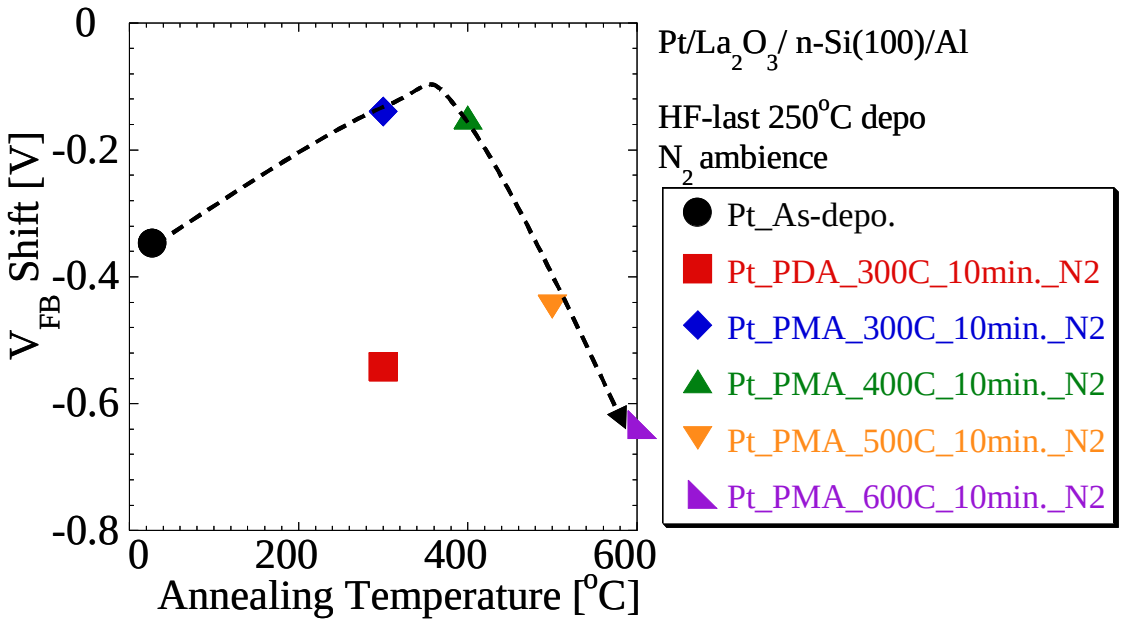

Figure 3-54: The values of the V_{FB} shift versus annealing temperature plot

3.4.3.2 Dependence on the Annealing Time of PMA with Platinum Upper Electrodes

The dependence on the annealing time for PMA with platinum upper electrodes was investigated same as aluminum and gold upper electrodes. Figure 3-55 shows the C-V characteristics dependent the time of PMA with platinum upper electrodes. Annealing time was examined from 0 sec to 100 minutes. The results of As-deposition and PDA samples were shown in same graph as well. Roughly speaking, there was almost no difference in C-V characteristics up to 10 minutes by a variation of the time of PMA. However, some changes of the characteristics such as slight V_{FB} shift, a decrease of capacitance value or an appearance of hysteresis were observed in the case of PMA for 100 minutes. To be more precise, the values of EOT of PMA slightly decreased with an increase in annealing time up to 10 minutes as shown in Figure 3-56. Moreover, the value of EOT of PDA was lower than the ones of PMA same as the case of aluminum upper electrodes. Figure 3-57 shows the plot of V_{FB} shift dependent on annealing time. It was found that the V_{FB} shift slightly recovered with increase in annealing time. And it was also found that PDA caused V_{FB} to shift toward negative side same as the case of aluminum upper electrodes.

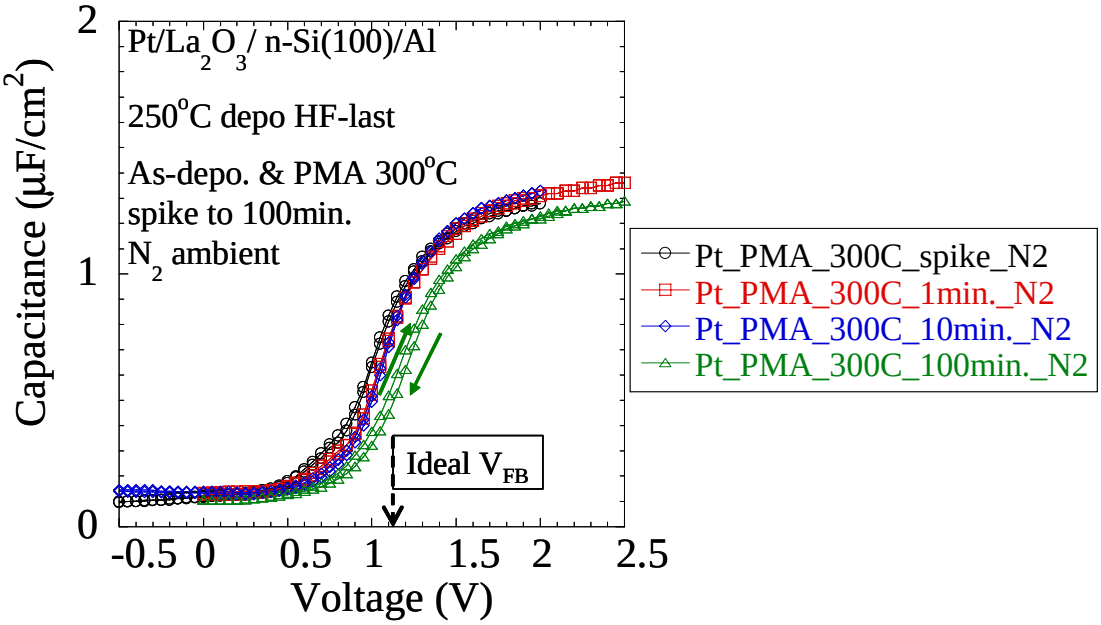

Figure 3-55: The C-V characteristics dependent the time of PMA

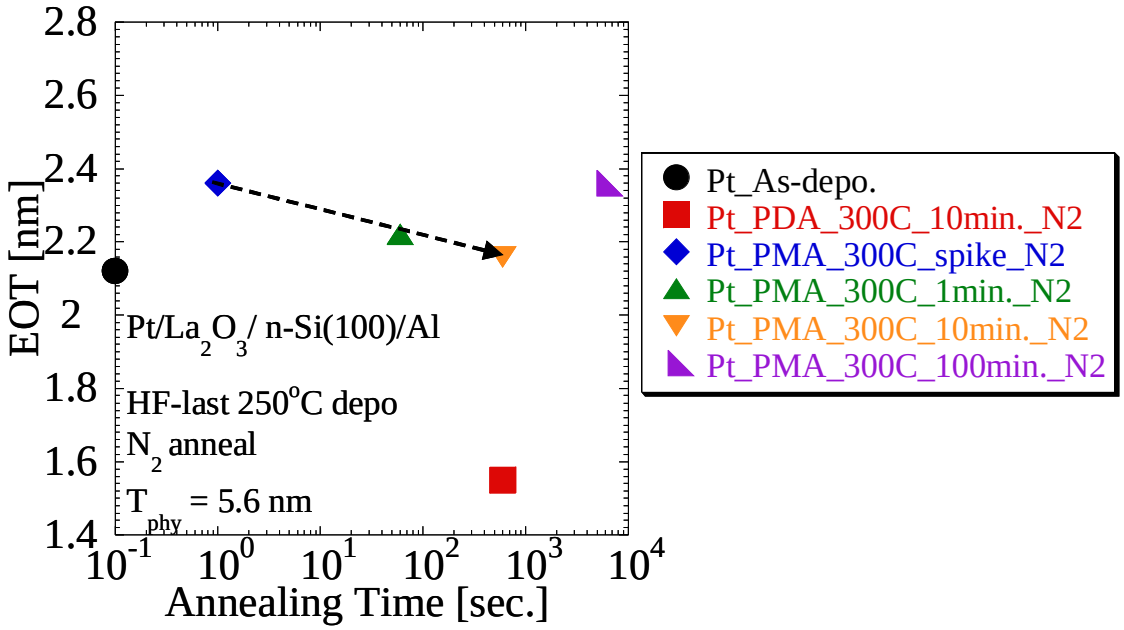

Figure 3-56: The values of EOT dependent on annealing time

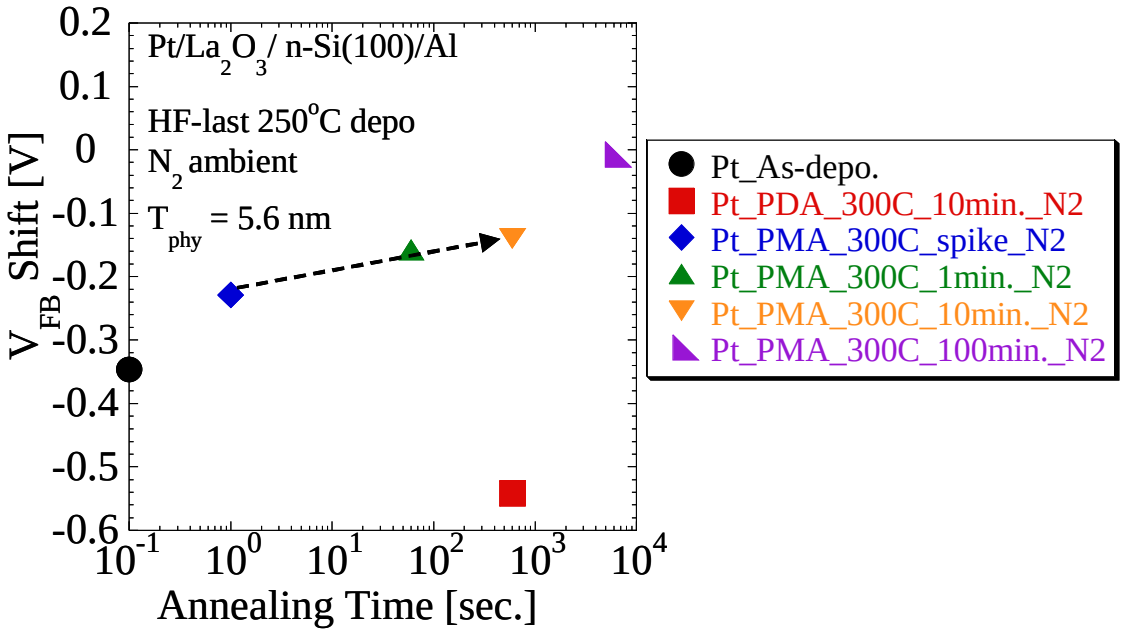

Figure 3-57: The values of V_{FB} shift dependent on annealing time

3.4.3.3 Dependence on the Ambience of PMA with Platinum Upper Electrodes

Up to this point, all of experiments in terms of PMA with platinum upper electrodes were done fixed to nitrogen ambience. Then, the influence of the annealing ambience through PMA was examined same as PMA with the case of aluminum and gold upper electrodes.

Figure 3-58 shows the comparison of the C-V characteristics of PDA between nitrogen and forming gas ambience and PMA between nitrogen, oxygen and forming gas ambience. All of samples were annealed for 10 minutes. It should be noted that the values of V_{FB} shift were quite dependent on annealing ambience in the case of not only PDA but PMA although there were almost no dependence on annealing ambience in terms of V_{FB} shift in the case of aluminum and gold upper electrodes. Moreover, it was also found that the annealing in forming gas ambience shifted V_{FB} to negative side less than the ones in nitrogen ambience in the case of PDA. On the other hand, a recovery of V_{FB} shift by PMA in forming gas ambience was less than the ones by PMA in nitrogen ambience. And the annealing in oxygen ambience brought the best recovery of V_{FB} shift but also a decrease of capacitance value.

Figure 3-59 shows the comparison of the C-V characteristics between nitrogen and forming gas ambience on each time of PMA from 0 second to 100minutes. On each annealing time, it was confirmed that the annealing in nitrogen ambience made the V_{FB} shift recover more than the ones in forming gas ambience. And the appearance of hysteresis classified into mobile charge type in the case of spike annealing in forming gas ambience, and charge injection type in the case of 100 minutes annealing in nitrogen ambience were observed respectively.

In order to verify from numerical view, the plots of the V_{FB} shift dependent on annealing time was shown in Figure 3-60. It can be confirmed that the difference of V_{FB} shift between the case of nitrogen and forming gas ambience was maintained on almost same level up to the annealing for 10 minutes. However, it was also found that variations of V_{FB} shift behaved quite different way, toward more positive side in the case of nitrogen ambience, and toward negative side in the case of forming gas ambience, on the annealing for 100minutes.

On the other hand, there was almost no dependence on annealing ambience in terms of EOT as shown in Figure 3-61.

The frequency dependence of C-V characteristics by various annealing time and ambience were compared to investigate the effect of annealing ambience. The result of nitrogen and forming gas ambience were shown in Figure 3-62 and 3-63 respectively. It was observed that in the case of the annealing in nitrogen, frequency dependence remained at weak inversion region on the all results of annealing time. On the other hand, in the case of the annealing in forming gas ambience, the frequency dependence gradually decrease with increase in annealing time, and it was completely eliminated at last by the annealing for 100minutes.

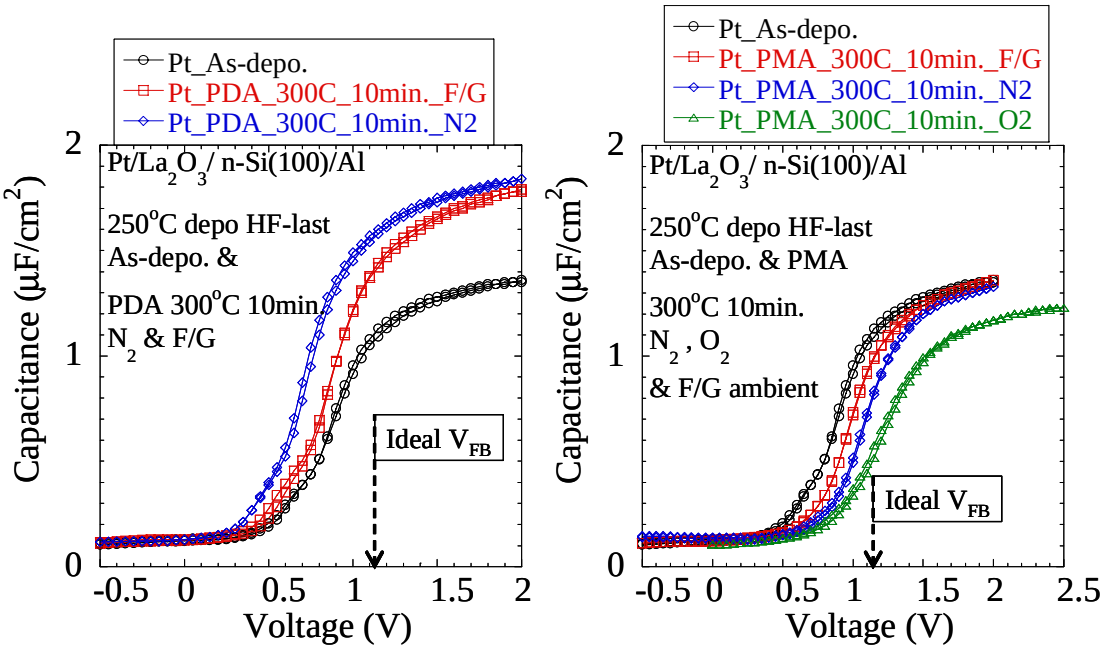

(a) PDA (b) PMA

Figure 3-58: The comparison of C-V characteristics
(a) PDA in nitrogen and oxygen ambience
(b) PMA in nitrogen, oxygen and forming gas ambience

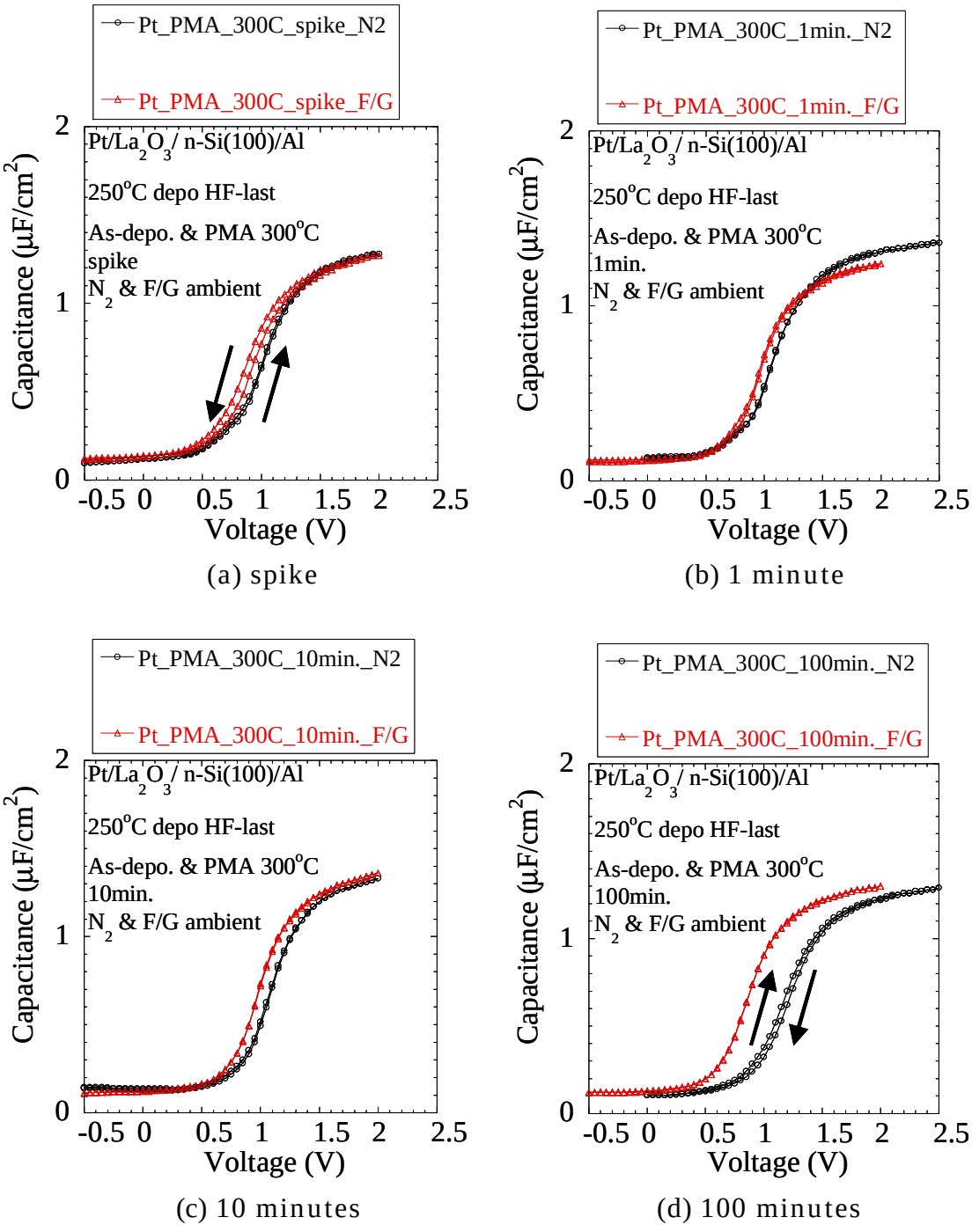

Figure 3-59: The comparison of the C-V characteristics between the case of nitrogen and forming gas ambience on each annealing time
(a) spiked (b) 1 minute
(c) 10minutes (d) 100minutes

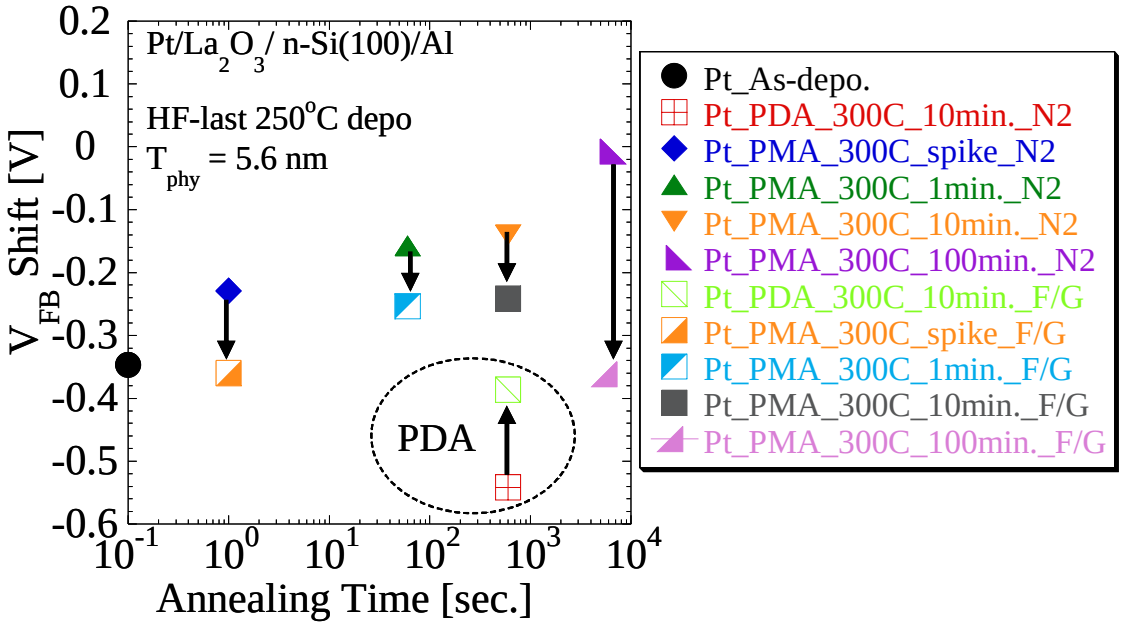

Figure 3-60: The plots of V_{FB} shift dependent on annealing time

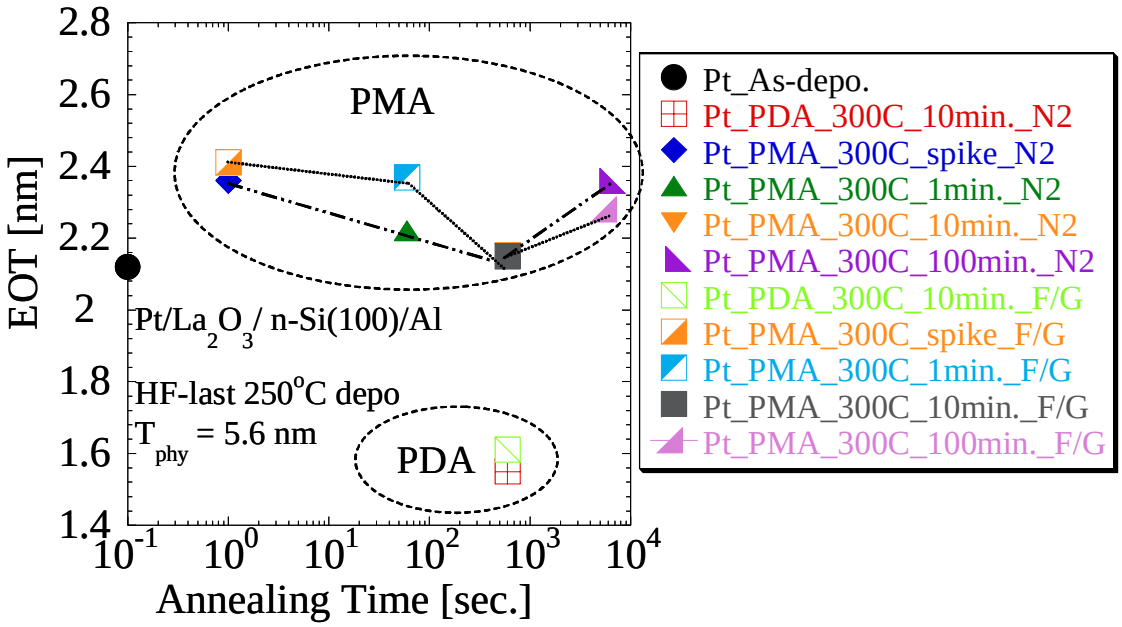

Figure 3-61: The plots of EOT dependent on annealing time

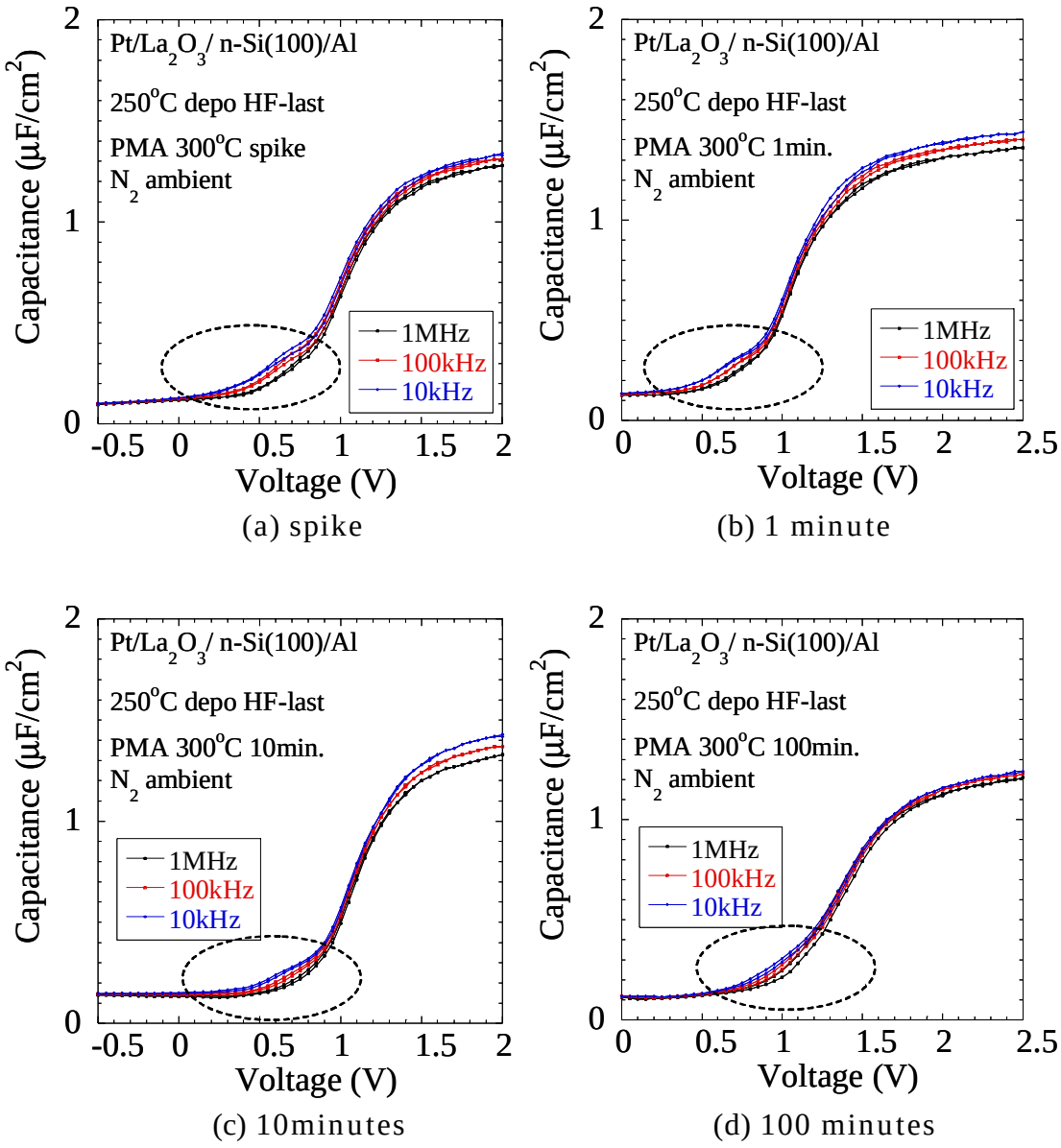

Figure 3-62: Frequency dependence of C-V characteristics fabricated by nitrogen annealing for
(a) spike (b) 1 minutes
(c) 10 minutes (d) 100minutes

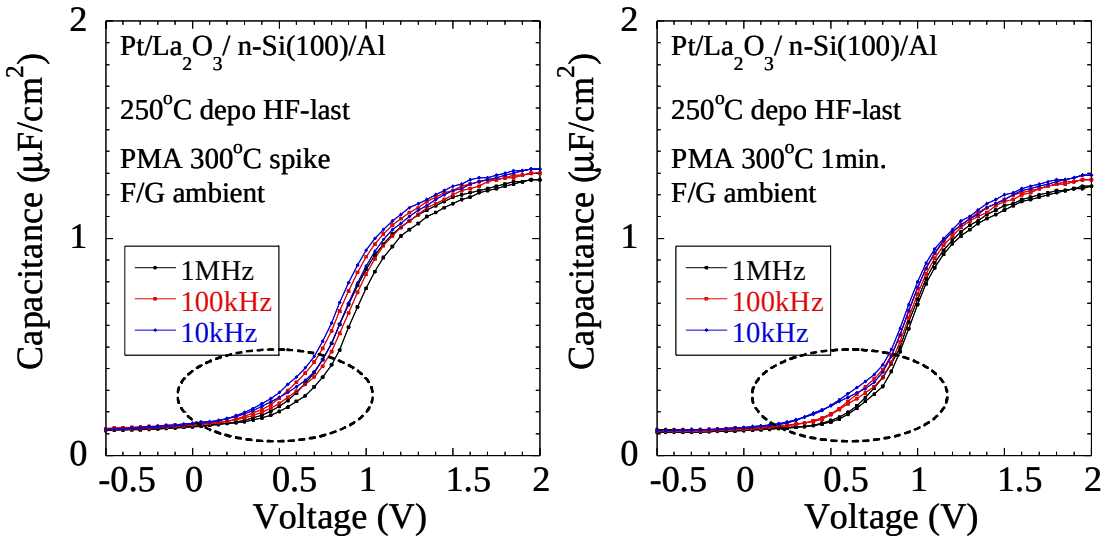

(a) spike

(b) 1 minutes

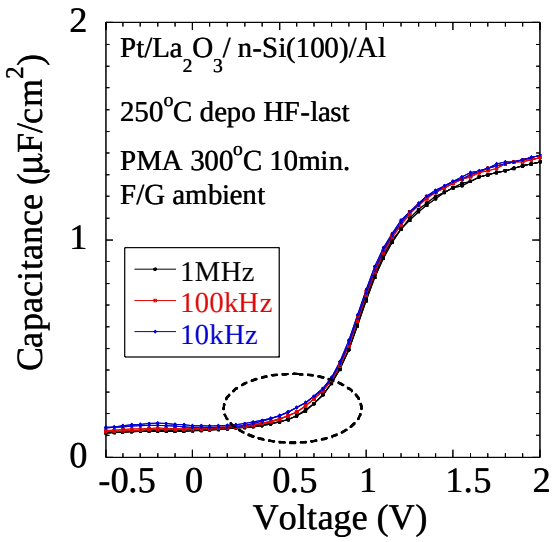

(c) 10 minutes

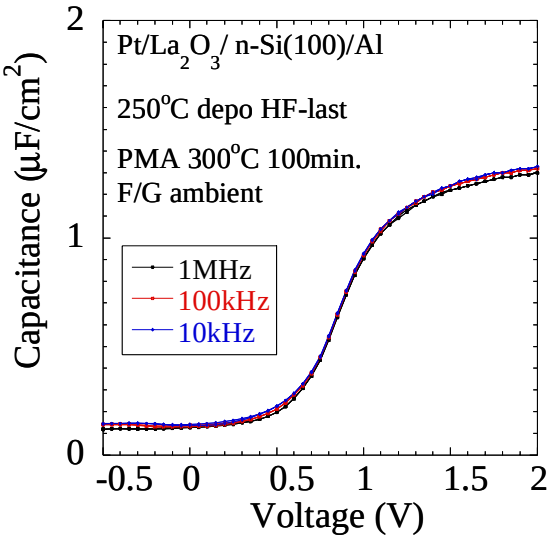

(d) 100 minutes

Figure 3-63: Frequency dependence of C-V characteristics fabricated by forming gas annealing for (a) spike (b) 1 minutes (c) 10 minutes (d) 100 minutes

3.4.3.4 The Summary of This Section

Up to this point, various annealing conditions for La_2O_3 thin films with platinum upper electrodes were investigated. As the summary of these investigations, the comparison of C-V characteristics between PDA and PMA are shown in Figure 3-64. The tendency that PDA increased the capacitance value but also shifted V_{FB} toward negative side is quite similar to the case of aluminum upper electrodes. However, there were several differences between both behaviors such as a way of recovering the V_{FB}, variation of EOT dependent on the condition of PMA, the range of variations of EOT and V_{FB} or influence of annealing ambience and so on. Therefore the reason why PMA with platinum could recover the V_{FB} shift might be different from the ones of aluminum. In order to explain these phenomena, more investigation must be done by adopting other metal material as upper electrodes.

Finally, plots of EOT versus V_{FB} shift is shown in Figure 3-65. It should be noted that major plots of V_{FB} shift stayed within -0.4 V. These results could be the evidence that the mechanism of variations of V_{FB} shift in the case of platinum upper electrodes is different from ones of aluminum upper electrodes because V_{FB} shift varied drastically owing to the annealing conditions in the case of aluminum upper electrodes. And same as the case of aluminum, trade-off relationship between EOT and V_{FB} shift exists and there are 3 plots on the line which means the best result, PMA for 100minutes in nitrogen ambience, PMA for 10minutes in nitrogen ambience and PDA for 10 minutes in forming gas ambience. Hence, combining these annealing conditions could bring much better results such as recovering V_{FB} shift without an increase of EOT.

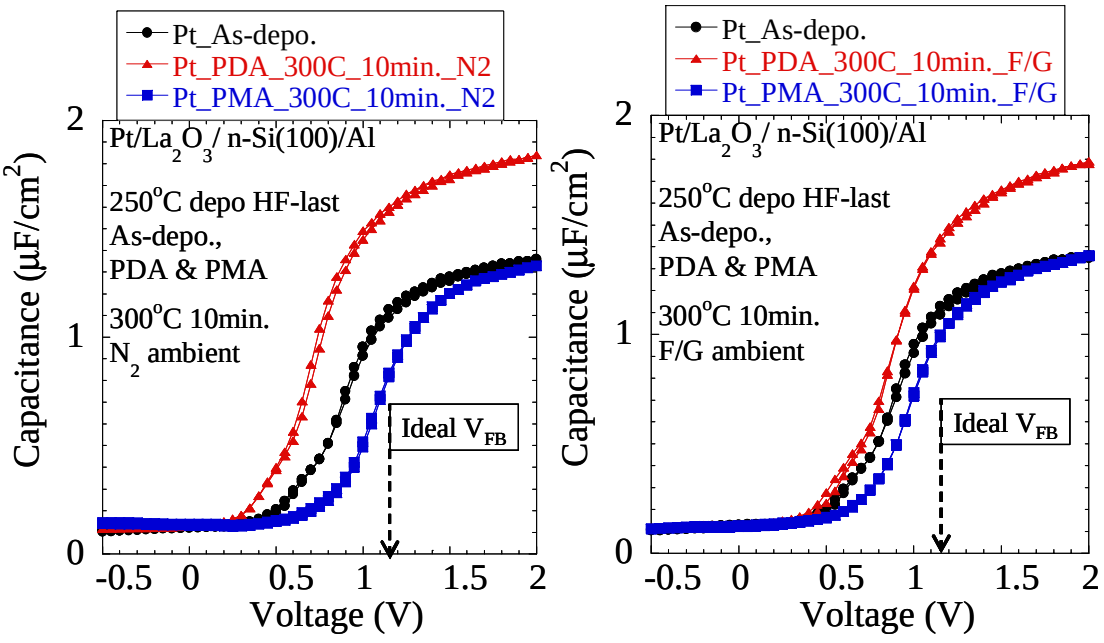

(a) Nitrogen ambience (b) Forming gas ambience

Figure 3-64: The comparisons of C-V characteristics between PDA and PMA in (a) nitrogen ambience (b) forming gas ambience

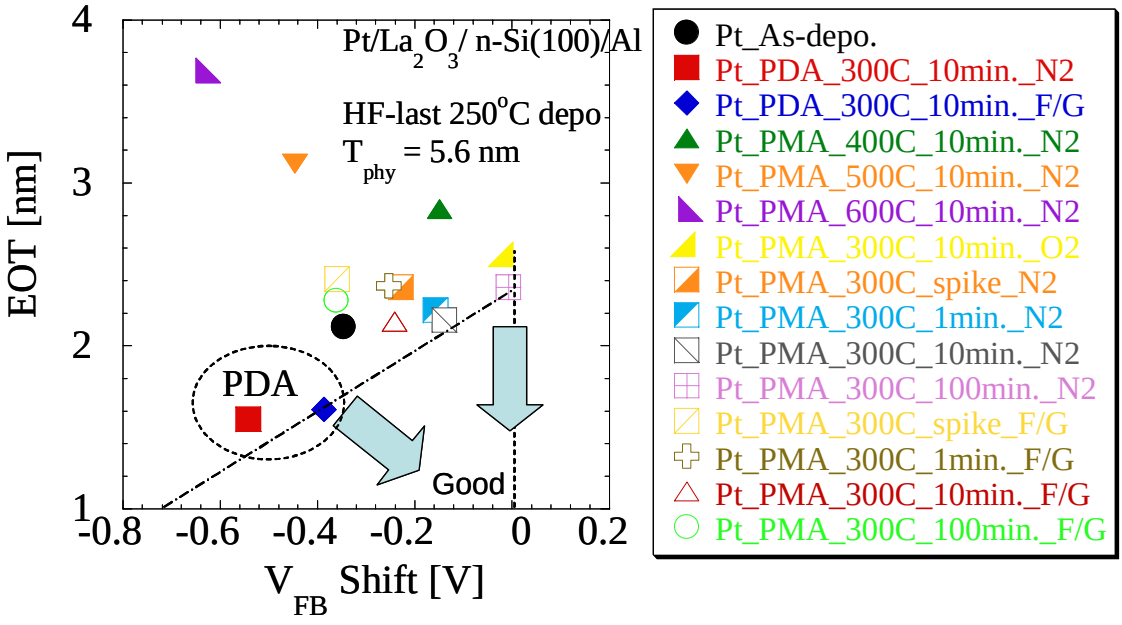

Figure 3-65: EOT versus V_{FB} shift plots

3.4.4 Examination of PMA for Another Rare Earth Oxide

In order to investigate a relationship between a recovery of V_{FB} caused by PMA with aluminum upper electrodes and La_2O_3 thin films, PMA for another rare earth oxide was examined for the purpose of the comparison with La_2O_3 thin films. In this examination, Gd_2O_3 were used. Figure 3-66 shows the comparison of C-V characteristics between PDA and PMA for Gd_2O_3 thin films with aluminum upper electrodes. It should be noted that V_{FB} shift recovered toward positive side in the case of Gd_2O_3 shin films same as in the case of La_2O_3 thin films. Moreover, the similar tendency such as a slight increase of hysteresis was also observed. From these results, it can be said that the effects of PMA were not dominated by the materials of gate insulator, but by the materials of upper metal electrodes, and this assumption indicates that PMA treatment investigated in my study could be applied to other materials which have the problem of V_{FB} shift toward negative side. Finally, it was found that PDA for Gd_2O_3 decrease the capacitance value compared to the ones of as-deposition (not described) although the value of PMA was maintained on a level with the one of as-deposition. This phenomenon was quite contrary to the case of aluminum upper electrodes.

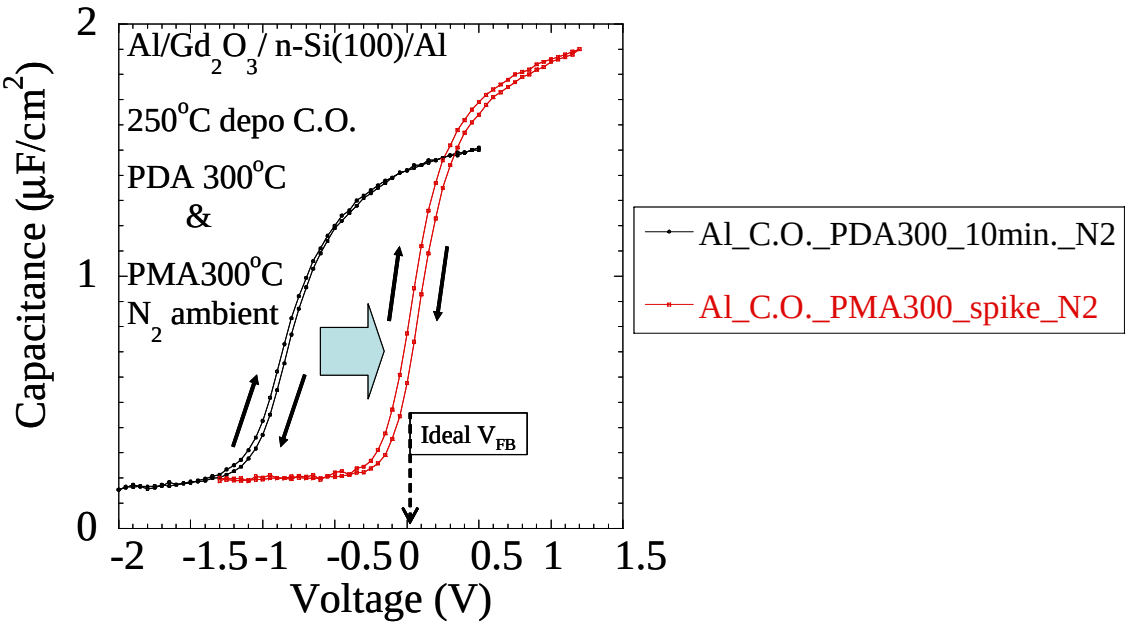

Figure 3-66: The comparison of C-V characteristics between PDA and PMA for Gd_2O_3 thin films with aluminum upper electrodes

Chapter 4

Conclusions

4.1 Summary of This Investigation

In my study, various annealing conditions for three kind of metal upper electrodes, aluminum, gold and platinum were investigated. Finally, obtained data will be summarized by itemizing in following pages as the conclusions.

4.1.1 Summary of the Investigation into the Annealing with Aluminum Upper Electrodes

PMA for La_2O_3 thin films with aluminum upper electrodes were investigated. As a result,

1. PDA decreased the values of EOT with increase in annealing temperature, but also shifted the V_{FB} toward negative side.
2. PMA recovered V_{FB} shift toward positive side and decreased leakage current as compared with PDA at same temperature, but also increased the value of EOT.
3. As compared with the case of HF-last treatment, chemical oxidation treatment suppressed leakage current, decreased the value of EOT slightly and recovered V_{FB} toward positive side in the case of PMA, but shifted V_{FB} toward negative side in the case of PDA.
4. Longer time annealing shifted V_{FB} toward negative side in the case of PDA, but shifted toward positive side in the case of PMA.
5. As a result of the examinations into the annealing in three ambiences, nitrogen, oxygen and forming gas, there was almost no dependence on annealing ambience
6. The combination of PDA and PMA brought good results, a recovery of V_{FB} shift with suppressing a decrease of capacitance value.

4.1.2 Summary of the Investigation into the Annealing with Gold Upper Electrodes

PMA for La_2O_3 thin films with gold upper electrodes were investigated. As a result,

1. PMA shifted V_{FB} toward negative side and increased leakage current, but also decreased the value of EOT.
2. As compared with the case of HF-last treatment, chemical oxidation treatment suppressed leakage current, decreased the value of EOT slightly in the case of PMA, but shifted V_{FB} toward negative side in the case of both PDA and PMA.
3. Longer time annealing increased the value of EOT in the case of PDA, but decreased in the case of PMA.
4. Oxygen ambience decreased the value of EOT as compared with nitrogen ambience..

4.1.3 Summary of the Investigation into the Annealing with Platinum Upper Electrodes

PMA for La_2O_3 thin films with platinum upper electrodes were investigated. As a result,

1. PMA recovered V_{FB} shift toward positive side until the annealing at 300^{o}C, but shifted toward negative side from the annealing at 400^{o}C, and increased the value of EOT as compared with the case of PDA
2. Longer time annealing recovered V_{FB} toward positive side and decreased the value of EOT until 10minutes annealing in the case of PMA
3. As compared with the annealing in nitrogen ambience, PMA in oxygen ambience recovered V_{FB} toward positive side, but increased the value of EOT.
4. As compared with the annealing in nitrogen ambience, the annealing in forming gas ambience recovered V_{FB} toward positive side in the case of PDA, but shifted toward negative side in the case of PMA.

4.1.4 Summary of the Effects of PMA for Gd_2O_3 Thin Films with Aluminum Upper Electrodes

PMA for Gd_2O_3 thin films with aluminum upper electrodes were investigated. As a result,

1. PMA recovered V_{FB} shift toward positive side same as the case of PMA for La_2O_3 thin films and V_{FB} shift was only 0.05 V from theoretical V_{FB} by PMA.
2. Contrary to the case of PMA for La_2O_3 thin films, the higher capacitance value than the one of PDA was confirmed by PMA.
3. The similar tendency of hysteresis to the case of PMA for La_2O_3 thin films was observed.

Finally, the tables of summary in regard to V_{FB} shift and EOT after annealing at various conditions were shown in Table 4-1 and 4-2 respectively.

Table 4-1: Summary of my investigation regarding to V_{FB} shift

	V_{FB}		
	Aluminum	Gold	Platinum
Dependence on Temperature-PDA	To Negave Side	not examined	not examined
Dependence on Temperature-PMA	To Positive Side	To Negave Side	To Negave Side (From 400°C)
Chemical Oxidation Treatment-PDA	To Negave Side	To Negave Side	not examined
Chemical Oxidation Treatment-PMA	To Positive Side (Up to 300°C)	To Negave Side	not examined
Dependence on Annealing Time-PDA	To Negave Side	No Dependence	not examined
Dependence on Annealing Time-PMA	To Positive Side	No Dependence	To Positive Side
Oxygen Ambience-PDA Compared to Nitrogen	No Dependence	To Positive Side	not examined
Forming gas Ambience-PDA Compared to Nitrogen	To Positive Side Slightly	not examined	To Positive Side
Oxygen Ambience-PMA Compared to Nitrogen	No Dependence	No Dependence	To Positive Side
Forming gas Ambience-PMA Compared to Nitrogen	No Dependence	not examined	To Negave Side

Table 4-2: Summary of my investigation regarding to EOT

	EOT		
	Aluminum	Gold	Platinum
Dependence on Temperature–PDA	Decrease	not examined	not examined
Dependence on Temperature–PMA	Increase	Decrease	Increase
Chemical Oxidation Treatment–PDA	No Dependence	No Dependence	not examined
Chemical Oxidation Treatment–PMA	Decrease	Decrease	not examined
Dependence on Annealing Time–PDA	No Dependence	Increase	not examined
Dependence on Annealing Time–PMA	Slight Increase	Decrease	Decrease (Up to 10 minutes)
Oxygen Ambience–PDA Compared to Nitrogen	No Dependence	Slight Increase	not examined
Forming gas Ambience–PDA Compared to Nitrogen	No Dependence	not examined	No Dependence
Oxygen Ambience–PMA Compared to Nitrogen	No Dependence	Decrease	Increase
Forming gas Ambience–PMA Compared to Nitrogen	No Dependence	not examined	No Dependence

4.2 Considerations about an Occurrence and a Recovery of V_{FB} Shift

By some conditions of PMA, V_{FB} shift toward negative side was completely and dramatically recovered. However, not only the mechanism of this recovery but also the mechanism of V_{FB} shift toward negative side has not clarified yet. From the results we have obtained, some assumptions for this phenomenon can be enumerated and some of them will be cited in the pages that follow.

It can be considered that there are principally two possibilities to bring about the V_{FB} shift toward negative side. The one is the absorption of moisture ambience into rare earth oxides thin films. It is well known that all of rare earth oxides have the property of absorbing readily moisture, and this absorption could make the rare earth oxides change into hydroxide as shown in Figure 4-1.

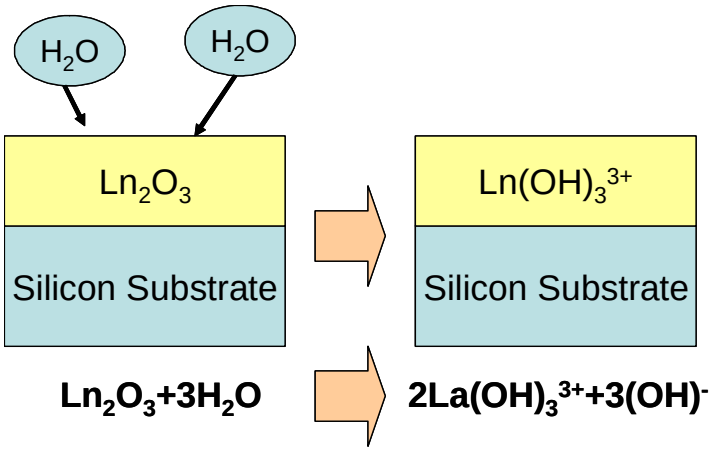

Figure 4-1: Schematic illustration of hydroxylation mechanism

The presence of $(OH)^-$ ion place of O^{2-} site could become a primary factor of the V_{FB} shift toward negative side.

Another is the oxygen deficiency. If the oxygen leaves from rare earth oxides films by some reasons, stoichiometry can not be preserved, and that result in the generation of positive charge in films. Three possibilities can be considered when oxygen vacancies occur as shown in Figure4-2. The one is a moment when rare earth oxides are deposited on silicon substrates in ultra high vacuum. This presumption seems to be consistent because the V_{FB} shift toward negative side was observed in as-deposited sample in my

results. The second is the time when the annealing process is performed. This one also seems to be consistent because larger V_{FB} shift toward negative side than as-deposited sample was also observed in PDA sample in my results. The third is the time when the aluminum upper electrodes are evaporated on the rare earth oxides thin films. It is well known that aluminum has the property of the strong affinity with oxygen and this property worked on this result. In other words, aluminum inhales the oxygen in rare earth oxides at a moment aluminum cone into contact with rare earth oxides thin films. This assumption also seems to be reasonable because the value of V_{FB} shift in the case of aluminum upper electrodes was larger than the one in the case of platinum upper electrodes.

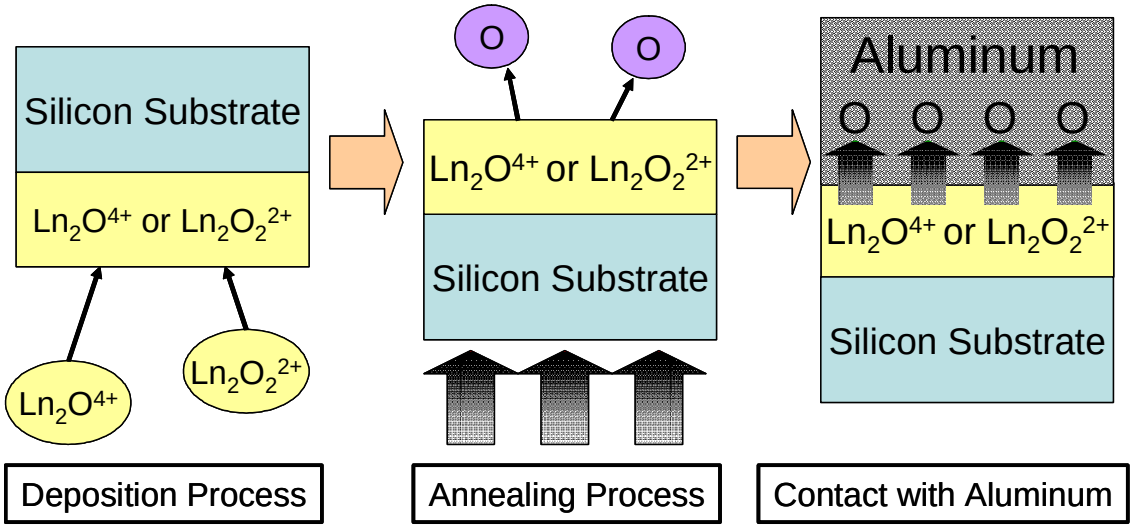

Figure 4-2: Schematic illustrations of oxygen vacancies mechanism

Then, the reason why V_{FB} shift toward negative side recovered by PMA with aluminum must be made clear. There are also two possibilities here. One is the effect of covering surface of rare earth oxides films before the annealing process. That seems to prevent oxygen from getting away to outside. However, this assumption is leaving one question. If this assumption is correct, PMA with all kind of metal upper electrodes is supposed to have an effect on the suppression of V_{FB} shift toward negative side. Actually, however, PMA with gold upper electrodes did not only yield

any recovery of V_{FB} shift, but shifted V_{FB} toward more negative side. Hence, this assumption does not seem to be correct. Another is the reaction between metal upper electrodes and rare earth oxides. In the case of aluminum upper electrodes which realized a recovery of V_{FB} shift, it is natural to consider that aluminum oxides (Al_2O_3) or lanthanum aluminate ($LaAlO_3$) was formed if there were some reactions between aluminum upper electrodes and rare earth oxides. And this assumption seems to become much more reasonable that these reactions formed aluminum oxides, not lanthanum aluminate. This assumption is well substantiated by three facts obtained by this investigation. One is a decrease of capacitance value after PMA with aluminum upper electrodes compared to one of PDA. It is well known that aluminum oxides have the lower dielectric constant (8~10) compared to lanthanum aluminate (20~25) and rare earth oxides (15~30). The second is the fact that PMA with gold upper electrodes increased the capacitance value in contrast to the case of PMA with aluminum upper electrodes. The third is an effect of a recovery of V_{FB} shift for Gd_2O_3 by PMA with aluminum as described in sub-section 3.3.4. This result also greatly supports this assumption. Therefore, it is conceivable that the formation of aluminum oxides decreased the capacitance value. Another, and this is the most significant part, is the fact that aluminum oxides have the property of shifting V_{FB} toward positive side. Aluminum oxide has been widely investigated as the one of the most promising and realistic next generation gate insulator material and this V_{FB} shift toward positive side has been commonly reported. And these reactions might occurred not only in the films but also at the interface between lanthanum oxides and aluminum, and that reaction could increase the own film thickness. These assumptions explained up to this point is illustrated in Figure 4-3.

Finally, it can be suggested that the formation of higher quality aluminum oxides between rare earth oxides which have high dielectric constant such as laminate structure could realize the zero flat band shift with preserving higher capacitance value.

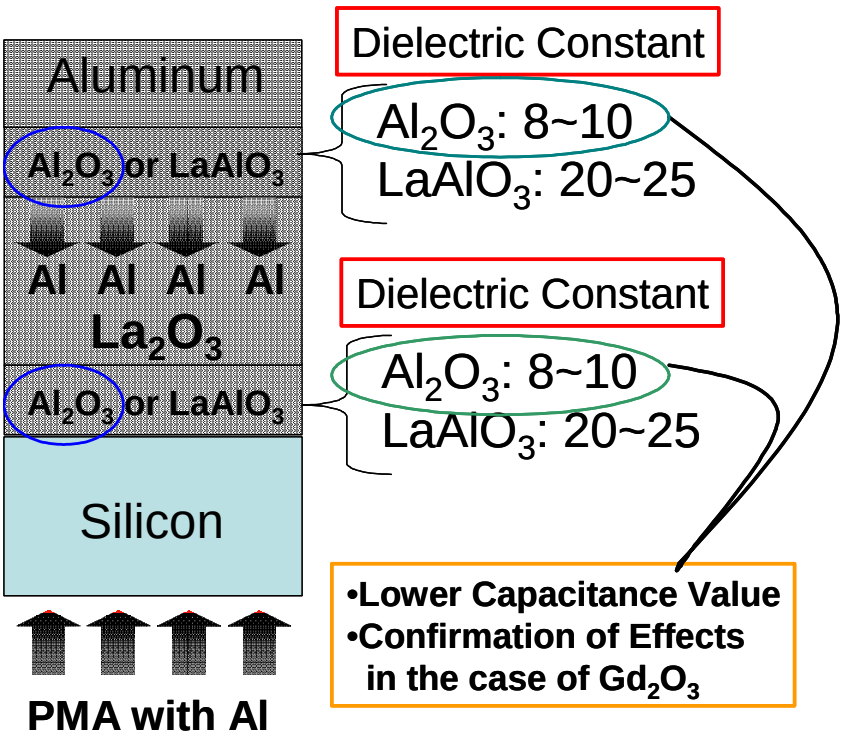

Figure 4-3: Illustration of the mechanism of a V_{FB} shift recovery

4.3 Future Issues

A recovery of V_{FB} shift was achieved by PMA with aluminum and platinum. However, the mechanisms of their recoveries, especially PMA with platinum were not clarified, and the reasons why PMA with gold electrodes did not yield any recovery of V_{FB} were not also investigated. From my results, it seems that some reactions enormously exert an influence on V_{FB} shift. Consequently, further examinations of these reactions in electrical, physical and chemical aspects will be required for elucidations of these mechanisms. And it can be anticipated that the mobility of MOSFET fabricated by PMA treatment could become higher as compared with the one fabricated by PDA treatment because PMA treatment could recover the V_{FB} shift toward almost theoretical value without fixed charge that cause the degradation of mobility owing to Coulomb scattering. Accordingly, the evaluation of mobility should be examined through fabricating MOSFET treated by PMA and the comparison with the one of PDA should be also done. Moreover, these material investigated in my study were not necessarily next generation gate electrode materials. Therefore, PMA for more promising materials as next generation gate electrodes such as TiN, TaN or nickel silicide must be examined.

Acknowledgement

In the first place, the author would like express my gratitude for Professor Hiroshi Iwai for his excellent guidance and continuous encouragement.

The author would like to express my sincere appreciation to Associate Professor Shun-ichiro Ohmi of his very useful advices and heartening encouragement through my research.

The author would like to thank Associate Professor Kazuo Tsutsui for his magnificent advices and encouragement.

The author would like to thank Professor Hiroshi Ishiwara very much for his tremendous supports for my research.

The author would like to thank Professor Kazuya Masu very much for his advices and supports.

The author would like to thank Associate Professor Eisuke Tokumitu for his supports for my research.

The author would like to thank Dr. K. Aizawa, Mr. T. Kurita and Mr. D. Shoji for their supports and useful advices.

The author would like to thank Dr. Yoshishige Tsuchiya for his generous supports and advices.

The author would like to thank Mr. sadahiro Akama, Ms. Chizuru Ohsima, Ms. Ikumi Kashiwagi, Mr. Akira Kikuchi, Mr. Junichi Taguchi, Hiroyuki Yamamoto and Mr. Yoshiaki Yoshihara for his great advices and wonderful friendship.

The author would like to thank Mr. Isao Ueda for his great discussions and wonderful supports

The author would like to thank his laboratory's colleagues, Mr. Jun-ichi Tonotani, Mr. Kyousuke Ohsima, Mr. Yongshik Kim, Mr. Jin Aun Ng, Mr. Joel Morina, Mr. Hendriansyah Sauddin, Mr. Youichi Kobayashi, Mr. Takahisa Sato, Mr. Kunihiro Miyauchi, Mr. George Yoshida and Katsuhiro Takagi for his wonderful friendship and heartening supports.

The author would like to express sincere and hearty appreciation to his laboratory's secretaries, Ms. Noriko Sato, Ms. Yuki Mihara, Ms. Kyoko Kubo, Ms. Masako Nishizawa, Ms. Nobuko Iizuka, Ms. Nahoko Hayashi and Ms. Yukie Morita of their great supports.

This study was partially supported by Semiconductor Technology Academic Research Center (STARC). The author would like to thank Dr. N. Nishikawa, Dr. J. Yugami, K. Tsunashima, T. Kato and K. Fujita for their useful advices and discussions.

This study was partially supported by Grant-in-Aid for Scientific Research Priority Areas (A): Highly Functionalized Global Interface Integration.

Finally, the author would like to express sincere and hearty gratitude for all of his friends and family for their wonderful supports.

Atsushi KURIYAMA

Yokohama, ***Japan***

19. February. 2004

Reference

[1] International Technology Roadmap for Semiconductors 2003 Edition.

[2] Keiji Tachikawa, IEDM Technical Digest, pp. (2003)

[3] S. Inumiya, K. Sekine, S. Niwa, A. Kaneko, M. Sato, T. Watanabe, H. Fukui, Y. Kamata, M. Koyama, A. Nishiyama, M. Takayanagi, K. Eguchi and Y. Tsunashima, Symposium on VLSI Technology, pp.17-18 (2003).

[4] T. Nabatame, K. Iwamoto, H. Ota, K. Tominaga, H. Hisamatsu, T. Yasuda, K. Yamamoto, W. Mizubayashi, Y. Morita, N. Yasuda, M. Ohno, T. Horikawa and A. Toriumi, Symposium on VLSI Technology, pp.25-26 (2003).

[5] C.H. Choi, S.J. Rhee, T.S. Jeon, N. Lu, J.H. Sim, R. Clark, M. Niwa and D.L. Kwong, IEDM Technical Digest, pp.857-860 (2002).

[6] H. Iwai, S. Ohmi, S. Akama, C. Oshima, A. Kikuchi, I. Kashiwagi, J. Taguchi, H. Yamamoto, J. Tonotani, Y. Kim, I. Ueda, A. Kuriyama and Y. Yoshihara, IEDM Technical Digest, pp.625-628 (2002).

[7] A. Chin, Y.H. Wu, S.B. Chen, C.C. Liao and W.J. Chen, Symposium on VLSI Technology, pp.16-17 (2000).

[8] S. Ohmi, C, Kobayashi, K. Aizawa, S. Yamamoto, E. Tokumitsu, H. Ishihara and H. iwai, Proceedings of ESSDERC, pp.235-238 (2001).

[9] U. Schwalke, Y. Stefanov, R. Komaragiri and T. Ruland, Proceedings of ESSDERC, pp.243-246 (2003).

[10] S.Guha, E. Cartier, M. A. Gribelyuk, N.A. Bojarczuk and C. Copel, Applied Physics Letters, Volume 77, Number17, 2710 (2000).

[11] Shin-ichi Saito, Yasuhiro Shimamoto, Kazuyoshi Torii, Yukiko Manabe, Matty Caymax, Jan Willem Maes, Masahiko Hiratani and Shin'ichiro Kimura, Extended Abstracts of SSDM, pp.704-705 (2002)

[12] Angus I. Kingon, Jon-Paul Maria, Dwi Wicaksana and Chris Hoffman, IWGI pp36-41 (2001)

[13] Jung-Hyoung Lee, Jong Pyo Kim, Jong-Ho Lee, Yun-seok Kim, Hyung-seok Jung, Nae-In Lee, Ho-Kyu Kang, Kwang-Pyuk Suh, Mun-Mo Jeong Kyu-Taek Hyun, Hion-Suck Baik, Young Su Chung, Xinye Liu, Sasangan Ramanathan, Tom Sidel, Jerald Winkler, Ana Londergan, Hae Young Kim, Jung Min Ha and Nam Kyu Lee, IEDM Technical Digest, pp221-224 (2002)

[14] M. Copel, E. Cartier and F. M. Ross, Applied Physics Letters, Volume 78, Number11, 1607 (2001)
[15] Takashi Shimizu, Hirotoshi Yamada, Akira Kurokawa, Kenichi Ishi and Eiichi Suzuki, IWGI pp196-201 (2001)